Using Non-Stationary Training Images from Process-Based Models for Multiple-Point Geostatistics Stochastic Generation of Fluvial-Dominated Delta Reservoir Model

Adhi Wibowo Prakoso

Delft University of Technology

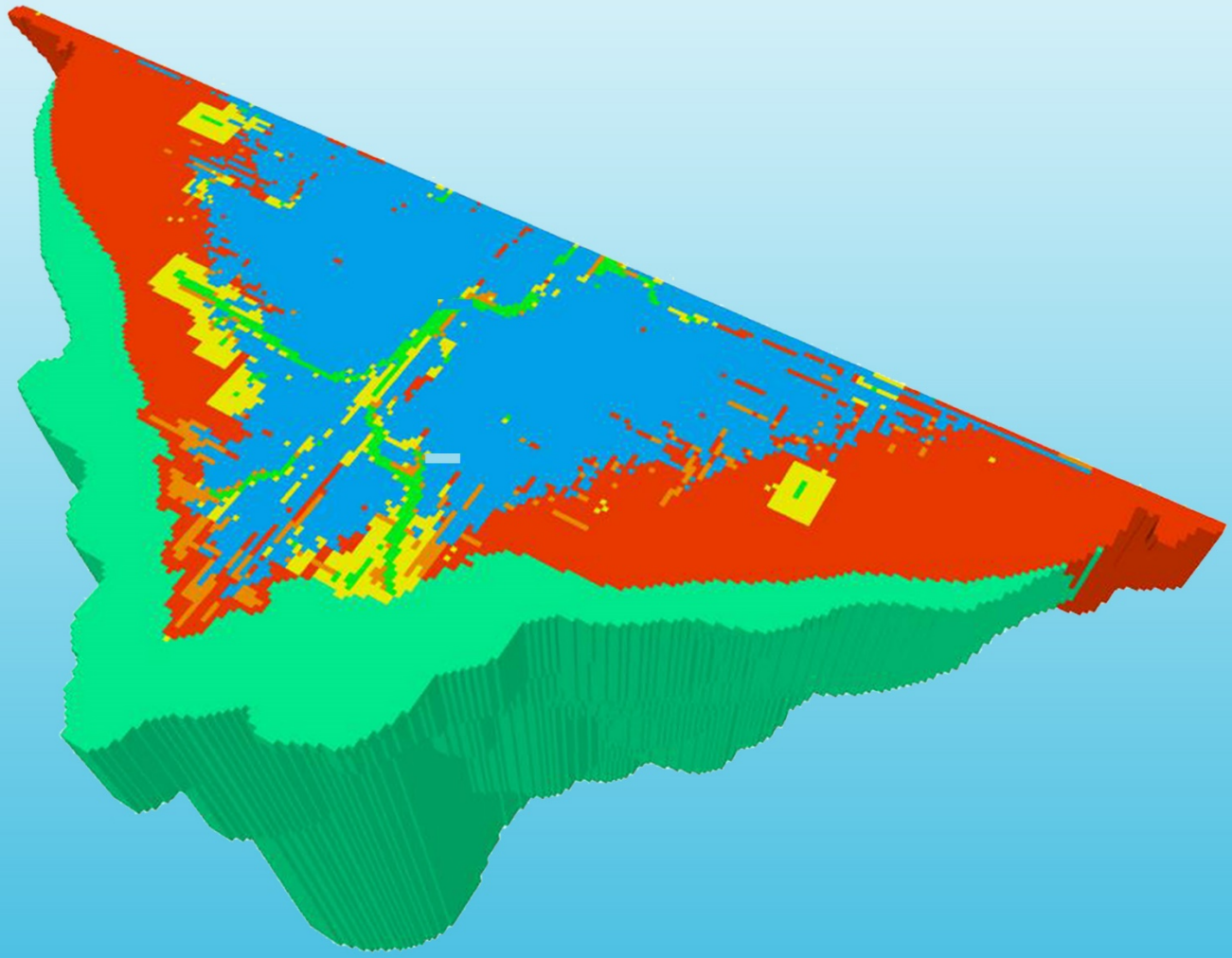

TU Delft

BAKER HUGHES a GE company

Using Non-Stationary Training Images from Process-Based Models for Multiple-Point Geo-statistics Stochastic Generation of Fluvial-Dominated Delta Reservoir Model

By

Adhi Wibowo Prakoso

in partial fulfilment of the requirements for the degree of

Master of Science
in Petroleum Engineering and Geosciences

at the Delft University of Technology,
to be defended publicly on Thursday November 29, 2018 at 10:30 AM.

Supervisor:	Dr. Joep Storms	TU Delft
Thesis committee:	Dr. Joep Storms	TU Delft
	Dr. Hemmo Abels	TU Delft
	Dr. ir. Femke Vossepoel	TU Delft
	Natalia Papatrecha, MSc	Baker Hughes, a GE company

An electronic version of this thesis is available at https://repository.tudelft.nl/

TU Delft

BAKER HUGHES a GE company

Abstract

Process-based method forward stratigraphic modelling provides advantages in reservoir modelling by simulating the geological process mathematically, and the genesis of geologic formations over time (Michael et al., 2010). In spite of its advantages, Miller et al. (2008) have recognised significant challenges in process-based simulation models, one of them is the incapability to condition to subsurface data. The problem in conditioning the data can be addressed by using an alternative method named multiple-point geostatistics (MPS) in modelling the subsurface since its introduction in 1993 by Guardiano and Srivastava. MPS considers the relationship between multiple data points that is different from the conventional geostatistical methods that are commonly limited to using a linear relationship between data (Guardiano and Srivastava, 1993). By using the process-based simulation model as training image (TI) for MPS simulation, MPS should be able to address the conditioning issue in process-based simulation model.

Over the past decade, most research in MPS has emphasized on new algorithms for improving efficiency of MPS (Mariethoz and Caers, 2014; Mariethoz and Lefebvre, 2014), but there are still issues remain for the workflow to be widely used in geosciences. Furthermore, using nonstationary TI such as process-based simulation model in MPS are still an issue because the workflow is always different for specific cases. Until recently, little published works are available in applicating nonstationary TI in MPS.

The principal objective of this project was to determine an optimised methodology that allows the use of nonstationary process-based simulation model for TI input with MPS simulation in the fluvial-dominated delta. The process-based simulation model used in the study is a post-processed data from numerical model done in process-based modelling software Delft3D (Lesser et al., 2004) which is the PhD work of van der Vegt in 2018. There were two different cases utilised in this study that represents the whole delta development: Case A with high repetition in the patterns and Case B with low repetition in the patterns.

In order to achieve the desired outcome, this study links process-based simulation model with MPS using unconditional and conditional 2D MPS simulation with two different approaches: zonation approach and control map approach. The realisations from the unconditional simulation have to be validated until successful unconditional MPS simulation. The conditional MPS simulation were carried out when the unconditional realisations have been acknowledged as the approved results in mimicking the patterns of the Delft3D model. Lastly, the results were evaluated with four methods: connectivity function, E-type models, conditional variance models, and analysis of distance (ANODI).

In all of the MPS simulation results, the use of control map approach with unilateral simulation path proved to deliver better realisations for unconditional and conditional MPS simulations. Also, this study has presented an optimised workflow of 2D MPS simulation on using process-based simulation model in fluvial-dominated delta environment as TI based on different conditions of patterns' repetition and hard data distribution.

Acknowledgements

There were a multitude of individuals who helped me to arrive at this point, and in this opportunity, I would like to express my gratitude. First and foremost, I would like to thank Dr. Joep Storms for his constant guidance, encouragement, and support through this thesis writing journey. He has offered very valuable advices on approaching unfamiliar aspects and problems in Multiple-Point Geostatistics to simple and understandable geology. His helpful and constructing character has made me a better person, both personally and academically.

Secondly, I wish to give a special thanks to Dr. Andre Jung and Baker Hughes, a GE Company for introducing this exciting topic that I hope will give a contribution in developing Multiple-Point Geostatistics application in reservoir modelling. Andre's knowledge and experience in Multiple-Point Geostatistics has provided valuable assistance in understanding MPS' complexity. He has also provided me with his enthusiasm to lend me a hand immediately whether I have questions, and hospitality in Baker Hughes whenever he is available.

I am also grateful to Helena van der Vegt, PhD for her eagerness and her aid in processing her work of Process-Based Model in order to be able to be used in this thesis. Her excellent work in the development of Process-Based Modelling has promote the ease in integrating her model in Multiple-Point Geostatistics at the start of my thesis. For that, I am most grateful.

Many thanks for Dr. Hemmo Abels, Dr. ir. Femke Vossepoel, and Natalia Papatrecha, MSc for being part of my graduation committee. Their critical and extensive feedbacks have helped me in completing this thesis as an academically-approved work.

My gratitude is also extended for Indonesia Endowment Fund for Education (LPDP) as my sponsor, without them I would not have been able to realise my lifelong dream of studying abroad. This allowed me to meet and collaborate with a lot of great people in TU Delft, one of the best institutions in the world. I will surely apply all the lesson and knowledge to the development of my homeland, Indonesia.

My acknowledgement would not be complete without thanking the fantastic people of TU Delft for helping me in various aspects of this thesis. Thank you for Stephan in helping me processing the data in MATLAB so it can be used properly. Thank you for Aulia for the free coffee and the discussion of the geological contents. Also, thank you for all the Indonesian companions in Petroleum Engineering and Geosciences for all the exam preparations in this 2-year academic journey. I owe a debt of gratitude to you all.

My warmest thanks are due to my parents for their never-ending care and always supporting every path I chose. Their weekend video calls have always keep the homesick feelings at bay. Also, my Indonesian friends and PPI Delft for making Delft a home far-away from home with their *nyinyiran*, late-night talks, weird YouTube videos, and exciting trips. I cannot wait to spend time together with you all again in the future.

Last but not least, I would not survive master study without Nabilah Adani and her emotional support albeit the 6936 km and 8-hour difference between Delft-Edmonton. Not an easy one, huh?

Terima kasih banyak, semuanya.

Contents

Abstract.....i

Acknowledgements.....ii

List of Figures.....vi

List of Tables.....xii

List of Abbreviations.....xiii

1 Introduction.....1

1.1 Process-based and Multiple-point Geostatistics (MPS) method in facies modelling.....1

1.2 Motivation and objective of the study.....2

1.3 The scope of the study.....4

2 Methodology.....5

2.1 Multiple-point geostatistics (MPS).....5

2.1.1 MPS algorithms.....6

2.1.2 Training image (TI) and its stationarity.....7

2.1.3 Source of TI.....8

2.2 Process-based modelling.....11

2.3 Modelling nonstationarity in MPS.....12

2.3.1 Zonation approach.....12

2.3.2 Control map approach.....14

2.4 MPS simulation path type.....15

2.4.1 Random simulation path.....15

2.4.2 Unilateral simulation path.....16

2.5 Conditioning in MPS simulation.....17

2.6 Evaluation of MPS simulation....18
2.6.2 Analysis of distance (ANODI)....21
2.7 Workflow....26
3 Data....28
3.1 Process-based simulation model as input data....28
3.2 Preparation of the input data....30
3.3 TI construction and its properties....32
3.3.1 TI for zonation approach....33
3.3.2 TI for control map approach....36
3.4 Hard data selection for conditional simulations....39
4 Results....41
4.1 Unconditional MPS simulation results....41
4.1.1 Case A....43
4.1.2 Case B....47
4.1.3 Evaluation of the results....50
4.1.4 Summary of the unconditional MPS simulation results....54
4.2 Conditional MPS simulation results....54
4.2.1 Case A....55
4.2.2 Case B....58
4.2.3 Evaluation of the results....60
4.2.4 Summary of the conditional MPS simulation results....72
5 Discussion....74
5.1 Unconditional MPS IMPALA simulation....74
5.1.1 Determining assumed stationarity zonations in unconditional MPS simulation....74

5.1.2 Comparing the realisations from zonation approach and control map approach in unconditional MPS simulation 74

5.1.3 The effect of various parameters in the connectivity function 76

5.1.4 Preference of unilateral simulation path in simulating channel features....76

5.2 Conditional MPS IMPALA simulation 76

5.2.1 Capability in honouring the hard data....76

5.2.2 Limitation of unilateral simulation path 77

5.2.3 Interpolation capability in conditional MPS simulation 77

5.2.4 Variability of realisations between zonation and control map approaches 78

5.2.5 ANODI scoring results compared to the other evaluation 79

6 Conclusions and future recommendation 80

6.1 Ideal TI for MPS simulation using nonstationary fluvial-dominated delta simulation model 80

6.2 The optimised method to unconditionally model the nonstationarity in fluvial-dominated delta reservoir model based on the study's methods 81

6.3 The optimised method to conditionally model the nonstationarity in fluvial-dominated delta reservoir model based on the chosen methods....82

6.4 Future recommendations 82

7 References 84

Appendix....89

Appendix....94

List of Figures

Figure 2.1. The illustration of a multiple-point event (Michael J. Pyrcz and Deutsch, 2014).....5

Figure 2.2. An example of SNESIM algorithm in simulating a cell (Zhang, 2008). 6

Figure 2.3. An example of TIs in fluvial environment. Left picture shows nonstationary TI, and right picture shows stationary TI. In stationary TI, the patterns shows enough repetition compared to the nonstationary TI (Arpat and Caers, 2007).....8

Figure 2.4. An example of constructing TI from Lena River Delta's satellite image (Feng and Wu, 2016). 9

Figure 2.5. An example of object-based method in generating TI using TiGenerator. The patterns represent channels with crevasse-splay (Maharaja, 2008). 10

Figure 2.6. The process-based simulation model of Delft3D software for deltaic environment (van der Vegt, 2018). 11

Figure 2.7. Example of the use of zonation concept in MPS modelling. Each zone (yellow and red) has its corresponding TI that shares the same channel facies (Daly and Caers, 2010).....12

Figure 2.8. Example of rotation and affinity zones in SNESIM algorithm (Liu, 2006). 13

Figure 2.9. Example of control maps in nonstationary MPS modelling. (a) and (a') represent the TI and its control maps, where (b) and (b') represent the simulation grid and its control map. Notice the patterns' orientation between the TI grid and simulation grid (Mariethoz and Caers, 2014). 14

Figure 2.10. Another example of control maps in nonstationary MPS modelling. By using the control map, the geomodeler can control the occurrence of the patterns in the simulation grid. The value in the control map is similar for each stationary zonation (Ephesia Consult, 2017). 14

Figure 2.11. An illustration of the random simulation path in MPS simulation. From left to right depicts the percentage of cells simulated (Mariethoz and Caers, 2014). 15

Figure 2.12. The illustration of the unilateral simulation path in MPS simulation in the +I+J direction (Mariethoz and Caers, 2014).....16

Figure 2.13. Training image and the realisations with using random and different unilateral simulation path (Mariethoz and Caers, 2014). 17

Figure 2.14. The illustration of MPS simulation using unilateral simulation path in -J+I direction in an example 4 x 4 grid. The simulation started at the top left corner, then increments through the +I direction after the column has been simulated in -J direction. The red node depicts the cell that is being simulated, the grey nodes depicts simulated cells, and the white nodes depict cells that have not been simulated. 17

Figure 2.15. The left picture depicts a typical L-shaped search template for unilateral simulation path simulation that started in the lower-left corner. The right picture depicts the conditioning with hard data. The green nodes represent hard data, the white nodes are the simulated nodes before the conditioning, and the pink nodes represent the conditioned simulated nodes (Mariethoz and Caers, 2014). 18

Figure 2.16. An example of connectivity function in x direction of TI compared to the MPS realisations. Similar connectivity functions indicates the similarity of the patterns between the TI and the MPS realisations (Pourfard, Abdollahifard, Faez, Motamedi, and Hosseinian, 2017)....19

Figure 2.17. Left picture shows the example of E-type model for conditional MPS simulation with the straight line as the hard data (Tahmasebi, Sahimi, and Caers, 2014), and the right picture shows the example of conditional variance model for conditional MPS simulation with circles as hard data (Pourfard et al., 2017). A good conditional MPS simulation would show similar facies around hard data (left picture, shown in red colour) and low values of variance around the hard data (right picture, shown in blue colour). 21

Figure 2.18. Example of similarity between scree-plot obtained from PCA and profile log-likelihood from MLE (Zhu and Ghodsi, 2006). 22

Figure 2.19. An example of a pyramid of 3 subresolutions from a single TI (Tan et al., 2014). ..23

Figure 2.20. An example of kernel k-means clustering (Honarkhah and Caers, 2010). 24

Figure 2.21. An example of TI and MDS space. The x-axis represents the largest eigenvalue, and the y-axis represents the second largest eigenvalue (Honarkhah and Caers, 2010). 25

Figure 2.22. The flowchart in using process-based simulation model in MPS simulation in this study. 27

Figure 3.1. Final bathymetry of the fluvial-dominated delta simulation output from Delft3D, shown in a vertical section. Each line in the vertical section represents time-slice in one time deposition. Note that the displayed data is the original simulation output data, not the post-processed data (van der Vegt, 2018). 28

Figure 3.2. The Delft3D simulation model in JewelSuite. The whole grid consists of variables including inactive cells that is also needed in the MPS simulation. Display without inactive cells were shown in middle and lower pictures to clearly show the sediment bodies. Each k-layer time-slice represents a period of deposition in a period of the order of a century to millennial scale, shown in a flat 2D layer. 31

Figure 3.3. Facies display of the architectural elements (facies) variable. Upper picture depicts Case A: 240th k-layer with high repetition, lower picture depicts Case B: 100th k-layer with low repetition. 32

Figure 3.4. Facies and its subenvironments of Case A and Case B. The subenvironments act as the stationary zonations for the zonation approach. 33

Figure 3.5. Dimension extraction from the Delft3D simulation model. There are three dimensions acquired from the channel accretion and the mouth bar facies (channel width, lobe width, and lobe length) which serve as the dimensions in the new TI construction. 34

Figure 3.6. The 240th k-layer for each of new TI for delta top and delta front subenvironment. ..35

Figure 3.7. The azimuth map used in the Case A and Case B. The zones will apply clockwise rotation to the patterns found on the zones. 35

Figure 3.8. The 100th k-layer for each of new TI for delta top and delta front subenvironment. ..36

Figure 3.9. The diameter, net-to-gross, and sorting variable of Case A and Case B....37

Figure 3.10. TI display of the 240th k-layer which shows low repetition in the fluvial patterns and its control map based on its subenvironment....38

Figure 3.11. TI display of the 100th k-layer which shows low repetition in the fluvial patterns.....39

Figure 3.12. Hard data placement for Case A and Case B. In sparse hard data distribution, the placement of the hard data took place in the distal area and the sandy deposit's facies that offers advantage in evaluating the unilateral simulation path. 40

Figure 4.1. Case A and its histogram for its facies. Case A has high repetition in its sandy deposit's facies, which are channel accretion and mouth bar facies. 42

Figure 4.2. Case B and its histogram for its facies. Case B has low repetition in its sandy deposit's facies, which are channel accretion and mouth bar facies. 42

Figure 4.3. Unconditional simulation results from Case A and its facies' histogram using Method I....43

Figure 4.4. Unconditional simulation results from Case A and its facies' histogram using Method II....44

Figure 4.5. Unconditional simulation results from Case A and its facies' histogram using Method III....45

Figure 4.6. Unconditional simulation results from Case A and its facies' histogram using Method IV. 46

Figure 4.7. Unconditional simulation results from Case B and its facies' histogram using Method I....47

Figure 4.8. Unconditional simulation results from Case B and its facies' histogram using Method II....48

Figure 4.9. Unconditional simulation results from Case B and its facies' histogram using Method III....49

Figure 4.10. Unconditional simulation results from Case B and its facies' histogram using Method IV. 50

Figure 4.11. Connectivity function of Method I, Method II, Method III, and Method IV in Case A. The similarity of the connectivity function reflects good patterns' reproduction between realisations and TI. Only 10 realisations are displayed in the plot to show better visual representation.....52

Figure 4.12. Connectivity function of Method I, Method II, Method III, and Method IV in Case B. The similarity of the connectivity function reflects good patterns' reproduction between realisations and TI. Only 10 realisations are displayed in the plot to show better visual representation.....53

Figure 4.13. Conditional simulation results from Case A using Method I. 55

Figure 4.14. Conditional simulation results from Case A using Method II. 56

Figure 4.15. Conditional simulation results from Case A using Method IV.....57

Figure 4.16. Conditional simulation results from Case B using Method III. 58

Figure 4.17. Conditional simulation results from Case B using Method IV.....59

Figure 4.18. Connectivity function of Method I, Method II, and Method IV in Case A with dense hard data. The similarity of the connectivity function reflects good patterns' reproduction between realisations and TI. Only 10 realisations are displayed in the plot to show better visual representation. 60

Figure 4.19. Connectivity function of Method I, Method II, and Method IV in Case A with sparse hard data. The similarity of the connectivity function reflects good patterns' reproduction between realisations and TI. Only 10 realisations are displayed in the plot to show better visual representation. 61

Figure 4.20. Connectivity function of Method III and Method IV in Case B with dense hard data. The similarity of the connectivity function reflects good patterns' reproduction between realisations and TI. Only 10 realisations are displayed in the plot to show better visual representation.....62

Figure 4.21. Connectivity function of Method III and Method IV in Case B with sparse hard data. The similarity of the connectivity function reflects good patterns' reproduction between realisations and TI. Only 10 realisations are displayed in the plot to show better visual representation.....62

Figure 4.22. E-type and conditional variance models of Method I for conditional MPS simulations in Case A. The channels accretion facies in the E-type model was shown by the value of 1. 63

Figure 4.23. E-type and conditional variance models of Method II for conditional MPS simulations in Case A. The channels accretion facies in the E-type model was shown by the value of 1. 64

Figure 4.24. E-type and conditional variance models of Method IV for conditional MPS simulations in Case A. The channels accretion facies in the E-type model was shown by the value of 1. 65

Figure 4.25. E-type and conditional variance models of Method III for conditional MPS simulations in Case B. The channels accretion facies in the E-type model was shown by the value of 1. 66

Figure 4.26. E-type and conditional variance models of Method IV for conditional MPS simulations in Case B. The channels accretion facies in the E-type model was shown by the value of 1. 67

Figure 4.27. Left picture shows scree-plot for case A with eigenvalue in normal scale, and the right picture shows scree-plot for Case A with logarithmic scale for the eigenvalues. 68

Figure 4.28. Left picture shows scree-plot for case B with eigenvalue in normal scale, and the right picture shows scree-plot for Case B with logarithmic scale for the eigenvalues. 68

Figure 4.29. MDS plot of Case A with dense hard data. The left plot depicts the x-y plot, and the right plot depicts the x-y-z plot. 69

Figure 4.30. MDS plot of Case A with sparse hard data. The left plot depicts the x-y plot, and the right plot depicts the x-y-z plot. 69

Figure 4.31. MDS plot of Case B with dense hard data. The left plot depicts the x-y plot, and the right plot depicts the x-y-z plot. 70

Figure 4.32. MDS plot of Case B with sparse hard data. The left plot depicts the x-y plot, and the right plot depicts the x-y-z plot. 70

Figure 5.1. An example of comparation between Method II (zonation approach with unilateral simulation path) and Method IV (control map approach with unilateral simulation path). Method IV has rougher edges between the boundaries of the facies.....75

Figure 5.2. An example of incapability of unilateral simulation path in conditional MPS simulation with Method IV (control map approach with unilateral simulation path) in Case B. The circle represents the discontinuity of the facies before it encountered the hard data.....77

Figure 5.3. Interpolation capability in reproducing new channel in a specific location with Method IV in Case B. Notice the arrow indicating the same length to the new channel in the realisation, E-type model and conditional variance model. 78

Figure 7.1 Unconditional simulation results from Case A using Method I. 89

Figure 7.2. Unconditional simulation results from Case A using Method II. 90

Figure 7.3. Unconditional simulation results from Case A using Method III. 90

Figure 7.4. Unconditional simulation results from Case A using Method IV. 91

Figure 7.5. Unconditional simulation results from Case B using Method I. 91

Figure 7.6. Unconditional simulation results from Case B using Method II. 92

Figure 7.7. Unconditional simulation results from Case B using Method III. 92

Figure 7.8. Unconditional simulation results from Case B using Method IV. 93

Figure 7.9. Conditional simulation results from Case A using Method I for dense and sparse hard data.....94

Figure 7.10. Conditional simulation results from Case A using Method II for dense and sparse hard data.....95

Figure 7.11. Conditional simulation results from Case A using Method IV for dense and sparse hard data.....96

Figure 7.12. Conditional simulation results from Case B using Method III for dense and sparse hard data.....97

Figure 7.13. Conditional simulation results from Case A using Method IV for dense and sparse hard data.....98

List of Tables

Table 4.1. ANODI scores for Case A with dense hard data. 71

Table 4.2. ANODI scores for Case A with sparse hard data. 71

Table 4.3. ANODI scores for Case B with dense hard data. 72

Table 4.4. ANODI scores for Case B with sparse hard data 72

List of Abbreviations

2D Two Dimensions

3D Three Dimensions

ANODI Analysis of Distance

ASM Automatic Segmentation Method

CCDF Conditional Cumulative Distribution Function

CHP Cluster-Based Histograms of Patterns

CPU Central Processing Unit

GEO-EAS Geostatistical Environmental Assessment Software

GSLIB Geostatistical Software Library

IMPALA Improved Parallel Multiple-point Algorithm Using a List Approach

JS Jensen-Shannon

m Metres

mm Millimetres

MDS Multidimensional Scaling

MLE Maximum Likelihood Estimate

MPH Multiple-Point Histograms

MPS Multiple-Point Geostatistics

NETCDF4 Network Common Data Form version 4.0

PCA Principal Component Analysis

PDF Probability Distribution Function

RAM Random Access Memory

SEDSIM Sedimentary Sequence Simulation

SNESIM Single Normal Equation Simulation

SSM Spatial-Similarity Method

TI Training Image

1

Introduction

Reservoir characterisation is essential in the field of earth sciences. One of the most challenging problems in reservoir characterisation is the limitation of the subsurface information, which is required to construct accurate geological models. The subsurface condition is often heterogeneous and complex, combined with different subsurface information coming from various sources at different scales and detail, the uncertainty in the modelling process is unavoidable. Geostatistics, a part of statistics that focuses on spatial or spatiotemporal data, provides the idea of estimating the correlations between the spatially close subsurface property values to those unsampled locations. The estimation is then used to capture the model uncertainty with the stochastic simulation of the reservoir properties, provided by the alternative, equiprobable solutions (Michael J. Pyrcz and Deutsch, 2014). The produced reservoir model is presented in a grid-based mathematical representation of the reservoir, which is comprised of different data from various sources, such as seismic, well logs, core, dynamic and analogue data.

The advances of the computer-based technology and computational power compared to the past times makes possible of the complex calculations which are not practical in the previous times. These advances in technology create new and improved geostatistical reservoir characterisation methods that would improve the realism of the geostatistical numerical models for complex geologic features and leads to enhanced subsurface prediction. Some of the most advanced geostatistical techniques used in the study are presented in the following sections, which are the process-based simulation and multiple-point geostatistics (MPS).

1.1 Process-based and Multiple-point Geostatistics (MPS) method in facies modelling

In the process of reservoir modelling, facies modelling is one of the essential procedures in the whole process. Each of the facies defines the geometry of the reservoir rocks and the distribution of their petrophysical properties, such as porosity and permeability. In this case, geostatistics method plays a significant role in controlling the distribution of the facies in the model simulation by estimating the unsampled locations and produce it as a simulation model.

Some of the latest advances in the geostatistical method used in the reservoir modelling are process-based method modelling and multiple-point geostatistics (MPS) (Pyrcz and Deutsch, 2014; Mariethoz and Lefebvre, 2014).

Process-based method forward stratigraphic modelling provides an excellent way to model complex subsurface geology because it simulates the geological process mathematically, and the genesis of geologic formations over time (Michael et al., 2010). The facies properties generated by the process-based simulation model were defined by the initial and the boundary conditions, with the geologic processes associated within the modelling software. Some of the purposes of constructing the process-based models are useful in helping developing theory and the interaction of processes, the development of conceptual models, and composing reservoir framework in large-scale modelling (Michael J. Pyrcz and Deutsch, 2014).

In spite of the advantages in modelling with process-based methods, Miller et al. (2008) have recognised significant challenges in process-based simulation models, one of them is the incapability to condition to subsurface data. The problem in conditioning the data, for instance in facies properties, can be addressed by using an alternative method named multiple-point geostatistics (MPS) in modelling the subsurface since its introduction in 1993 by Guardiano and Srivastava.

MPS considers the relationship between multiple data points that is different from the conventional geostatistical methods that are commonly limited to using a linear relationship between data, represented by variogram models (Guardiano and Srivastava, 1993). Instead of using a variogram, it introduces the use of a training image (TI), which considers the multiple-point numerical conceptual representation of the variables deemed to be present in the modelled reservoir (Strebelle and Chevron, 2012).

TI represents a grid-based numerical representation that includes the information of the reservoir in a two or three-dimensional grids. The properties in the TI grid can be facies properties, porosity, grain size, or other reservoir properties. It is under the assumption that the TI has the same multiple-point statistics and contains the same complexity of the geological features of the area of interest, or in other words, assumed stationary (Michael J. Pyrcz and Deutsch, 2014). The assumption of stationarity means that the area considered has the same statistical properties throughout, while in reality, there is no stationary data, termed nonstationary, where the properties are always changing following the processes applied.

The TI can be constructed from various techniques such as object-based methods, process-based method, or from available training image databases (Michael J. Pyrcz and Deutsch, 2014). Those methods generated various variables, including facies variable which the facies pattern will be used as the input. With using process-based simulation model as TI, MPS will infer and reproduce facies' patterns in the TI, honour both hard and soft data, and deliver results within low computational costs (Journel, 2003; Mariethoz and Caers, 2014; Strebelle and Chevron, 2012). It directly uses empirical multivariate distributions deduced from training images, so any complex architecture of geological facies is dependent to the geomodeller's knowledge of the depositional environment in building the training images (Boisvert, Pyrcz, and Deutsch, 2007). In the process, MPS can accommodate the nonstationarity within its TI by several means that will be discussed in the following sections. Therefore, the training-image based approach can use the process-based simulation model as the TI, hence can handle the complexity, nonstationarity, and conditioning matter that pose the significant challenges.

1.2 Motivation and objective of the study

Over the past decade, most research in MPS has emphasized on new algorithms for improving efficiency in dealing pattern matching, searching, and synthesis (Mariethoz and Caers, 2014;

Mariethoz and Lefebvre, 2014), but there are still issues remain for the workflow to be widely used in geosciences. Furthermore, the solution for using nonstationary TI such as process-based simulation model in MPS are still an issue because the workflow is always different for specific cases. Very little published works available in applicating nonstationary TI in MPS. Some of the most notable and recent ones did not address the workflow and best practices along and the data-to-model evaluation applicable with industry or academic (Mariethoz and Kelly, 2011; Mariethoz, Renard, and Straubhaar, 2010; Michael et al., 2010; Strebelle, 2002).

Based on the background described previously, there are some questions that are addressed in combining the process-based simulation models as training images for MPS simulation:

- How does the nonstationary data need to be prepared to be suitable for MPS?
- How to optimise the workflow in using process-based simulation model as TI in unconditional MPS simulation?
- What is the conditioning capability in MPS simulation with using process-based simulation model as TI?

Previous successful attempts to model nonstationarity in MPS simulation has used zonation (Honarkhah and Caers, 2012) and control maps, also called auxiliary variables (Chugunova and Hu, 2008). Some of the problems addressed in the combining process were the nonstationarity in the process-based model which can be challenging to reproduce location-specific features and trend (Hoffimann, Scheidt, Barfod, and Caers, 2017; Michael et al., 2010).

MPS in facies modelling is still a relatively new topic, and recently is rapidly growing in popularity by providing the modeller with the flexibility of modelling complex geometries which still have a long academic history ahead. The use of MPS also being adapted in modern commercial and non-commercial reservoir modelling software such as BHGE's JewelSuite, Schlumberger's Petrel, Halliburton's DecisionSpace Geosciences, and Stanford University's SGeMS. The extensive usage of MPS motivates the study to discuss the MPS even further by improving the previous works and making new approaches by using nonstationary TI in a particular case, so we can establish optimised workflow in MPS simulation using nonstationary TI with most general use of MPS algorithm by most geoscientists.

This study focuses on deltaic reservoir in the application of MPS in with nonstationary TI. There are three main types of deltaic system: fluvial-dominated, wave-dominated, and tidal-dominated delta (Orton and Reading, 1993). Through the years, science has approached the understanding of deltaic environment sedimentation processes has been based on field data. The recent addition of process-based forward stratigraphic modelling can serve further information on understanding the sedimentary processes within the deltaic environment. We used a fluvial-dominated reservoir model generated from process-based forward stratigraphic modelling which contains nonstationarity in its fluvial patterns.

By considering the underlying questions in using process-based simulation models on MPS simulation, the primary objective of the study is to determine an optimised methodology that allows the use of nonstationary process-based simulation model for TI input with MPS simulation in the fluvial-dominated delta. The method should be capable of measuring the capability of generating unconditional and conditional MPS simulation model that is based on the process-based simulation model.

The structure of this study is summarily described in the following section. Methodology which contains detailed explanation in the stochastic geostatistical method of this study is firstly described in Chapter 2. Then, followed by the data that encompasses the preparation of the data, and the selection of hard data for conditioning in Chapter 3. In Chapter 4, the results from the unconditional and conditional MPS simulations are presented, including the evaluation of the results. Chapter 5 discusses the results from previous chapter; and lastly, Chapter 6 gives the conclusions and future recommendations for the improvement of the topic.

1.3 The scope of the study

This study focuses on the restrictions and boundaries of the nonstationarity in the fluvial-dominated delta process-based model which can be used in the MPS method. These two aspects are compared by using visual inspection and data-to-model statistical evaluation to ensure that the realised MPS simulation model represents a proper realisation from the process-based model it is based on.

With the nature of the MPS simulation, the main idea of the simulation is not to create a copy of the process-based simulation model, but to generate stochastic simulation model realisations that mimic the patterns and geostatistical properties of the TI. Similar patterns are assumed to resemble similar geostatistical properties for the compared models.

This study used MPS' IMPALA algorithm in JewelSuite software, an improvement of the SNESIM algorithm in the search tree component. Both algorithms considered same in the basis of nodes' simulation. SNESIM is one of the most popular MPS algorithms and being used in most of commercial and non-commercial reservoir modelling software available in the market. The other softwares used in the study are MATLAB R2016b and SGeMS version 2.1.

Also, this study is limited to the usage of 2D facies model in both training image and realisations, which reasons are described in the section 3.2.

Since this study is based on the numerically simulated physical processes of the process-based model in the work of van der Vegt in 2018, so several pre-defined parameters of the delta model are addressed, such as the accommodation space, the hydrodynamic conditions, the sediment supply, and time. All pre-defined parameters are based on a detailed literature study, to emulate delta progradation onto shelves with low slopes. For more detailed parameters of the input data, see (van der Vegt, 2018).

2

Methodology

2.1 Multiple-point geostatistics (MPS)

Multiple-point geostatistics (MPS) is a recent branch of geostatistics that has been developed to characterise spatial continuity over more than two points (Mariethoz and Caers, 2014). It is an improvement proposed by Guardiano and Strivastava in 1993 to overcome the limitations of the conventional variogram-based simulation methods. This method would be able to provide correlations between three or more locations at a time (Figure 2.1).

MPS can benefit some improvements over the conventional variogram-based simulation methods because the latter cannot characterise curvilinear features and ordering relationships (Michael J. Pyrcz and Deutsch, 2014). Those curvilinear characters, such as sinuous fluvial channels, and higher order relationship are commonly present in the real world. To achieve that improvement over conventional variogram-based simulation methods, MPS makes use of training images (TI) to distinguish the spatial variability of the natural phenomena, then simulated in a stochastic way (Mariethoz and Caers, 2014). MPS has a capability in recreating complex geometries within geological features in inferring the statistics from the TI.

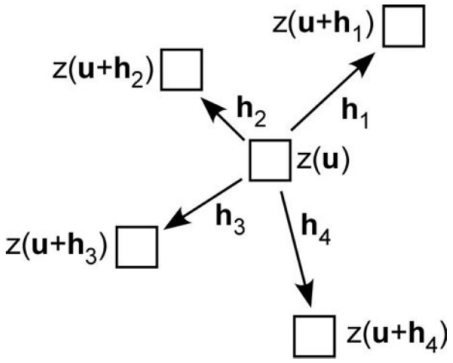

Figure 2.1. The illustration of a multiple-point event (Michael J. Pyrcz and Deutsch, 2014).

Many different MPS algorithms available and being developed. These algorithms have different methods to be applied to making a stochastic geostatistical simulation. Mariethoz and Caers wrote in 2014 about the classification of those MPS algorithms into two types: pixel-based and pattern-

based algorithm. The primary difference between of those two methods is the way algorithm visiting the training image grid and simulation grid nodes. The pixel-based method simulates the properties on the Cartesian grid by visiting the grid nodes one at a time (Saripally and Caers, 2008). On the other hand, the pattern-based method extracts the data event defined by the pattern template then scans through all the patterns in the training image to find the most similar one (Honarkhah and Caers, 2010).

2.1.1 MPS algorithms

The MPS simulation in this study will use the pixel-based method, which is IMPALA (Straubhaar et al., 2011) based on the SNESIM (Strebelle, 2002) algorithm. The next section will explain the following algorithms.

2.1.1.1 Single Normal Equation Simulation (SNESIM) algorithm

Single Normal Equation Simulation (SNESIM) was introduced in 2002 by Strabelle, with the improvement in the TI events storage in a search tree data structure instead of searching the TI each every time for each conditioning data template, resulting in a much-decreased duration in simulation (Strebelle, 2002). Fast retrieval of required conditional probabilities is now possible with using the search tree data structure, with the one-time scanning of the TI.

The name itself came from the use of a single normal equation in the process of property probability modelling, Bayes relation defining a conditional probability. With SNESIM, the TI is scanned by utilising a pre-defined search template for each pattern, searches for replicates of the pattern and then fetches the corresponding histogram of the central value (Figure 2.2).

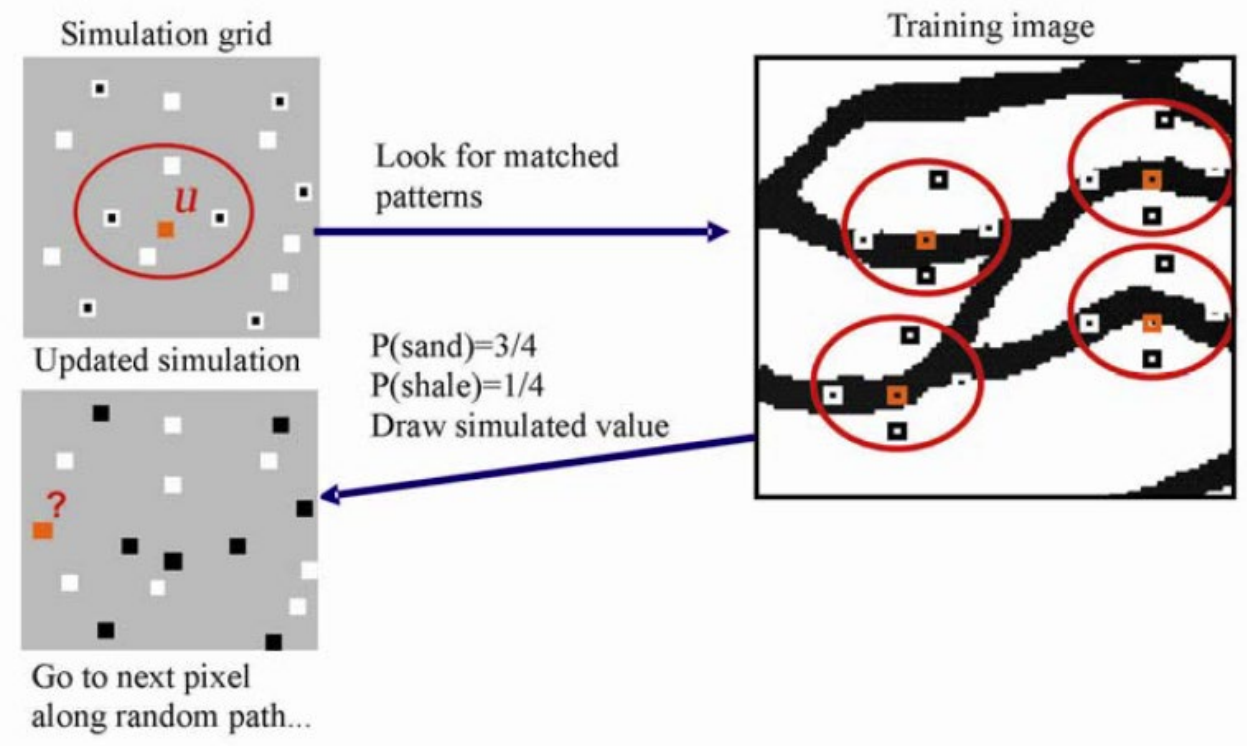

Figure 2.2. An example of SNESIM algorithm in simulating a cell (Zhang, 2008).

For instance, based on the sand/no-sand facies in Figure 2.2, if a data patterns in the simulation grid within the search template is found ten times in the TI, with the central node is being a sand facies seven times, then the conditional sand probability is 0.7. After that, SNESIM draws a simulated value back to the simulation grid, with the sand facies probability of the central node with the value of 0.7. The data simulated is stored in the search tree.

Nonetheless, several drawbacks occur in the SNESIM algorithm. The search tree only store data patterns that is present in the TI. When the data pattern is not repeated often enough in the TI, especially in the complex TI and large search templates, the algorithm will drop one datum of that event, generally the datum that is the farthest from the centre datum and repeats the pattern search process until the pattern matches (Strebelle, 2002). This will potentially lead to a removal of many data in the search template, reducing the information which follows into a poor reproduction of the TI patterns.

One of the solutions to this problem is to use a pattern-rich TI, but the memory required for the simulation will be more significant because it is based on the number of unique events present in the TI. For example, one MPS simulation using very large and rich TIs will lead to several gigabytes of Random-Access Memory (RAM) of the computer. Alternatively, several methods have been developed for making the process more efficient, and one of the methods is explained in the following section.

2.1.1.2 Improved Parallel Multiple-point Algorithm Using a List Approach (IMPALA) algorithm

A further improvement to SNESIM algorithm is Improved Parallel Multiple-point Algorithm Using a List Approach (IMPALA) algorithm, developed by Straubhaar et al. in 2011. They proposed to replace the tree, which is a construction of the search tree by a list. This IMPALA list structure requires much less RAM which is a significant problem in SNESIM in dealing up with complex and rich TI.

It has three advantages: (1) it allows for the use of larger templates, (2) the list structure is efficient, can be extended to include additional information, (3) allows one to parallelise the part of the algorithm in which the conditional probability density function is computed. By decreasing the RAM consumption in the process, the higher Central Processing Unit (CPU) of the computer is costed. Despite the memory advantages and parallelisation in the process, IMPALA behaves precisely similar to the SNESIM algorithm.

Ephesia Consult implements IMPALA algorithm that is used in this study in the JewelSuite 2018.1 software from Baker Hughes, a GE company.

2.1.2 Training image (TI) and its stationarity

Training image (TI) by definition is a two or three-dimensional numerical grids that quantify the heterogeneity from the properties of the reservoir (Mariethoz and Caers, 2014). The TI acts as the representative of the geological concept of the area of interest, and the statistics required by the stochastic algorithm can be inferred from the TI (Journel, 2003). It is also able to provide the constraints of the spatial variability within the patterns in the TI, and also provide sufficient freedom to produce the variability in each of the realisations (Mariethoz and Caers, 2014). In the MPS simulations, the idea is not to reproduce almost identical patterns in the TI, but to generate similar features by inferring to the TI, while keeping an aspect of randomisation to the simulation.

Like any other geostatistical approaches, MPS assumes the stationarity to simulate the reservoir characterisation, and TI as the input have to meet this requirement of stationarity, or else the calculation of the geostatistics would not be achievable. Mariethoz and Caers in 2014 explain stationarity of a process in a spatial context as the assumption of the similarity of the statistical variation of the entire spatial domain. It means that if in a specific location domain lies a statistic property, the statistics, such as mean and variance, will be similar to any other portion of the domain. An ideal TI that meets the stationarity requirement should have patterns that is plausibly homogeneous with enough repetition all over the TI grid (Maharaja, 2008), or else, considered as nonstationary TI. Figure 2.3 illustrates nonstationary and stationary TI with fluvial patterns. In nonstationary TI, we can see that the channels are nonhomogeneous and have varying patterns throughout the grid.

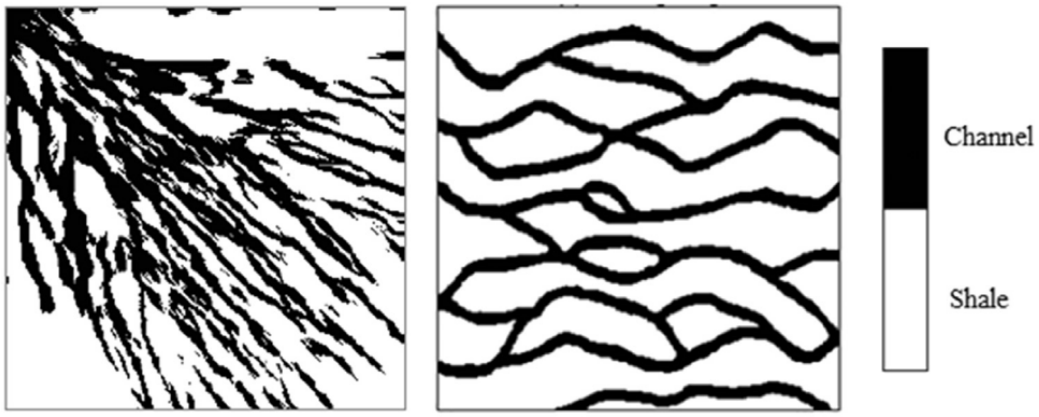

Figure 2.3. An example of TIs in fluvial environment. Left picture shows nonstationary TI, and right picture shows stationary TI. In stationary TI, the patterns shows enough repetition compared to the nonstationary TI (Arpat and Caers, 2007).

Despite the fact of the assumption of the stationarity in the TI for MPS simulation, most of the physical processes that happened in the world are nonstationary. Stationarity in MPS is a decision of the geomodeler, and the geomodeler has to choose the TI that has enough data for getting sufficient geostatistical inference without overfitting the local data and underestimating model uncertainty (Michael J. Pyrcz and Deutsch, 2014). Also, the data in TI has to be pooled close enough with similar properties and has enough repetitions in the pattern, so it may show significant reservoir heterogeneity and not overestimating the model uncertainty (Zhang, Bombarde, Strebelle, and Oatney, 2006).

2.1.3 Source of TI

The construction of the TI is the subjectivity of the geomodeler to incorporate the representing statistics in the desired reservoir model. The TI has to describe natural processes which often complex and random, and also can be used in the MPS simulation. Establishing TI has the same manner with establishing conceptual geological model; it must be able to represent the actual reservoir model and be specific to the case that is being modelled.

There are several sources to obtain the suitable TI for the simulation, and one of the approaches integrates the available model from another methods.

2.1.3.1 TI from analogue data

A direct approach to construct TI is by using the data directly as patterns. The data can be obtained from idealised conceptual geological models from literature, analogue photos (Ringrose and Bentley, 2015), satellite images (Feng and Wu, 2016) (Figure 2.4), or tomographic images (Lochbühler, Pirot, Straubhaar, and Linde, 2014). Those data are usually converted and processed into a simplified model of a reservoir that shows the key elements of the corresponding environment.

The geomodeller can utilise built-in graphical module in commercial reservoir modelling software such as JewelSuite and Petrel to make the representing patterns manually based on the analogue data. Another method would be drawing the patterns using commercial and non-commercial graphical software such as Photoshop and GIMP, then convert it into numerical representation file. An improvement also made by Fadlelmula F., Killough, and Fraim in 2016 by making a software called TiConverter to easily convert raster image into numerical representations. The patterns derived from the analogue data contains the representative patterns and will be used in simulations.

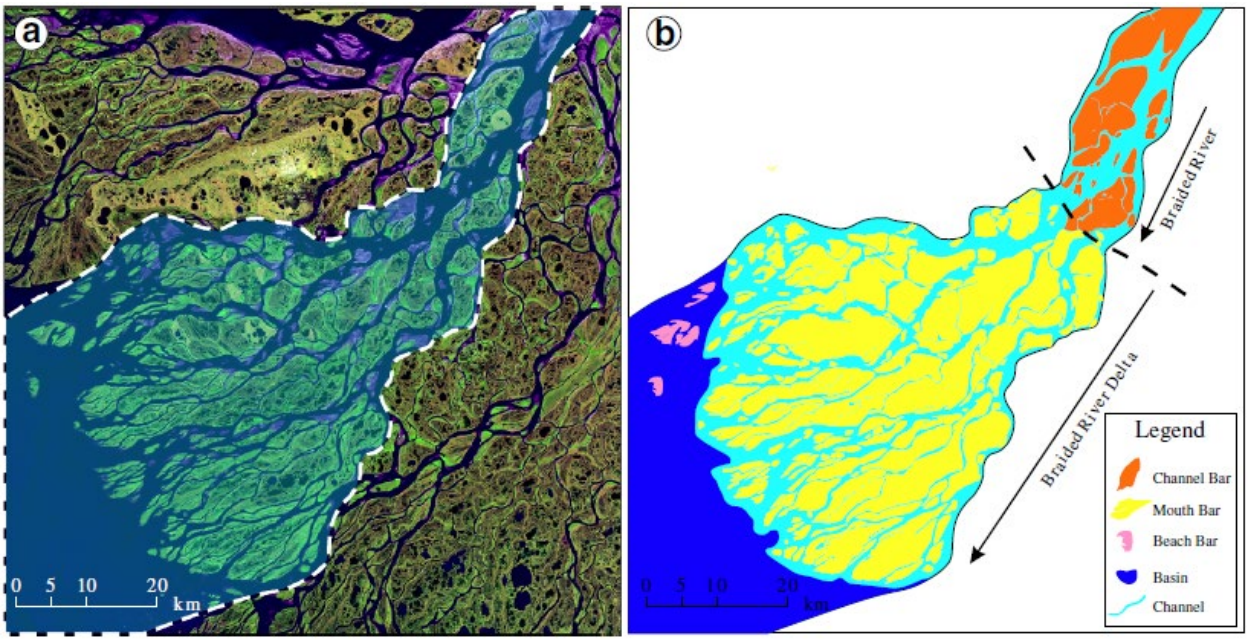

Figure 2.4. An example of constructing TI from Lena River Delta's satellite image (Feng and Wu, 2016).

2.1.3.2 TI from databases

TI databases has been created as deterministic methods to provide a ready-to-use TI in MPS simulation. The databases comprise of architectural features like geometry, spatial distribution, and specific patterns combined with variety of filters which enables the user to easily construct the desired TI. Several notable examples of the TI databases are:

- FAKTS (Colombera, Felletti, Mountney, and McCaffrey, 2012). The database provides fluvial reservoir TI that includes fluvial architectural data obtained from literature- and field-derived modern rivers and ancient successions.

- Carbdb (Jung and Aigner, 2012). Presenting a hierarchical classification of carbonate bodies that includes carbonate systems from outcrops, the subsurface, and modern environments. The classification comprised of depositional time, depositional system, depositional zone, depositional shape, depositional element, and facies.
- Database for fluvial and deepwater reservoirs by M. J. Pyrcz, Boisvert, and Deutsch (2008). The database presents a program for creating object-based TI for fluvial and deepwater environment, which includes TI from idealised surface-based, event-based, and object-based models such as FLUVSIM (Deutsch and Tran, 2002).

2.1.3.3 TI from object-based methods

Object-based methods populates the grids with predefined objects in 2D or 3D using specific algorithms. The objects' shape are generated with using non-iterative, unconditional Boolean simulation (Maharaja, 2008) (Figure 2.5). One of most notable object-based methods software available is TiGenerator (Maharaja, 2008). In using TiGenerator, the geomodeler could decide on the shape of the object by setting the geometry, and the algorithm would set the rules between the interacting simulated objects.

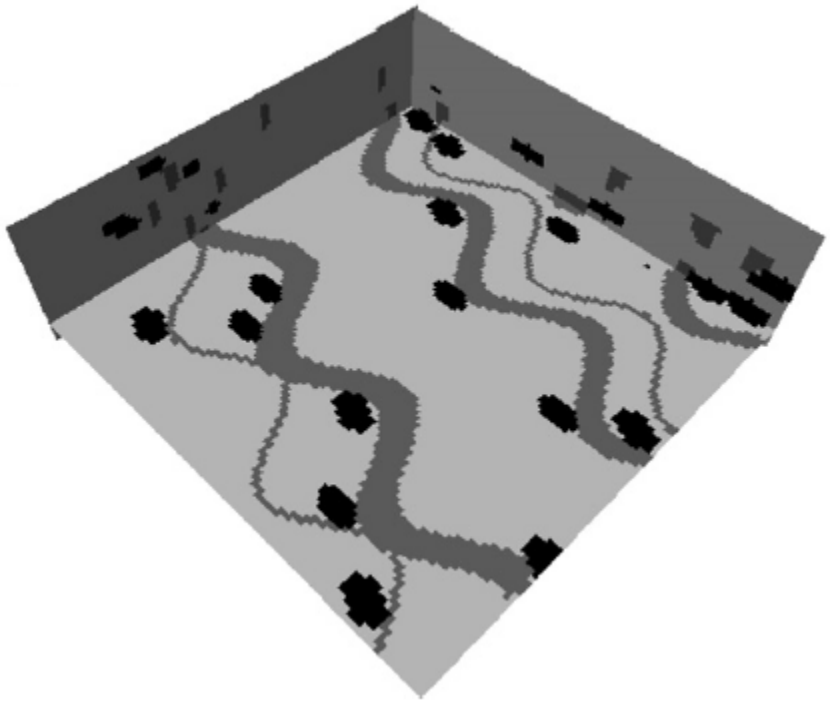

Figure 2.5. An example of object-based method in generating TI using TiGenerator. The patterns represent channels with crevasse-splay (Maharaja, 2008).

Main advantages of using object-based method is the fast and simple approach of making the patterns. The graphical user interface has made it easy for the geomodeler to set the constraints by setting and specifying the parameters. While some of the drawbacks are the lack of flexibility and oversimplification in modelling complex structures (Mariethoz and Caers, 2014).

2.1.3.4 TI from process-based simulation models

Process-based simulation models can serve as a working TI because the process-based simulation models are made with the idea of numerically forward simulate the processes of the sedimentation (Mariethoz and Caers, 2014). Technically, process-based simulation model serves as a conceptual geological model in geological modelling workflow. The use of process-based simulation model as TI can fine tune the model by conditioning it through MPS simulation, although the workflow of applicating process-based simulation model is not that simple because of the nonstationarity.

The explanation of the process-based simulation model and the application in MPS workflow will be discussed in detail in the next section.

2.2 Process-based modelling

Process-based modelling is a numerical forward-modelling method that integrates geological information controlled by geological rules (Michael J. Pyrcz and Deutsch, 2014). The idea of forward-modelling of the reservoir is to construct the layers of the model sequentially based on the chronological geologic processes so that it mimics how the sedimentation processes in the real-world situation (Michael J. Pyrcz and Deutsch, 2014). Many of the different process-based algorithms have been developed, such as DIONISOS (Granjeon and Joseph, 1999), (SEDSIM (Tetzlaff, 1990), and Delft3D (Lesser, Roelvink, van Kester, and Stelling, 2004).

With using a predefined description of underlying physical processes, several modules of the modelling method which describe different processes (Dastgheib, Roelvink, and Wang, 2008) that ended up with a modelling result in high detail (Figure 2.6). In making a realistic process-based simulation model that captures the complex heterogeneities within the model, the simulation needs extensive characterisations of paleo-conditions that occurred during the actual reservoir formation (Michael J. Pyrcz and Deutsch, 2014). The process-based method simulation can only set the initial conditions and boundary conditions of the model, alas the forward evolution of the simulation is out of control of the modeller.

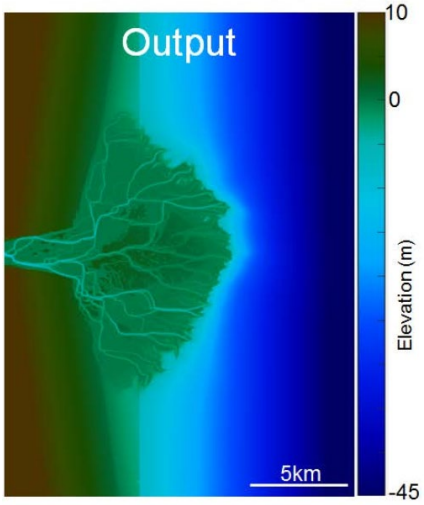

Figure 2.6. The process-based simulation model of Delft3D software for deltaic environment (van der Vegt, 2018).

Miller et al. (2008) have recognised five significant challenges in process-based modelling, including: (1) accurate quantification of geologic processes, (2) complex and unknown input parameters with unknown initial conditions, (3) potential for non-unique solutions, (4) computational effort, and (5) incapability to condition to subsurface data. The latter is one of the most critical issues in using the process-based model in reservoir characterisation. Reservoir modelling in reproducing well and seismic data is essential, and its failure to condition makes the typical process-based workflow in including the heavy modifications on the input to match the wells and seismic observation.

The nonstationarity in the statistical variation of the process-based simulation is also expected in the model. The statistics within the model vary with location and time. For example, in Figure 2.6, the transitional patterns of the facies are developing through the slope, following the boundaries and condition in the functions defined. The statistics property of the facies developing in the proximal part is different compared to those emerging in the distal part of the shelf. Preparing nonstationary TI such as process-based simulation model is different than stationary TI. There are two different ways to prepare the TI that is going to be explained in detail in the next section: (1) make a new separate TI within the assumed stationary zonations, and (2) use the process-based simulation model directly.

2.3 Modelling nonstationarity in MPS

Intricate patterns in the area of interest with high-order nonstationarity cannot be described by regular MPS algorithm. The trends are usually present with complicated patterns with a wide range of different scales. The replication of the patterns is more severe in more complex and high-order nonstationarity. To handle the nonstationarity, several mechanisms can define the location for each pattern in the TI and simulation grid: zonation and control map approaches.

2.3.1 Zonation approach

Zonation, or region concept, split the entire nonstationary TI into zones that are considered stationary, and then simulating each zonation with different TI specific to the zone (Wu, Zhang, and Boucher, 2007). The considered stationary zonations are treated as they were separated TI, so a new stationary TI is needed to represent each stationary zone (Figure 2.7). The new TI is constructed with patterns and facies that are present in the previous zonations.

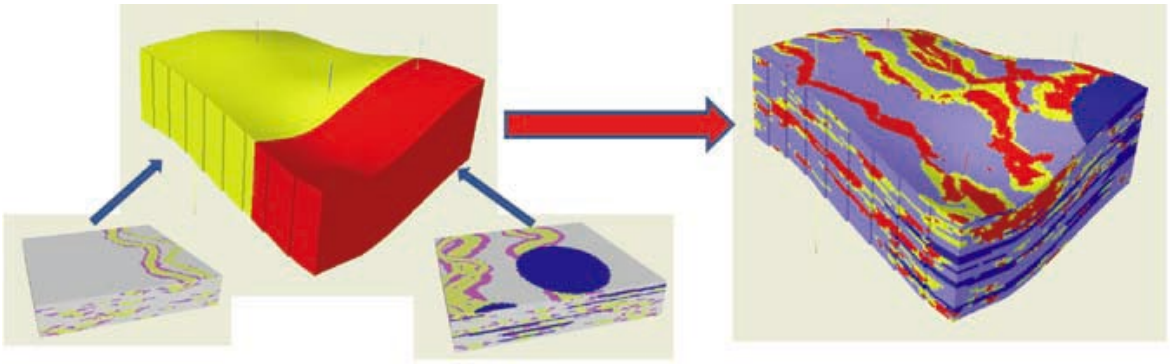

Figure 2.7. Example of the use of zonation concept in MPS modelling. Each zone (yellow and red) has its corresponding TI that shares the same channel facies (Daly and Caers, 2010).

By having different zonations with each zonation is considered stationary, the MPS simulation will take place independently in each zonation using the appropriate stationary TI. To achieve a good continuity between the boundaries, the TIs in interacting zonations must share the same facies (Wu et al., 2007). For example, in Figure 2.7, both TI for each zone share the same channel facies. The simulation will occur independently in each zonations, and the presence of the channel facies ensures the smooth transition between the boundaries, shown in the simulation result.

Deciding the stationarity is a matter of geomodeller's subjectivity to decide the structures differ significantly from one zonation to another. Also, the geomodeler has to be able to create the representing TI from each zonations. The process is often complicated following the order of non-stationarity and complexity of the TI.

Additional step to increase the similarity of the results to the TI is to apply rotation to the simulation. The use of rotation provides a means of mimicking the patterns, especially in zones with different orientation over the domain (Mariethoz and Caers, 2014).

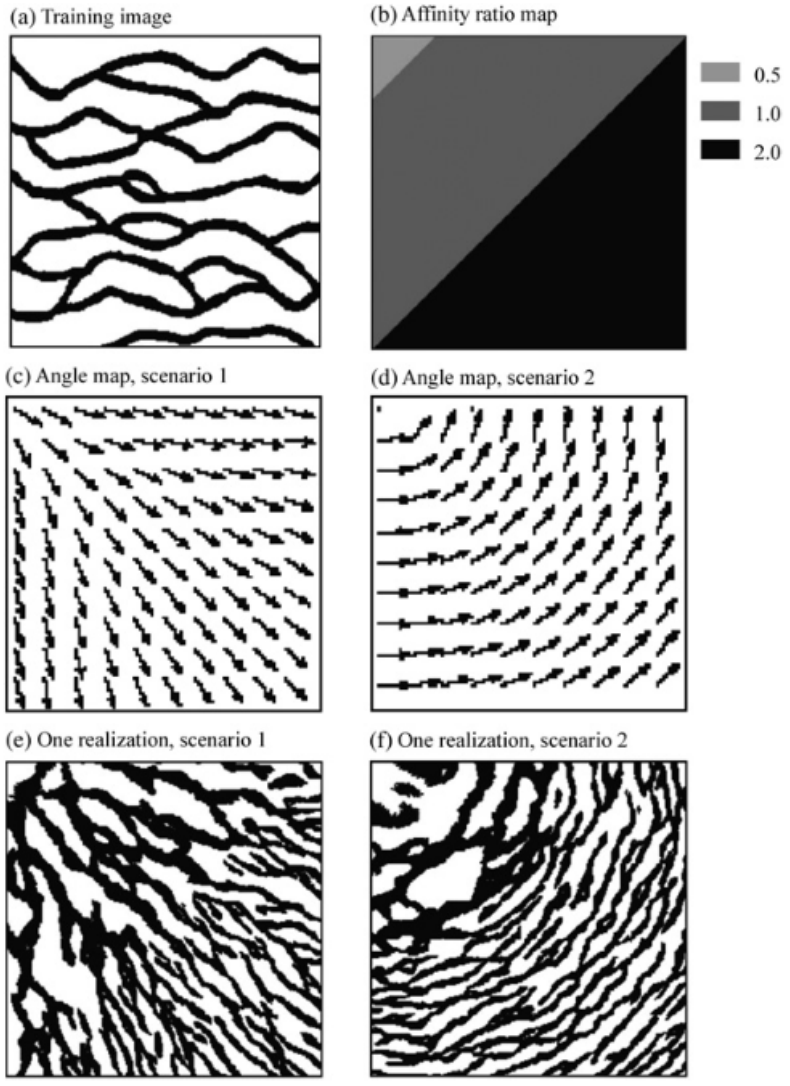

Figure 2.8. Example of rotation and affinity zones in SNESIM algorithm (Liu, 2006).

2.3.2 Control map approach

When the restriction of the zonation method is too rigid for the simulation case, control maps can be the solution to handle the nonstationarity. Often the patterns in the TI show a smooth transition which caused difficulty in determining the boundary of the stationarity. Hu and Chugunova in 2008 introduced the idea control maps, containing continuous variables that are defined in the TI and simulation grid (Figure 2.9 and Figure 2.10). Control maps will decide which patterns in the TI would occur in the simulation grid with defining its location.

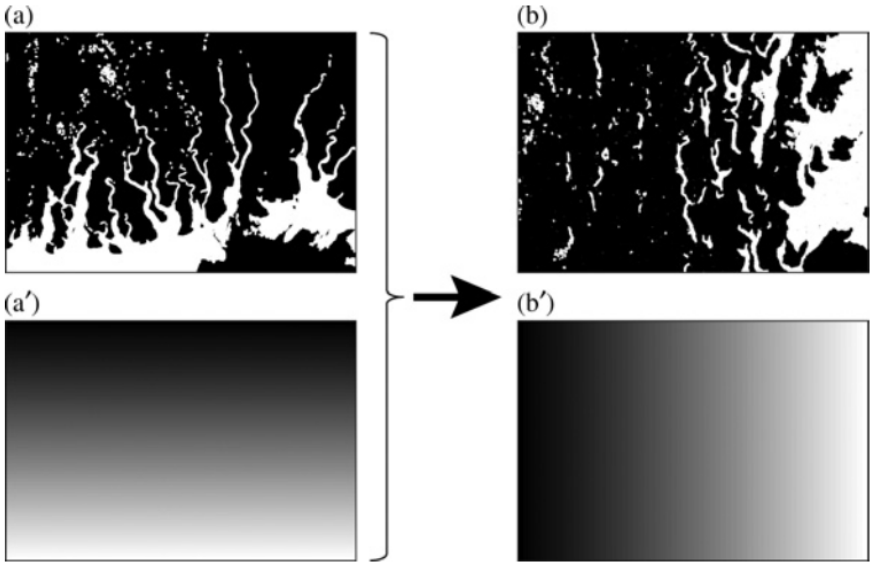

Figure 2.9. Example of control maps in nonstationary MPS modelling. (a) and (a') represent the TI and its control maps, where (b) and (b') represent the simulation grid and its control map. Notice the patterns' orientation between the TI grid and simulation grid (Mariethoz and Caers, 2014).

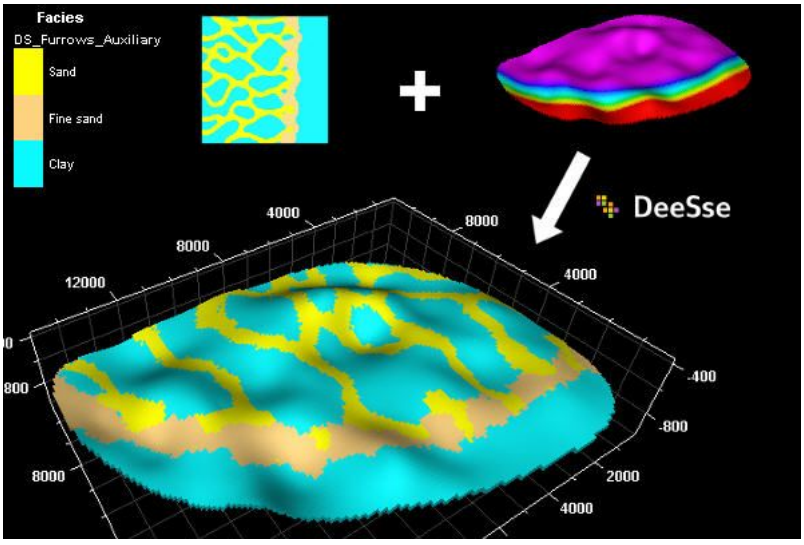

Figure 2.10. Another example of control maps in nonstationary MPS modelling. By using the control map, the geomodeler can control the occurrence of the patterns in the simulation grid. The value in the control map is similar for each stationary zonation (Ephesia Consult, 2017).

Each of the similar values of the control map is present in both the TI and simulation grid, so the joint probability of the simulation grid is inferred from the TI and its control map. Consequently, for every pair control map value in the simulation grid and the TI grid will also infer the similar patterns, so the control map describes the presence of a trend in both grids (Hu and Chugunova, 2008). For most of the cases, the control maps are based on the distance to the coastline or along the depositional gradient, while more complex control maps are needed for the more difficult cases. Riou, Höcker, and Hughes in 2015 suggested the use of the available data from the model, such as net-to-gross or grain size can be used to define the connection between the nonstationary patterns.

To make a usable control map, we can see the application from Figure 2.9 and Figure 2.10 where the control map defined the patterns in the TI in regards of the distance to coastline. The values of the control map can either be continuous for the whole grid like in Figure 2.9, or non-continuous as long as the same values are representing the assumed stationary zones like in the case of Figure 2.10.

The construction of control maps proves to be problematic for describing accurate nonstationarity in both TI and simulation grid. The control map has to be accurately translated the trend into a continuous variable which relies on the modeller geological knowledge of the TI, and often the process is deterministic (Mariethoz and Caers, 2014).

2.4 MPS simulation path type

In the MPS simulation, one of the most decisive factors is the way MPS simulation visit the grid nodes, called simulation path. The simulation path determines the final result of the simulation because each pattern observed in the TI are unique; hence appropriate visitation order is needed to deliver adequate results. Several paths are used in this study, that will be discussed in the following section.

2.4.1 Random simulation path

The most common MPS simulation simulates sequentially along a random simulation path. This means the visitation of all uninformed nodes in the TI and simulation grid are in random order (Mariethoz and Caers, 2014). The first nodes simulated show a tendency in the further away from its neighbour, resulting large-scaled features first; then as the close neighbour frequency increases, it starts to generate small-scale features (Figure 2.11).

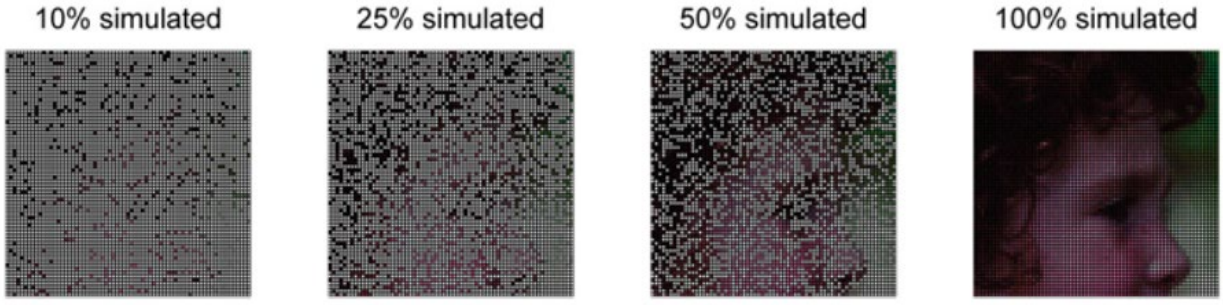

Figure 2.11. An illustration of the random simulation path in MPS simulation. From left to right depicts the percentage of cells simulated (Mariethoz and Caers, 2014).

In reproducing features with long-range continuity, such as fluvial channel patterns, the random simulation path would over-constrained the simulated nodes because of the relatively few multiple points in the early stage of the simulation, so they are weakly informed from the TI (Michael J. Pyrcz and Deutsch, 2014). The resulting outcomes would be the features are failing to connect within the random visitation of the cells and dismantling of the long-range features. Daly in 2005 suggested that the connectivity issues in reproducing long-range features with the random simulation path can be overcome by linearly visiting the nodes, called a unilateral simulation path.

2.4.2 Unilateral simulation path

In the unilateral simulation path, the grid nodes are visited in a sequential, non-random order. It starts with the node in one corner, then continuing along one of the directions at a time. The walking direction can be determined by adjusting the I, J, and K direction, where I, J, K is a Cartesian grid system. The convention of the direction of the path presented in positive or negative notation, while positive notation nods to a higher value of the Cartesian grid system coordinates.

For instance, say the origin node of the grid is in the lower-left corner, and we want to simulate with a unilateral simulation path in +I+J+K direction. The simulation will move to start from the origin node in the lower-left node, walking through the first row along the +I direction (from west to east) and when the first row is completed, it will continue to the next row along the +J direction (from south to north). The simulation will continue until the IJ plane is completed, then advance to the next plane in the +K direction (from bottom to top). The illustration of the unilateral simulation path in +I+J direction is shown in Figure 2.12.

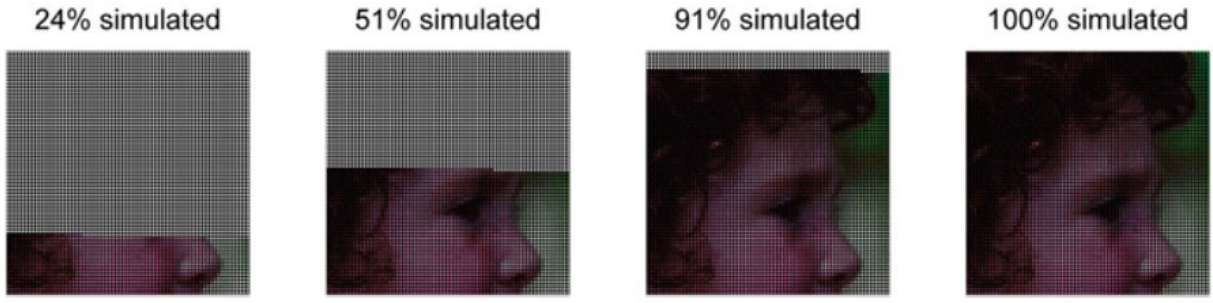

Figure 2.12. The illustration of the unilateral simulation path in MPS simulation in the +I+J direction (Mariethoz and Caers, 2014).

The output of the unilateral simulation path tends to be parallel to the first path direction and often leads to better reproduction of TI patterns and long-range continuity (Mariethoz and Caers, 2014). Especially in the case of long-range continuity, connected structures are represented better but appears elongated in the path direction (Figure 2.13).

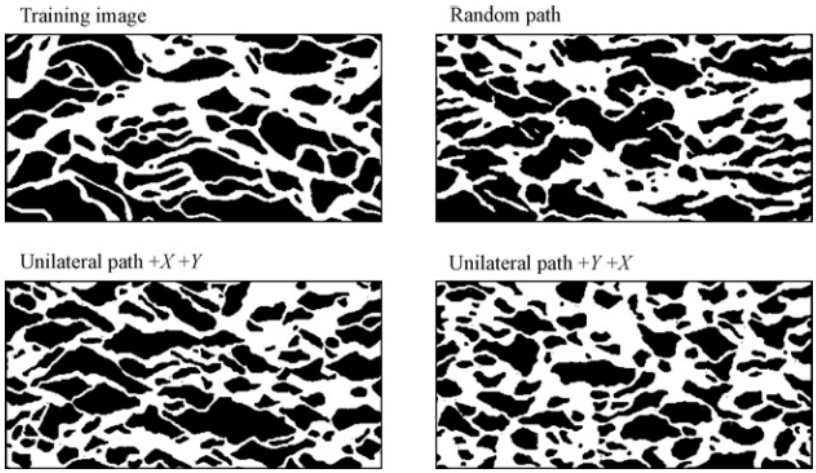

Figure 2.13. Training image and the realisations with using random and different unilateral simulation path (Mariethoz and Caers, 2014).

In this study, the direction of the unilateral simulation path used was -J+I direction based on the direction of the simulated delta from the source. The -J direction would simulate the column from north to south, then increments through the +I direction (left to right) when it arrives at the end of the column (Figure 2.14). The I-direction can be interchangeable (can be positive or negative), but for simplicity, we use the positive direction (started in the top left corner of the grid).

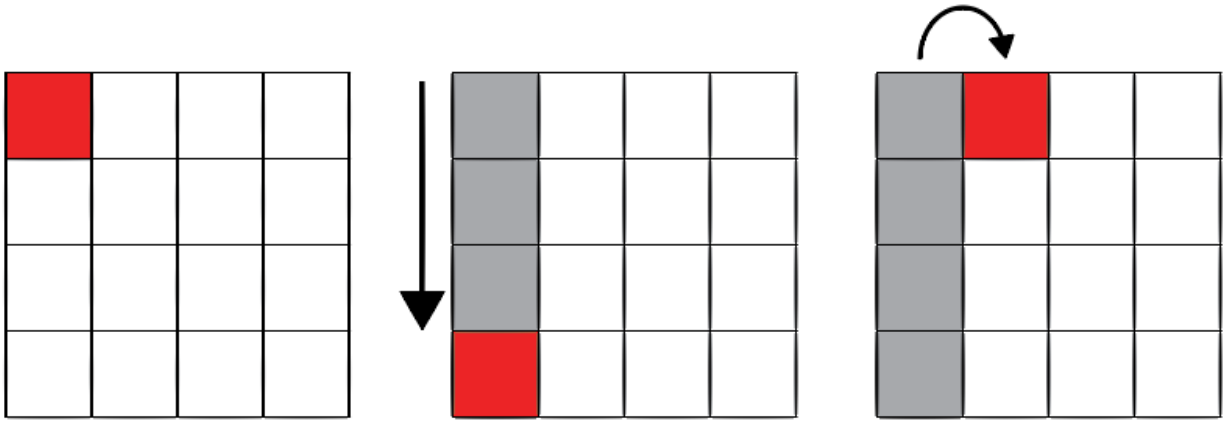

Figure 2.14. The illustration of MPS simulation using unilateral simulation path in -J+I direction in an example 4 x 4 grid. The simulation started at the top left corner, then increments through the +I direction after the column has been simulated in -J direction. The red node depicts the cell that is being simulated, the grey nodes depicts simulated cells, and the white nodes depict cells that have not been simulated.

2.5 Conditioning in MPS simulation

When using the hard date to condition in the MPS simulation, the MPS realisation model must honour the data in the specific data location. In using the process-based simulation model as its TI, MPS simulation can overcome the incapability of conditioning in the process-based simulation. Pyrcz and Deutsch in 2014 stated this situation in the data reproduction, that is may be linked to

the issues in the assignment to grid and conditioning in the simulation method. Checking the data reproduction in its according location may exhibit the performance of the MPS algorithm.

The nature of the pixel-based algorithm such as IMPALA should not confront the problem in the hard data preservation, because the data are estimated at the data locations with zero kriging variance (Michael J. Pyrcz and Deutsch, 2014). However, the hard data will affect the continuity in the case of channel patterns reproductions around the data, especially in using the unilateral simulation path where the data ahead of the path may not be compatible with the structures that built preceding the simulation data (Daly, 2005; Parra and Ortiz, 2011). Usually, the conditioned data values influenced the simulation only when data points are encountered in the search template (Figure 2.15).

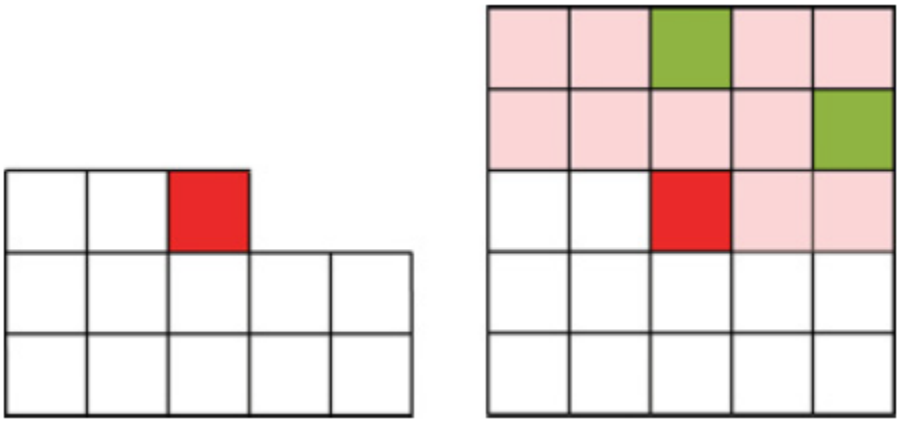

Figure 2.15. The left picture depicts a typical L-shaped search template for unilateral simulation path simulation that started in the lower-left corner. The right picture depicts the conditioning with hard data. The green nodes represent hard data, the white nodes are the simulated nodes before the conditioning, and the pink nodes represent the conditioned simulated nodes (Mariethoz and Caers, 2014).

2.6 Evaluation of MPS simulation

2.6.1.1 Visual inspection

One of the most basic things and may be the most important one is checking through visual inspection. The objective of the MPS stochastic modelling is to mimic a realistic geological model through MPS that follow the geological rules in its structures of the patterns. While it is hard to judge the similarity only with human eyes, we can highlight several features in both TI and realisations, such as low and high-valued areas, trends, and continuity (Michael J. Pyrcz and Deutsch, 2014). For example, if we want to simulate delta reservoir model in MPS simulation that have mouth bar connected to the channels, the resulting MPS simulation models must have the same features as the original model.

Limitations of the MPS simulation also need to be considered. The features of the realisation models may not be giving the impression of being geologically plausible, considering the limited model resolution or the limitation of the TI itself in conveying a geologic model (Michael J. Pyrcz and Deutsch, 2014). Those reasons make allowances for the acceptance of the MPS simulated realisations in case of visual inspection, as long as the TI's features are recreated correctly.

2.6.1.2 Connectivity function

The connectivity function considers the probability between two locations, say A and B, separated by lag distance h along a particular direction to be connected (Pardo-Igúzquiza and Dowd, 2003). If between those locations are connected, then the probability for two locations A and B are present (Figure 2.16). A collection of adjacent grid nodes of the same connected category, called geobody, represents the connectivity between those locations. For example, if those two locations belong to the same geobody, then they are connected and have the probability of connection; or else, disconnected. The application is useful to evaluate the similarity between the realisations and TI with connecting patterns like fluvial environment,

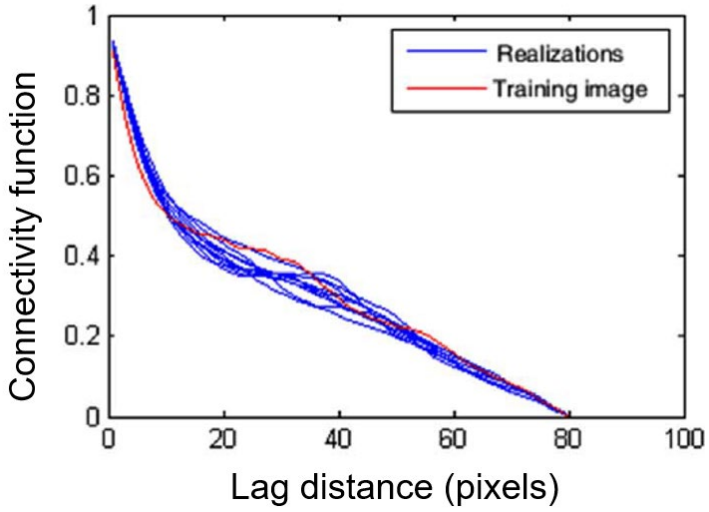

Figure 2.16. An example of connectivity function in x direction of TI compared to the MPS realisations. Similar connectivity functions indicates the similarity of the patterns between the TI and the MPS realisations (Pourfard, Abdollahifard, Faez, Motamedi, and Hosseinian, 2017).

The workflow of the connectivity functions is as follows, using MATLAB:

1. Import the TI and realisations with GSLIB format
2. Decide which facies that want to be evaluated and change the facies' code with number 1, else is 0
3. Identify and label each geobodies
4. Calculate the connectivity function in the defined direction

The mathematical expression expresses the connectivity function:

$$\hat{\tau}(h) = \frac{\#N\ (u \Leftrightarrow u+h | u, u+h \in S)}{\#N(u, u+h \in S)} \qquad (II.2.4)$$

where $\hat{\tau}(h)$ is the estimate of the connectivity function for distance h, $\#N\ (u \Leftrightarrow u+h | u, u+h \in S)$ is the number of cells separated by distance h, that belong to the phase S and are connected. $\#N(u, u+h \in S)$ is the number of cells separated by distance h that belong to the phase S and may or may not be connected.

In the validation between the MPS realisations and the TI, connectivity functions are generated for each realisation and then compared. The similarity between the functions indicates the similarity of the patterns between the TI and its realisations (Mariethoz and Caers, 2014).

2.6.1.3 E-type and conditional variance model

Usual approaches to compare the performances of the conditional simulation is to use the E-type and conditional variance model. Both models can be generated with using MATLAB or SGeMS software. E-type model is the local average of all realisations at each location in the model (Goovaerts, 1997) (Figure 2.17), where E is short for “expected value”. This model allows a result of the most likely value in each reservoir property at each location.

The study uses SGeMS to calculate the E-type and conditional variance models, where the workflow is as follows:

1. Import the TI and realisations in GSLIB format
2. Calculate the E-type and conditional variance models for each method

The expected value $\bar{z}$ at each location u_α is presented in the next mathematical expression:

$$\bar{z}(u_\alpha) = \frac{1}{L}\sum_{l=1}^{L} z^l(u_\alpha), \qquad \forall \alpha \in V \tag{II.2.5}$$

Where L is the realisations of the property z at all locations within the volume of interest V. By using the E-type model, we can see how the tendency of the simulated patterns in all realisations produced.

Conditional variance model measures the variance of the local realisations at each location (Figure 2.17) (Goovaerts, 1997). The conditional variance σ^2 at each location u_α is expressed with:

$$\sigma^2(u_\alpha) = \frac{1}{L}\sum_{l=1}^{L}[z^l(u_\alpha) - \bar{z}(u_\alpha)]^2, \qquad \forall \alpha \in V \tag{II.2.6}$$

Using those two models would supply a visualisation of the reproduction of trends in the presence of conditioning data by comparing the similarity of the E-type and conditional variance model value near the conditioning data. A good conditional MPS simulation results at around hard data location would have similar E-type value to the hard data, and small value of conditional variance.

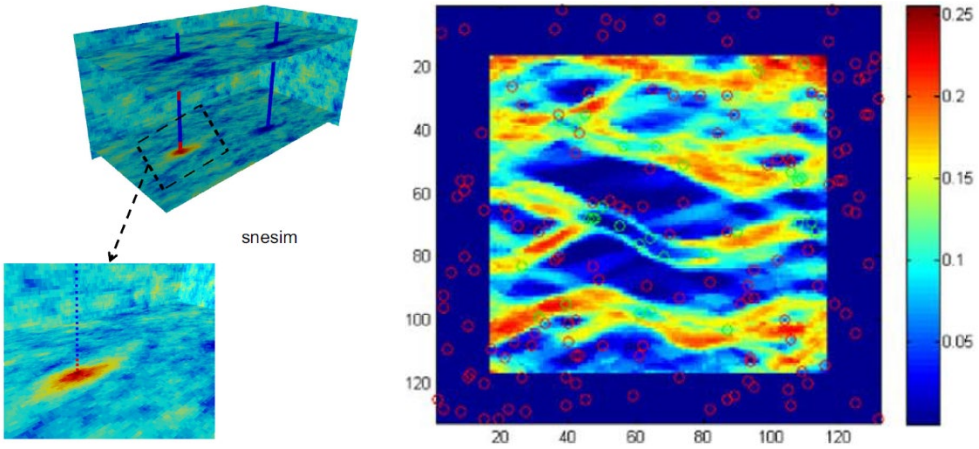

Figure 2.17. Left picture shows the example of E-type model for conditional MPS simulation with the straight line as the hard data (Tahmasebi, Sahimi, and Caers, 2014), and the right picture shows the example of conditional variance model for conditional MPS simulation with circles as hard data (Pourfard et al., 2017). A good conditional MPS simulation would show similar facies around hard data (left picture, shown in red colour) and low values of variance around the hard data (right picture, shown in blue colour).

2.6.2 Analysis of distance (ANODI)

This methodology uses a distance of the statistics as the basis of the comparison between realisations and the TI (Tan, Tahmasebi, and Caers, 2014). Analysis of distance (ANODI) aims to rank the algorithms based on two aspects of distance, which are: the spatial uncertainty (variability between the realisations, termed “between-realisation”) and pattern reproduction (resemblance between realisations and the TI, termed “within-realisation”). The reason why distance is preferred over variances and covariances is the dimensionality problem (Tan et al., 2014). The dimensions of the covariances grow rapidly, but covariance or variance do not address the dimensionality problem by present as measure of linear relationship/variation. Hence, it is favoured to work with dot-products that associated to the Euclidean distance. For more information, see (Tan et al., 2014).

The study used MATLAB to perform ANODI[1], which has workflow as follows:

1. Determine the template size of TI using “elbow” in scree-plots
2. Create pyramid of subresolutions for TI and realisations, using bicubic interpolation
3. Classify patterns of TI and realisations as clusters for each subresolution in each method by:
    a. Extract the patterns using the template size
    b. Calculate dissimilarity matrix of the patterns using Euclidean distance for each TI and realisation

[1] The ANODI code is modified from https://github.com/SCRFpublic/ANODI (Tan et al., 2014).

   c. Cluster the patterns using kernel k-means analysis
4. Summarise the clusters as cluster-based histograms of patterns (CHP) for each TI and realisation in each subresolution
5. Compute the distances of CHP with JS-divergence distances and show the J-S divergence distances in MDS plot
6. Calculate the between-distances and within-distances for each method
7. Calculate the ratio of between-distances, within-distances, and total-distances between methods

First, we determine the template size of each grid is defined using "elbow" in scree-plots based on the correlation between the eigenvalues of the covariance matrix and its dimensions (Zhu and Ghodsi, 2006) (Figure 2.18). The values were obtained by performing principal component analysis (PCA) on the patterns, and the "elbow" is identified by a sharp decrease in eigenvalues then stabilise for the remaining points. The elbow is supported by maximum likelihood estimate (MLE), which also represents the dimension for which the covariance matrix decreases. For a more detailed explanation, see (Zhu and Ghodsi, 2006).

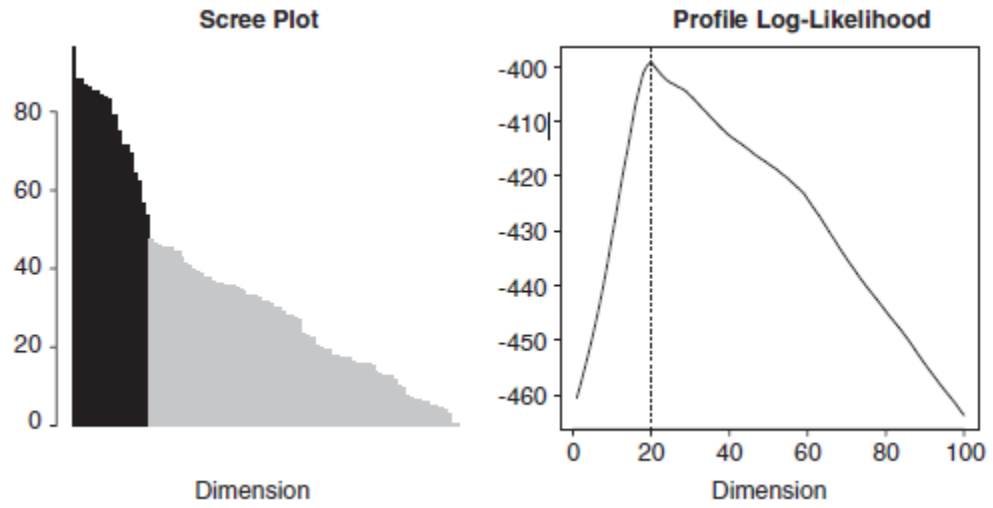

Figure 2.18. Example of similarity between scree-plot obtained from PCA and profile log-likelihood from MLE (Zhu and Ghodsi, 2006).

Then, a pyramid of multiple subresolutions (or multiresolutions) is created from every single realisation and training image using bicubic interpolation, owing to the presence of statistical variation that takes place at multiple scales (Tan et al., 2014). For higher subresolutions, previous resolution was divided into two between each level. For example, the original resolution is 101 x 101 cells, so the subresolutions 2 and 3 are 51 x 51 and 26 x 26 cells, respectively.

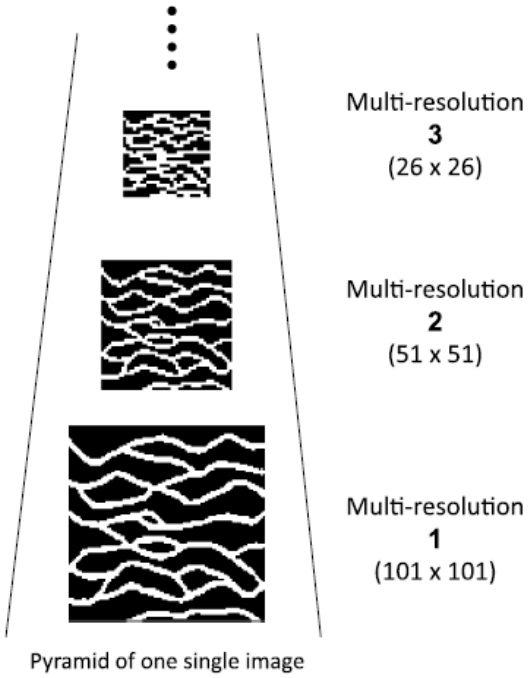

Figure 2.19. An example of a pyramid of 3 subresolutions from a single TI (Tan et al., 2014).

For each subresolution of the pyramid's statistics, we classify the patterns of TI and realisations by extracting the patterns using the template size acquired using the "elbow" from the scree-plot. The next step is we calculate the distance between the patterns in each template to cluster the patterns. Distance calculation used is using Euclidean distance function, which is given by:

$$d_E\left(pat_T^m(u), pat_T^n(u)\right) = \sum_{i=1}^{nT}\left(pat_T^m(h_i) - pat_T^n(h_i)\right)^2 \qquad (II.2.7)$$

Where the formula describes the Euclidean distance d_E for a pair of patterns from the pattern database T. Patterns with the high similarity, result in a small value, and different patterns result in a larger value (Suzuki and Caers, 2006). Within the range of similarity, one can cluster the patterns using kernel k-means analysis (see Campedel, 2005) (Figure 2.20).

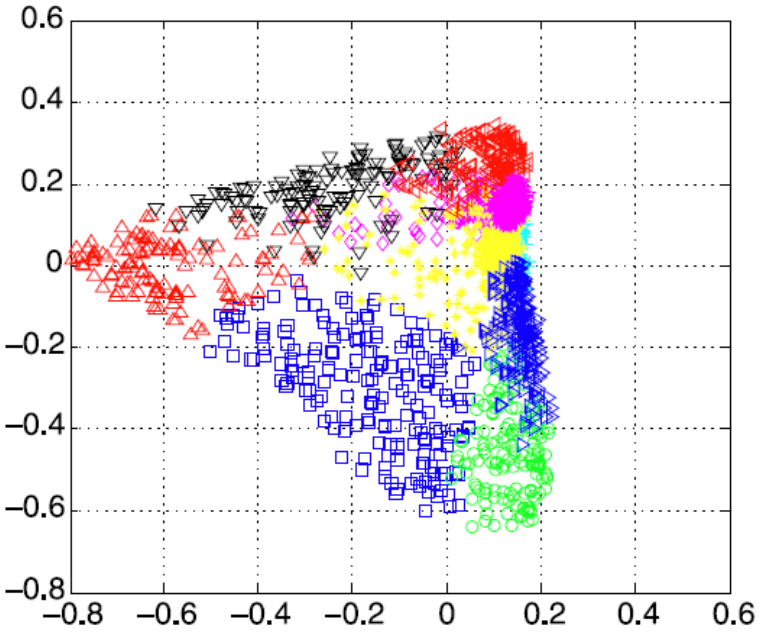

Figure 2.20. An example of kernel k-means clustering (Honarkhah and Caers, 2010).

We can summarise the clusters of patterns of each TI or realisations into multiple-point histograms (MPH) or cluster-based histograms of patterns (CHP), based on the more suitable way. We used CHP (see Honarkhah and Caers, 2010) for this study case because MPH can only handle small cases and binary variables, while the frequency table explodes when going to significant cases or dealing with multicategory (Tan et al., 2014).

The summarising process as CHP in TI and each specific realisation l are presented by:

$$\{ti_1, ti_2, \dots, ti_G\} \xrightarrow{summarize} \{CHP(ti_1), CHP(ti_2), \dots, CHP(ti_G)\}$$

$$\left\{re_1^{(l)}, re_2^{(l)}, \dots, re_G^{(l)}\right\} \xrightarrow{summarize} \left\{CHP\left(re_1^{(l)}\right), CHP\left(re_2^{(l)}\right), \dots, CHP\left(re_G^{(l)}\right)\right\} \quad (II.2.7)$$

Then, two types of distance can be calculated: (1) the distance between two given realisations (between-realisation) and (2) the distance between any realisation and the TI (within-realisation). The distance has to be able to summarise total differences between the CHPs of realisations and TI. Thomas and Joy in 2006 proposed a statistical measure of distance, termed Jensen-Shannon divergence where the divergence for two frequency distributions is the average of two Kullback-Leibler divergences. Regarding CHP, in each subresolution g, the Jensen-Shannon distance between the CHPs of lth realisation and TI in one algorithm k is:

$$d_g\left(re_k^{(l)}, ti_k\right) = \frac{1}{2}\sum_{c_g=1}^{C_g} CHP_{c_g}\left(re_{k,g}^{(l)}\right) \log\left(\frac{CHP_{c_g}\left(re_{k,g}^{(l)}\right)}{CHP_{c_g}(ti_g)}\right) + \frac{1}{2}\sum_{c_g=1}^{C_g} CHP_{c_g}(ti_g) \log\left(\frac{CHP_{c_g}(ti_g)}{CHP_{c_g}\left(re_{k,g}^{(l)}\right)}\right) \quad (II.2.8)$$

For calculating Jensen-Shannon distance between each realisation, the same formula is applied by changing the TI as the other realisation.

After the J-S distances between realisations and TI have been obtained, we can map the CHP as a set of points in space as multidimensional scaling (MDS) (Figure 2.21). MDS visualises the distances in each subresolution between clusters of realisations and the TI based on the eigen-value decomposition (Tan et al., 2014). MDS is needed to analyse the statistical variability in the change of dimension visually; the size of the cloud of data plotted reflected the variability of the data. The axis of the MDS plot shows the largest and second-largest eigenvalues.

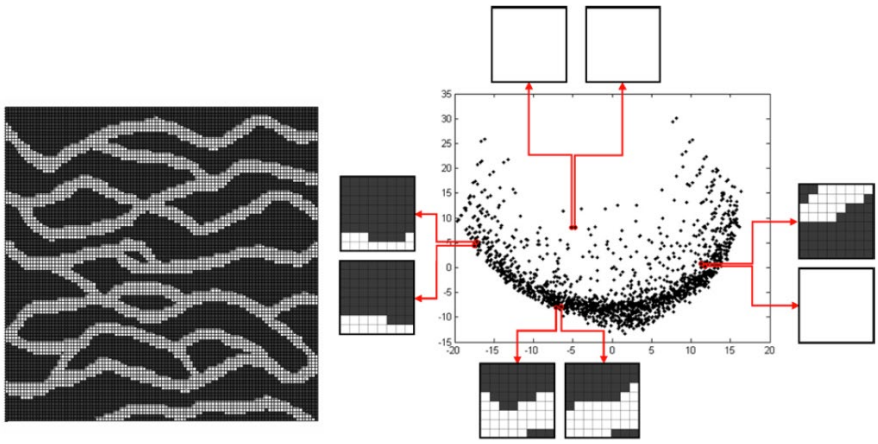

(a) Training Image (b) 2-d MDS space

Figure 2.21. An example of TI and MDS space. The x-axis represents the largest eigenvalue, and the y-axis represents the second largest eigenvalue (Honarkhah and Caers, 2010).

After that, we can now summarise the distance as variability (space of uncertainty) for within-realisation and between-realisation in one algorithm k for each subresolution g that is expressed by:

$$d_{g,k}^{between} = \frac{1}{L(L-1)} \sum_{l=1}^{L} \sum_{l'=1}^{L} d_g \left(re_k^{(l)}, re_k^{(l')} \right) \qquad (II.2.9)$$

$$d_{g,k}^{within} = \frac{1}{L} \sum_{l=1}^{L} d_g \left(re_k^{(l)}, ti_k \right) \qquad (II.2.10)$$

With realisation re, training image ti, distance d, one specific realisation l, and the total number of realisations L.

To obtain a single distance, the next step is to sum the variabilities from these subresolutions. By ranking of the algorithms, we have to compare between two algorithms to get the relative ordering. The ratios that quantify between-realisations and within-realisations differences between two algorithms k and m per subresolution grid are expressed as below:

$$r_{k,m}^{between} = \sum_{g=1}^{G} \frac{1}{2^g} \frac{d_{g,k}^{between}}{d_{g,m}^{between}} \quad (II.2.11)$$

$$r_{k,m}^{within} = \sum_{g=1}^{G} \frac{1}{2^g} \frac{d_{g,k}^{within}}{d_{g,m}^{within}} \quad (II.2.12)$$

The ratios are a weighted average, so the higher resolution grids get more weight than lower resolution grids. In essence, the grid with lower resolution will contain less information and have less variability than the grid with higher resolution, and shorter scale pattern is more essential than the larger scale pattern (Tan et al., 2014).

A good algorithm will reproduce higher spatial uncertainty between realisations (higher between-realisation distance) and better pattern reproduction based on the TI (lower within-realisation distance). Based on those criteria, the ratio of these distances will be calculated and be ranked. The ranking is presented by total ratio r, expressed by:

$$r_{k,m}^{total} = \frac{r_{k,m}^{between}}{r_{k,m}^{within}} \quad (II.2.13)$$

Where the best algorithm has the largest ratio compared to all other algorithms.

2.7 Workflow

There were three steps that became the basis in this study: data input preparation, linking process-based simulation model with MPS, and evaluation of the results. Figure 2.22 presents the overall workflow in a diagram.

Data input preparation includes importing the process-based simulation model into supported format in JewelSuite and TI construction for each particular approach. In this case, the NETCDF format file from the process-based simulation model data is converted into GSLIB format, so it can be supported and displayed properly in JewelSuite. Once the imported data has been processed, TI were constructed. Different approaches in MPS simulation requires different TI appropriate for the methods.

Linking process-based simulation model with MPS contains unconditional and conditional MPS simulation with two different approaches: zonation approach and control map approach. Before establishing conditional MPS simulation, the realisation from the unconditional simulations has to be validated by visual evaluation through trial-and-error processes started from the TI construction until successful unconditional MPS simulation. The conditional MPS simulation were carried out when the unconditional realisations have been acknowledged as the approved results in mimicking the patterns of the Delft3D model. In this way, we can evaluate the conditional capability from the methods by comparing unconditional and conditional MPS simulations' results (Arpat and Caers, 2007).

The last step evaluates the results with four methods: connectivity function, E-type models, conditional variance models, and analysis of distance (ANODI). The resulting evaluation will conclude

the optimised methodology in the study that allows the use of nonstationary process-based simulation model for TI input with MPS simulation in the fluvial-dominated delta.

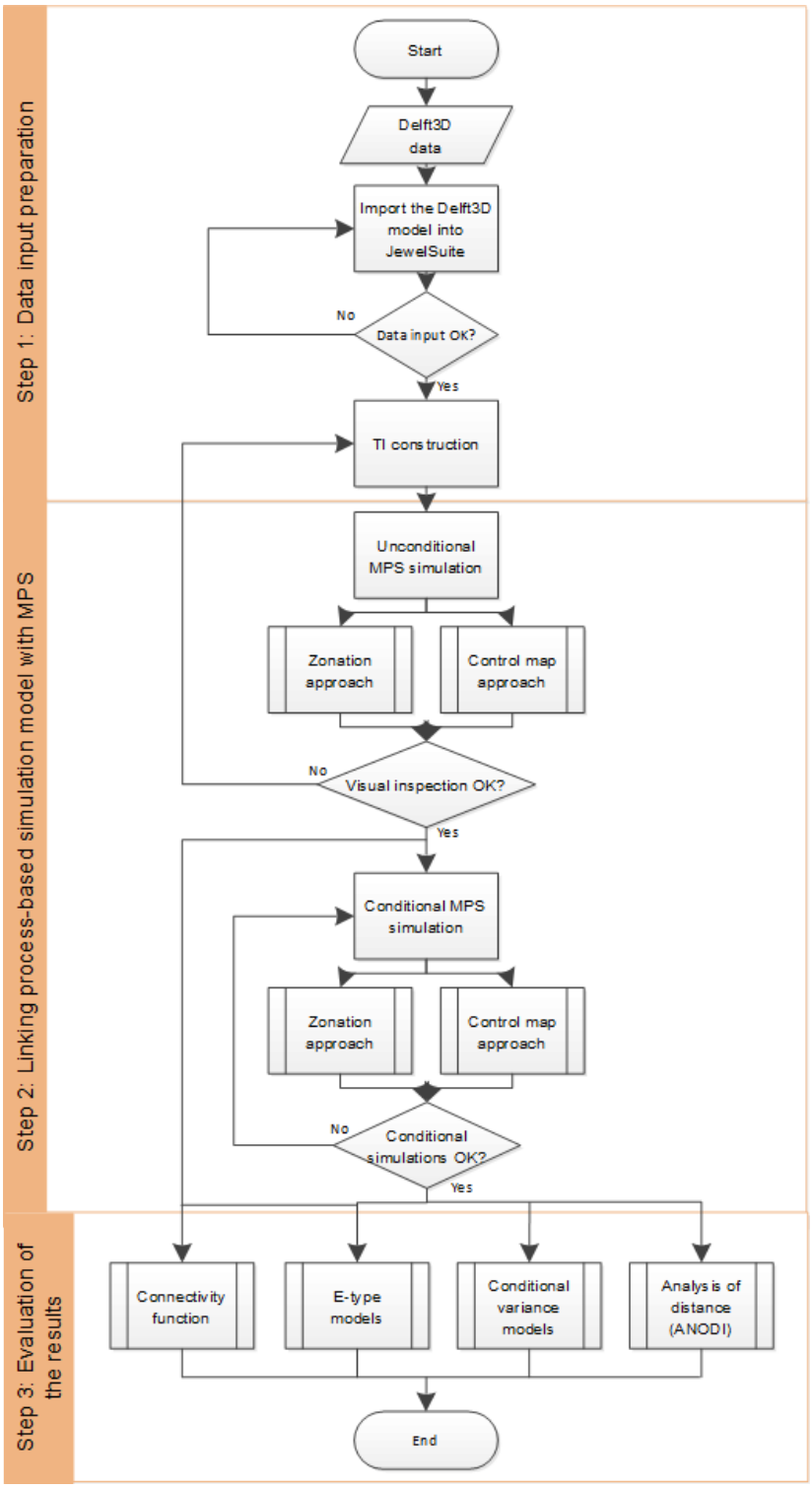

Figure 2.22. The flowchart in using process-based simulation model in MPS simulation in this study.

3

Data

3.1 Process-based simulation model as input data

The process-based simulation model used in the study is a post-processed data from numerical model done in process-based modelling software Delft3D (Lesser et al., 2004), which is the PhD work of van der Vegt in 2018 (Figure 3.1). The output from simulation is synthetic sediment bodies that requires post-processing to make the translation from simulation output to descriptions frequently used by geologists as fixed-size predefined calculation cells. The post-processing procedures identify the active channel network, describe delta architecture as subenvironments and facies, also analyse grain size distributions throughout the sediment bodies.

This study chose a model that comprises a dominantly medium sand composition delta that mimics fluvial-dominated delta progradation onto shelves with low slopes (van der Vegt, 2018) (Figure 3.1). For a more detailed explanation on the delta's parameters, see (van der Vegt, 2018). The post-processed files are in the NETCDF4 format, that allows the storage of a diverse set of parameters and their descriptions so that it can be later processed in most widely used programming software.

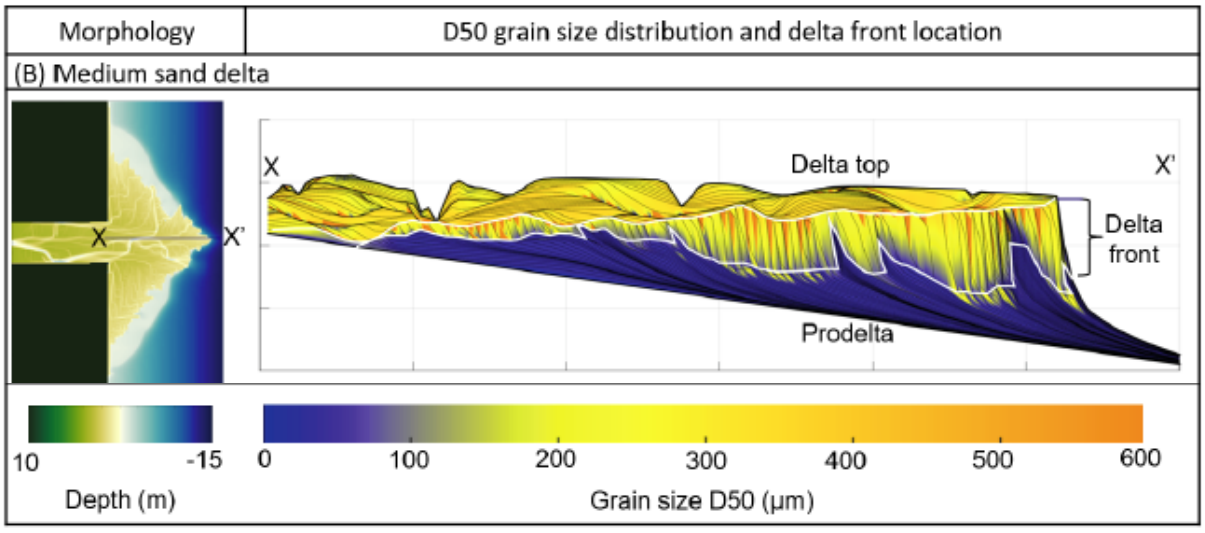

Figure 3.1. Final bathymetry of the fluvial-dominated delta simulation output from Delft3D, shown in a vertical section. Each line in the vertical section represents time-slice in one time deposition. Note that the displayed data is the original simulation output data, not the post-processed data (van der Vegt, 2018).

The total dimension of the NETCDF4 file is 282 x 302 x 321 (i x j x k) cells, each of the horizontal dimensions of the calculation cells used are 50 m x 50 m. The 3D grid of the NETCDF4 file does not necessarily show a 3D model of the reservoir, but only a display of 321 layers of time-slices (defined as k-layers in the k-axis) that each represents one layer of sediment that is being deposited in that period. The period is a user-defined amount of time defined as the hydrodynamic time, where an initial and final date is prescribed, in this case, is 320 days. Each day was applied a morphological scaling factor of 30 (Ranasinghe et al., 2001; as cited in van der Vegt, 2018), which means the one hydrodynamic year represents 30 years of deposition and erosion. The first layer is the layer with no deposition and erosion (start of the simulation).

Each grid in the layer is defined with one value of each property, such as thickness, facies, and depth value. The represented time in the process-based simulation model is expected to be in the order of a century to millennial scale, considering the volume of deltaic deposition (Li, Storms, and Walstra, 2018). The assumption taken in the simulation is the constant and high-level fluvial input, representing bankfull discharge when the most sediment is expected to be delivered in the basin. For a more detailed description on the data, see (van der Vegt, 2018).

Available post-processed data from Delft3D that can be used in this study as variables are:

- Subenvironment
- Architectural element (facies)
- Diameter
- Net-to-gross
- Sorting

The study focuses on the use of the facies' pattern in the MPS simulation, which resulted from the subdivision of the subenvironment variable. The subenvironment variables are:

- Delta top, including deposition below 5 m of water depth, deposition within the active channel network until the brink point depth, deposition above the brink point depth, any cell that is 0.5 m below the brink point and contains 1% sand.
- Delta front, including deposition down to 10 m of water depth, and deposition above the delta front limit that contains at least 1% sand
- Prodelta, including everything below the prodelta cut-off depth
- Inactive, including everything which have not at least 15 mm deposition in one time interval

The basis on the subenvironment definition is the hydrodynamic processes that is controlling how the grain size classes will be retained by the subenvironment, and which will be eroded (van der Vegt, 2018). Also, the sediment supply composition affects to the grain size classes available and affects the interaction within sediment. In the end, the whole processes combined with the sediment supply composition will determine the geometry, depositional, and reworking processes in each subenvironment (van der Vegt, 2018).

The subenvironments are further subdivided into seven architectural elements (Figure 3.2):

- Delta top subenvironment:
    - Channel accretion facies, defined as lateral and vertical accretion deposit as the channels migrate

    - Channel fill facies, defined as fining upwards deposit within previously active channels until it reaches the delta brink
    - Delta top background facies, defined as the remainder of the delta top deposit between the active distributary channels
- Delta front subenvironment:
    - Mouth bar facies, defined as sandy sediment deposited where sediment-laden jet exits channel mouth
    - Delta front background facies, defined as the lobate deposits travelling further than the mouth bar sands and the remainder sediments
- Prodelta subenvironment:
    - Prodelta facies, defined as the fine sediment deposited below the fair-weather wave base
- Inactive subenvironment:
    - Inactive facies, including everything which have not at least 15 mm deposition in one time interval of deposition

3.2 Preparation of the input data

The study used JewelSuite software to generate MPS realisations using process-based data as the TI. One of the supported grid data in JewelSuite is GSLIB, a simple ASCII format with no data compression or alphanumeric characters that have flexibility in changing and storing the data. This GSLIB format particularly using the simplified GEO-EAS format, in which each variable stored in vertical columns (Ziegel, Deutsch, and Journel, 1995). To convert the process-based model format in NETCDF into GSLIB format, MATLAB software was used. The data sequence was manipulated and converted into GSLIB format and be displayed in JewelSuite software whether the data has been formatted correctly or not.

Again, while the process-based simulation model grid itself is 3D, the output from the Delft3D software describes each time-slice as one layer of sediment which deposited in the range of each time layer and listed the grid properties as the properties of each cell. In the process-based simulation model, erosion might occur (depicted as a negative number of thickness value), and one time-slice layer grid might overlap with the other time-slice (showed by overlaying in the depth value).

JewelSuite's capability in importing the GSLIB data stores each grid into the grid counting system is limited, defining each cell in sequence within its grid counting system, instead of placing each cell in its according to the depth value. This results in importing the process-based simulation model into JewelSuite as a 3D grid, with each k-layer of time-slice as 2D map view with no difference in depth in each time-slice (Figure 3.2). Correspondingly, this study treated each time-slice as a 2D time-slice layer with a 50 x 50 x 50 m cube dimension in each cell.

Channel accretion and channel fill facies were two of the facies that comprises the channel sediments. A problem with the channel fill facies is that it shows scattered distribution to the TI grid, resulting in a chaotic pattern of the channels (Figure 3.2). A solution for the distribution problem is we combined two of the facies in order to create one channel facies, labelled as channel accretion facies for simplicity. The results were more consistent channels where little artefacts were found in the channel bodies (Figure 3.10) and (Figure 3.11).

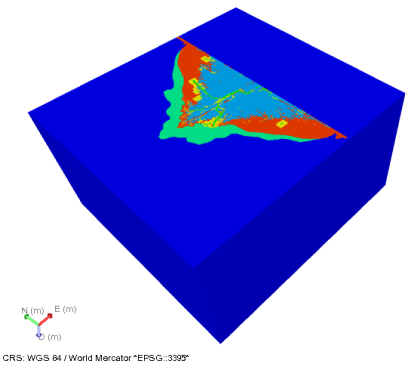

(a) Whole 3D grid of the data

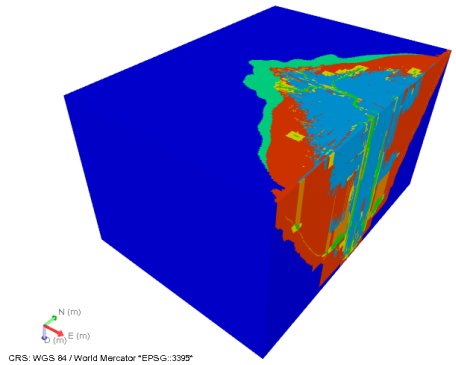

(b) Sliced 3D grid of the data

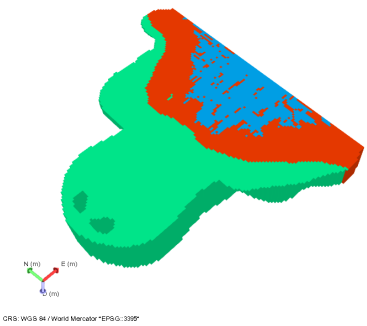

(c) Subenvironment for older, 250th k-layer

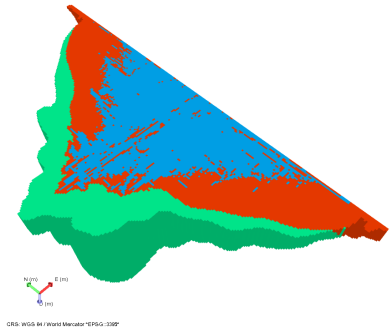

(d) Subenvironment for younger, 1st k-layer

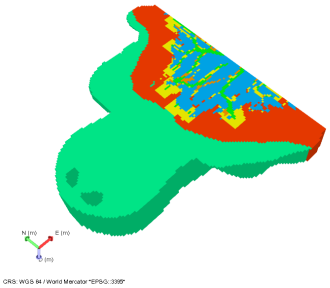

(e) Facies for older, 250th k-layer

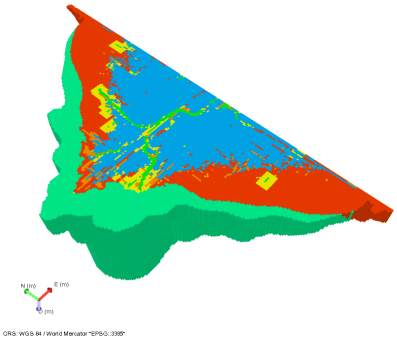

(f) Facies for younger, 1st k-layer

Figure 3.2. The Delft3D simulation model in JewelSuite. The whole grid consists of variables including inactive cells that is also needed in the MPS simulation. Display without inactive cells were shown in middle and lower pictures to clearly show the sediment bodies. Each k-layer time-slice represents a period of deposition in a period of the order of a century to millennial scale, shown in a flat 2D layer.

3.3 TI construction and its properties

The limitation of displaying the process-based model in JewelSuite without the difference of depth value made this study opted for the use of 2D grid in displaying of each time-slice. Consequently, the overlapping and the erosion of the sediment presented in simulation cells will not be apparent. This choice of 2D grid will show the patterns of the variable correctly in a map view.

Two approaches in handling nonstationarity were done in the study, which were zonation and control map approaches, and each of the approach needed different TI. Prior to commencing the construction of the TI, the decision of the suitable k-layer (layer in the k-direction) as time-slice were done to represents the while fluvial-dominated delta development. One of the most important of the adequate TI to be used in MPS simulation is the necessity of sufficient pattern repetition and broad enough so it is becoming unbiased and represents the range of variability (Michael et al., 2010). Judging from the facies patterns, the variations of repetitions lies in the channels represented by channel accretion and mouth bar facies, and their patterns become the basis of the TI time-slices selection.

This study chose two cases of the patterns' repetition in time-slices that represents the whole fluvial-dominated delta development: Case A with high repetition in the patterns, represented by the 240th k-layer and Case B with low repetition in the patterns, represented by the 100th k-layer (Figure 3.3).

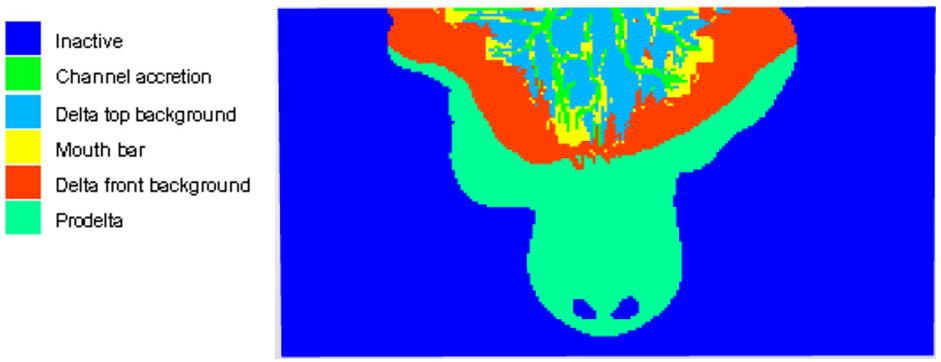

(a) Case A: TI 240th k-layer

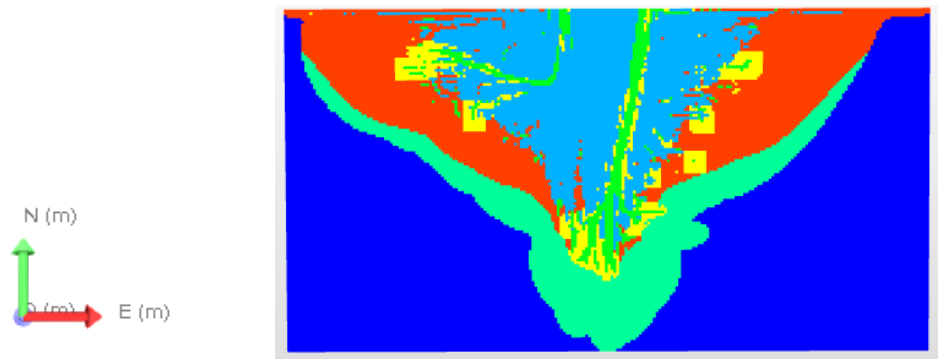

(b) Case B: 100th k-layer

Figure 3.3. Facies display of the architectural elements (facies) variable. Upper picture depicts Case A: 240th k-layer with high repetition, lower picture depicts Case B: 100th k-layer with low repetition.

Case A denotes early development of the delta (anabranching channels, high repetition in the patterns) and Case B for the later stages of the delta (meandering to straight channels, low repetition in the patterns). Those two time-slices assumed enough to illustrate the capability of MPS' IMPALA algorithm in handling the complexity of the various channels patterns. We also cropped the non-marine part of the delta where the sediment source originated, shown in the east (upper) part of the simulated delta so the MPS simulation could focus on the reservoir. The resulting TI grids is shown in the Figure 3.3, with the grid's dimension of 228 x 121 x 1 cells, which is also going to be used as the dimension of the simulation grid.

3.3.1 TI for zonation approach

The zonation approach implies that we identify several zones in the TI grid that are considered stationary and use new different TI specifically designed for the patterns in the zonation. The information on the statistics and structural geometry can be obtained from the Delft3D simulation model, then utilised on the new TI that has increased pattern repetition so that it can be assumed approaching stationarity.

The Delft3D simulation model defines the subenvironment based on the hydrodynamic processes and sediment supply composition; resulting in similar geometry, depositional, and reworking processes in each subenvironment (van der Vegt, 2018). Based on those rules that act as the principal, we can determine that each subenvironment is statistically assumed stationary with the same processes that controlled the processes and use each subenvironment as stationary zonation (Figure 3.4).

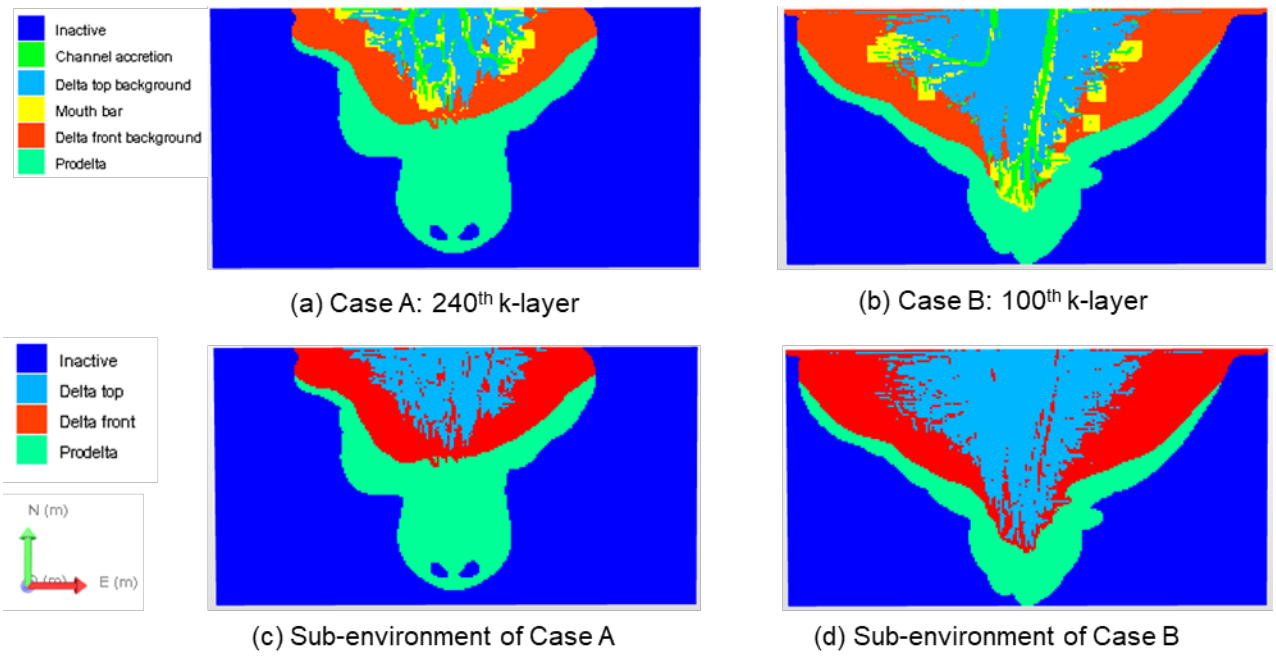

Figure 3.4. Facies and its subenvironments of Case A and Case B. The subenvironments act as the stationary zonations for the zonation approach.

There are no distinct sediment bodies with peculiar patterns within the prodelta and inactive zonations. With this consideration, those zonations will not be considered as required reservoir to be simulated in MPS simulation and will be applied with the same facies from the Delft3D data.

New TIs will only be required for each delta top and delta front zonations where both TI for each zonations share the same facies accretion facies for transition purposes in MPS simulation.

The striking variation of the patterns obtained in the sediment bodies which are the channel accretion and the mouth bar facies (Figure 3.3), both represent the distributary channels and the resulting sandy mouth bars building out at the end of the channels. The study then chose one representative channel and the delta lobes to has its dimension extracted to be used in the new TI construction (Figure 3.5), then constructed the new TI using the built-in graphical module in JewelSuite. Resulting new TIs were presented in the next sections.

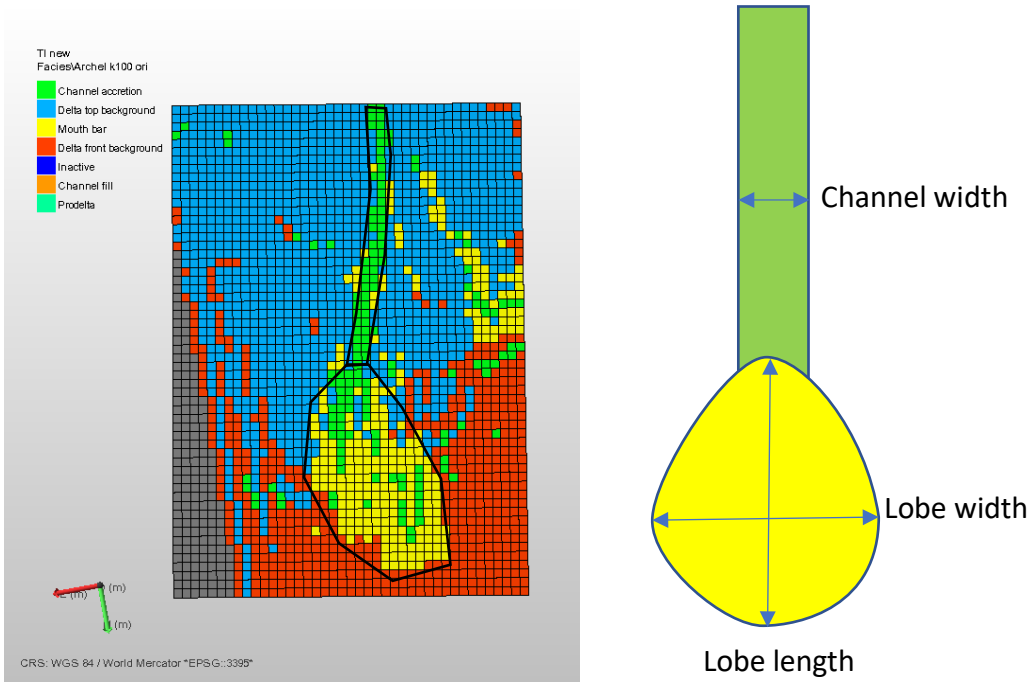

Figure 3.5. Dimension extraction from the Delft3D simulation model. There are three dimensions acquired from the channel accretion and the mouth bar facies (channel width, lobe width, and lobe length) which serve as the dimensions in the new TI construction.

3.3.1.1 Case A: high repetition

New smaller TIs were created for Case A with the dimensions of 50 x 50 x 1 cells. This grid size is suitable enough to capture the anabranching patterns of the facies and also the mouth bars. Between the delta top and delta front zonations, channel accretion facies acts as the bridge between the patterns across the zonations. For the delta top zonation, we created the anabranching channels pattern with the channel accretion facies. For the delta front zonation, single mouth bar and channel accretion facies are enough to accommodate the reproduction of the delta, so the MPS simulation will recreate mouth bars in the boundary of delta top and delta front zonations.

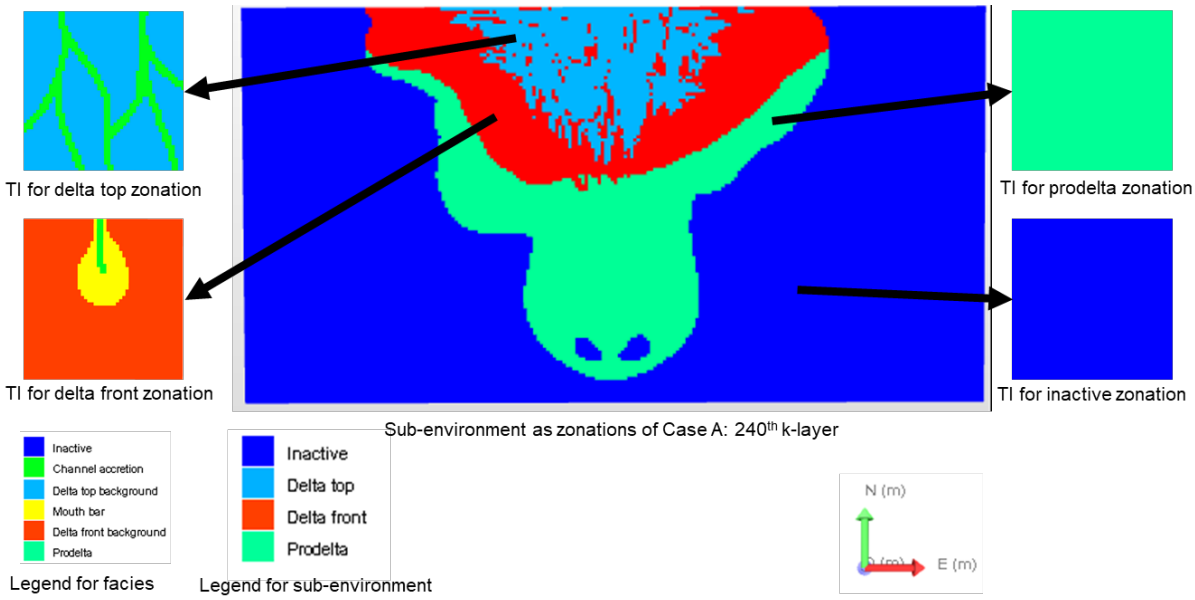

Figure 3.6. The 240th k-layer for each of new TI for delta top and delta front subenvironment.

From the Figure 3.3, this case has distributary channels that develop radially from the source of the sediment. To mimic the realisations to be as closely as possible to the original data had the need of data event transformation variable in the form of azimuth map. The azimuth map defines the rotation to the area it applied, so we can impersonate the radial distribution of the channels. We created an azimuth map that is divided into eight different azimuth zones, each of the zones has 30 degrees of clockwise rotation increment (Figure 3.7). It was considered that eight zones of azimuth rotation would similarly accommodate the rotation based on the Case A and Case B TIs.

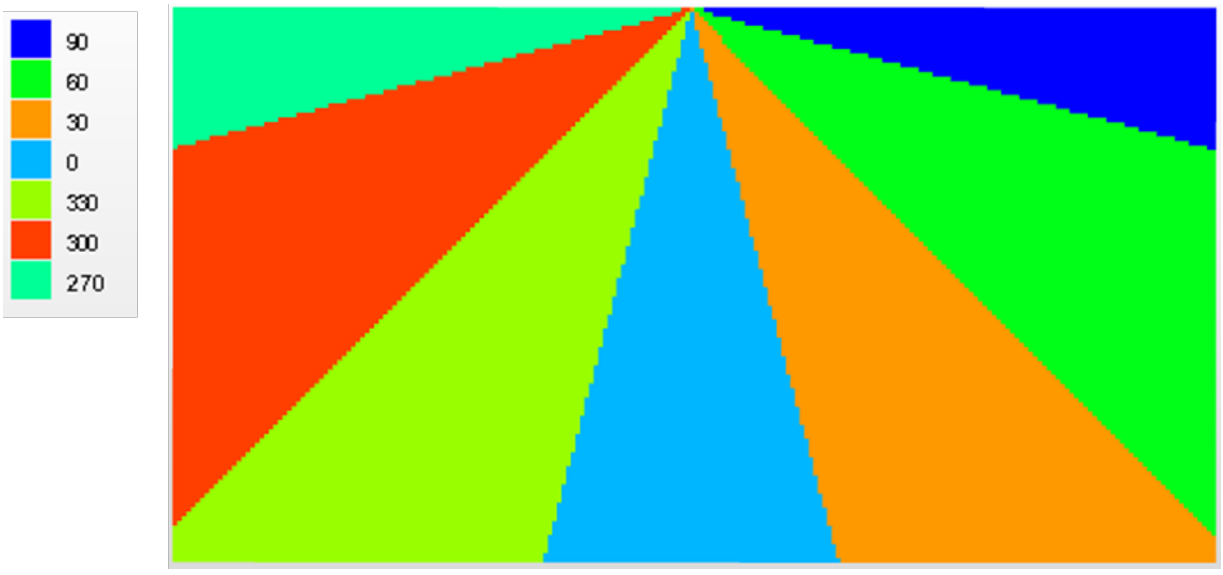

Figure 3.7. The azimuth map used in the Case A and Case B. The zones will apply clockwise rotation to the patterns found on the zones.

3.3.1.2 Case B: low repetition

The new TIs for Case B is similar to Case A, where new TIs were required in the delta top and delta front zonation. The grids have the same grid dimension (50 x 50 x 1 cells) and the same facies that are embodied in each zonations, but the difference is the patterns in the delta top zonation. Only two channel bodies in channel accretion facies compared to Case A whose channels were anabranching. These channels in Case B were branching in the south part of the TI grid to mimic the patterns in original Delft3D data.

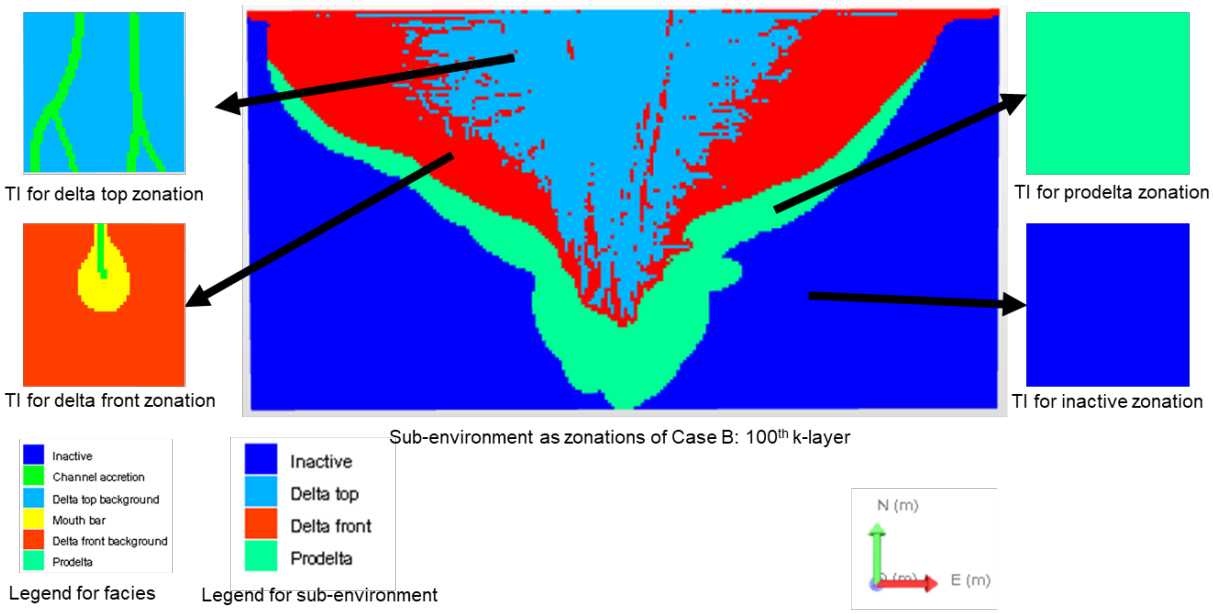

Figure 3.8. The 100th k-layer for each of new TI for delta top and delta front subenvironment.

Azimuth map needed in the Case B is similar to Case A, where the distributary channels are developing radially through the grid. Although the rotation is not necessarily the same, we decided to use the same azimuth map as Case A as it accommodated the rotation properly in Case B (Figure 2.1).

3.3.2 TI for control map approach

Handling nonstationarity in MPS simulation using control map utilises a single original TI as the input. No azimuth map is needed because the control map will decide which patterns that would occur in the simulation grid, including the data properties transformation such as rotation.

Riou, Höcker, and Hughes in 2015 stated the availability of the auxiliary variables from the data available can be used to define the connection between the nonstationary patterns. We have the diameter, sorting, net-to-gross fraction, and subenvironment variables from the input data (Figure 3.9). Those data were tried in MPS simulation to see its capability as the control map.

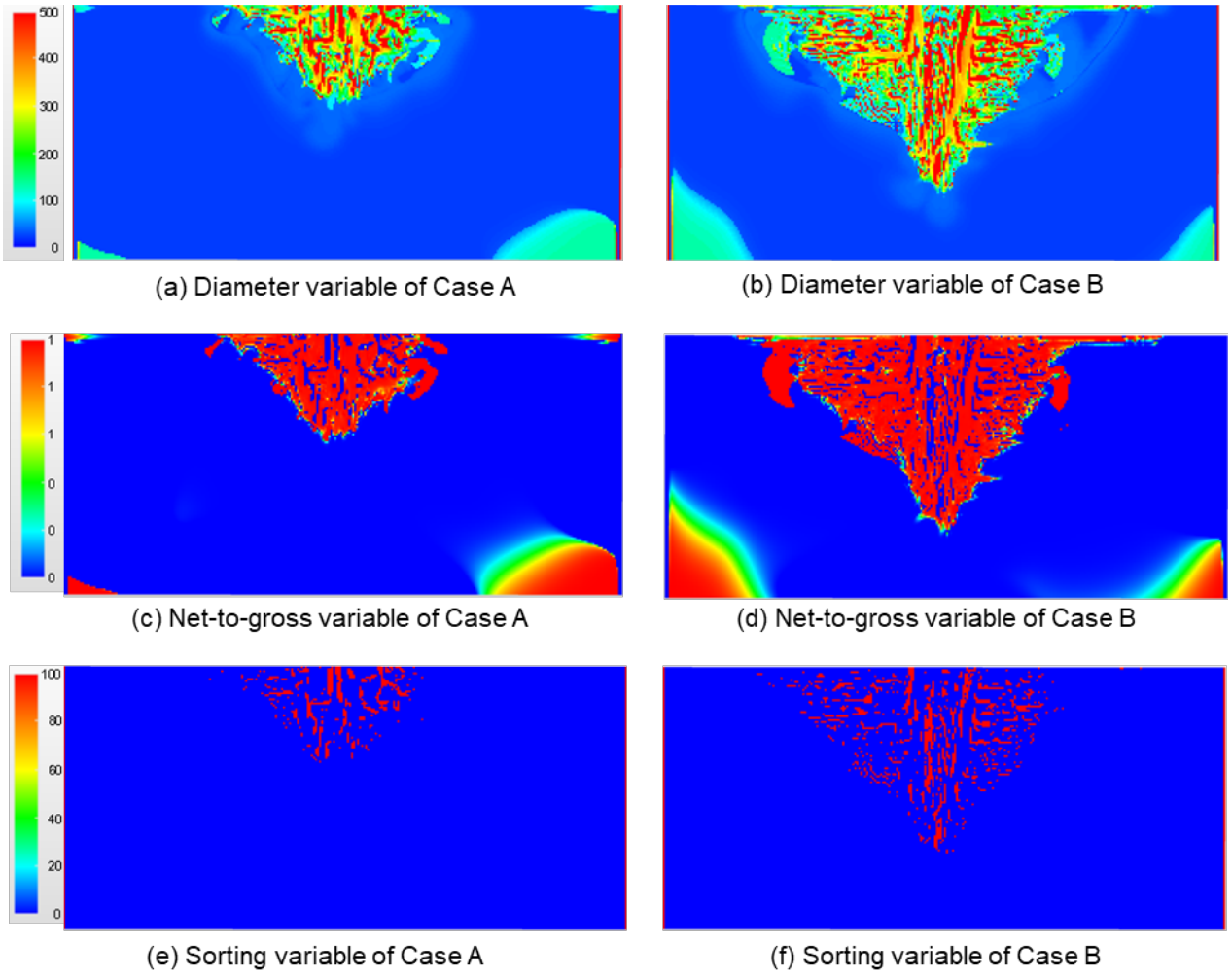

Figure 3.9. The diameter, net-to-gross, and sorting variable of Case A and Case B.

As can be seen from the Figure 3.9, the variables are either strictly positioned to the sediment body (diameter variable) or there is very little variation throughout the whole delta (net-to-gross and sorting variables). We decided not to constrain the delta development with the goal of creating freedom for the MPS simulation in simulating the facies by the control map. After all, the objective of the MPS simulation is to stochastically simulate the patterns to mimic the original data, not to force behaviour to the sediment body. The diameter, sorting, and net-to-gross fraction variables revealed to be too constrained in space (Figure 3.9), hence we utilised subenvironment (Figure 3.4) as the basis of our control map.

The decision to use subenvironment as control map was based on the hydrodynamic processes and the sediment supply composition that differ in every subenvironment. The MPS algorithm will have the freedom on simulating sediment bodies within each subenvironment and fulfil our objective of stochastic simulation.

3.3.2.1 Case A: high repetition

The TI used in Case A is the 240th k-layer from the Delft3D data. It has high repetition in the fluvial patterns, shown by anabranching channels from proximal part of the delta (Figure 3.10). The distribution of the fluvial patterns reveal radial patterns of the distributary channels development where multiple, interconnected channels were separated by the delta top background facies.

To commence the control map construction, the subenvironment variable was transformed into 0-1 values where the highest value is in the delta top subenvironment and the lowest value is in the inactive subenvironment. There is no definite rule on deciding the value, as long as the values were sorted from high to low and there are no overlapping values between the subenvironments. Once the variables have been converted into values, smoothing process were performed to ensure the smooth transition in the simulation process.

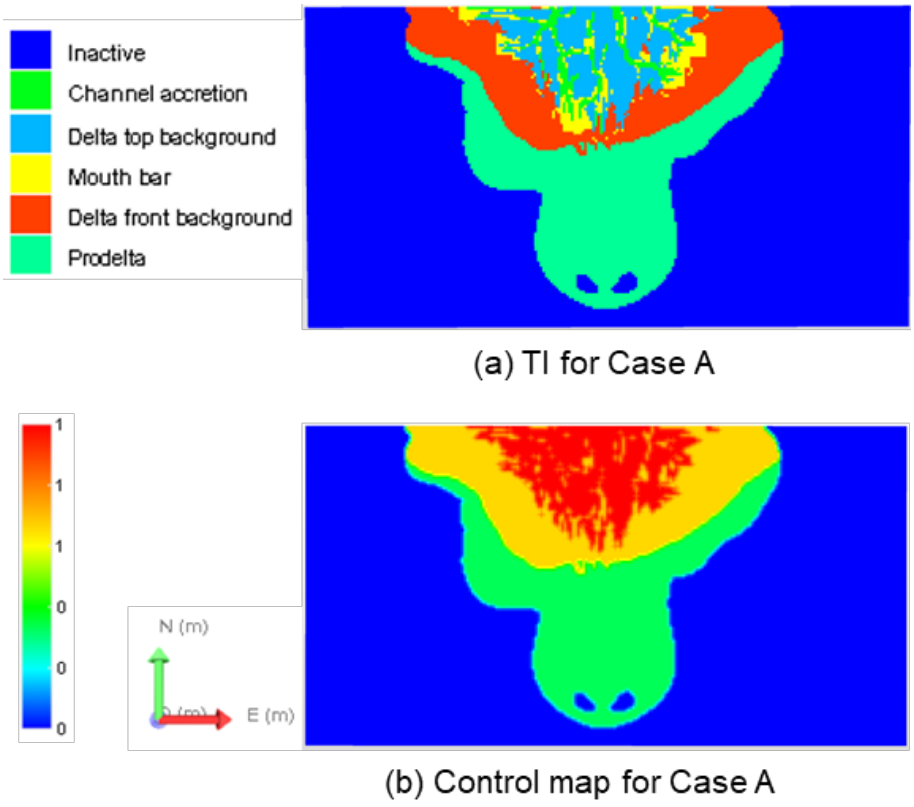

Figure 3.10. TI display of the 240th k-layer which shows low repetition in the fluvial patterns and its control map based on its subenvironment.

3.3.2.2 Case B: low repetition

The 100th k-layer of Delft3D data as TI in Case B has low repetition of patterns in the grid. Same steps have been taken to construct the control map in Case B where the subenvironment variable was converted into 0-1 values and then smoothened.

There are obvious difficulties in handling nonstationarity with low repetition of patterns, but the use of subenvironment as control map were considered able to overcome the limitation by simulating the patterns within the stationary subenvironment.

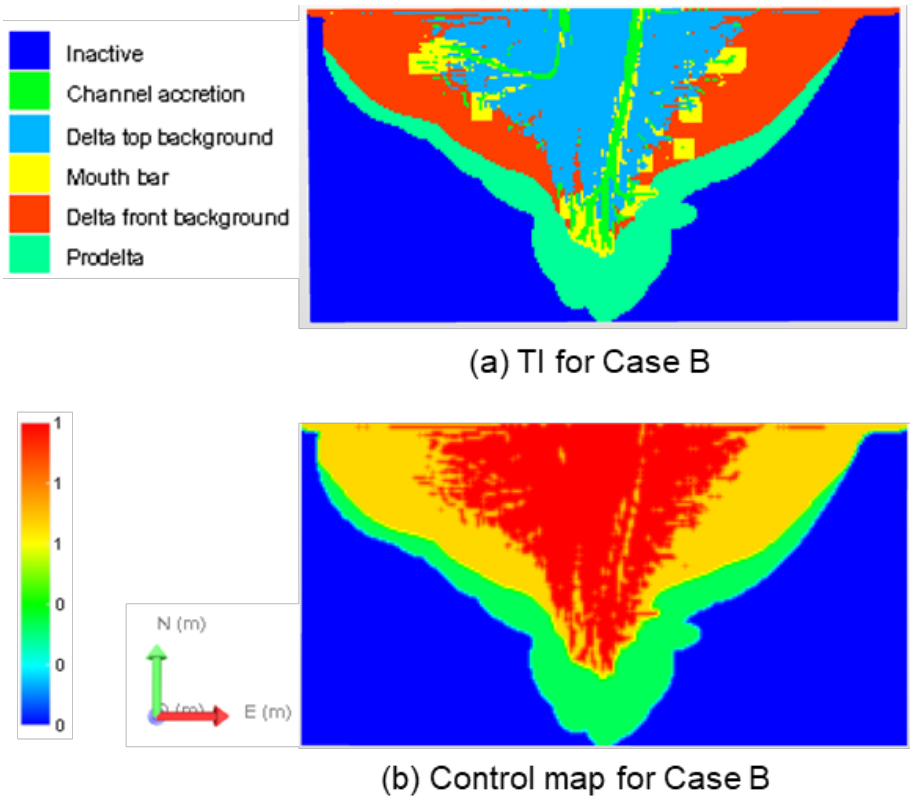

Figure 3.11. TI display of the 100th k-layer which shows low repetition in the fluvial patterns.

3.4 Hard data selection for conditional simulations

The presence of hard data in MPS simulation will define the similarity between the simulated model and real data. In this study, the hard data are grid cells comprised of facies variable from the Delft3D data. In an attempt to investigate the conditional capability of the IMPALA MPS algorithm, the study chosen dense and sparse hard data to be used in the conditional simulations. Both dense and sparse data will be affecting the conditional results of the MPS simulation.

The placement of the hard data was carried out in the area where the variation of the patterns takes place, which are the delta top and delta front subenvironments (Figure 3.12). Particularly in the sparse data case, the hard data were placed in the distal area where the channels already developed (Figure 3.12c and Figure 3.12d). Also, the hard data were put in sandy deposit (Figure 3.12c and Figure 3.12d), which are channel accretion and mouth bar facies, owing to the nature of the MPS' algorithm in using the search template size and the small width of the sandy deposit's facies. Positioning the hard data in this manner offers another advantage in evaluating the unilateral simulation path where the data ahead of the path may not be compatible with the structures preceding the simulation data (Daly, 2005).

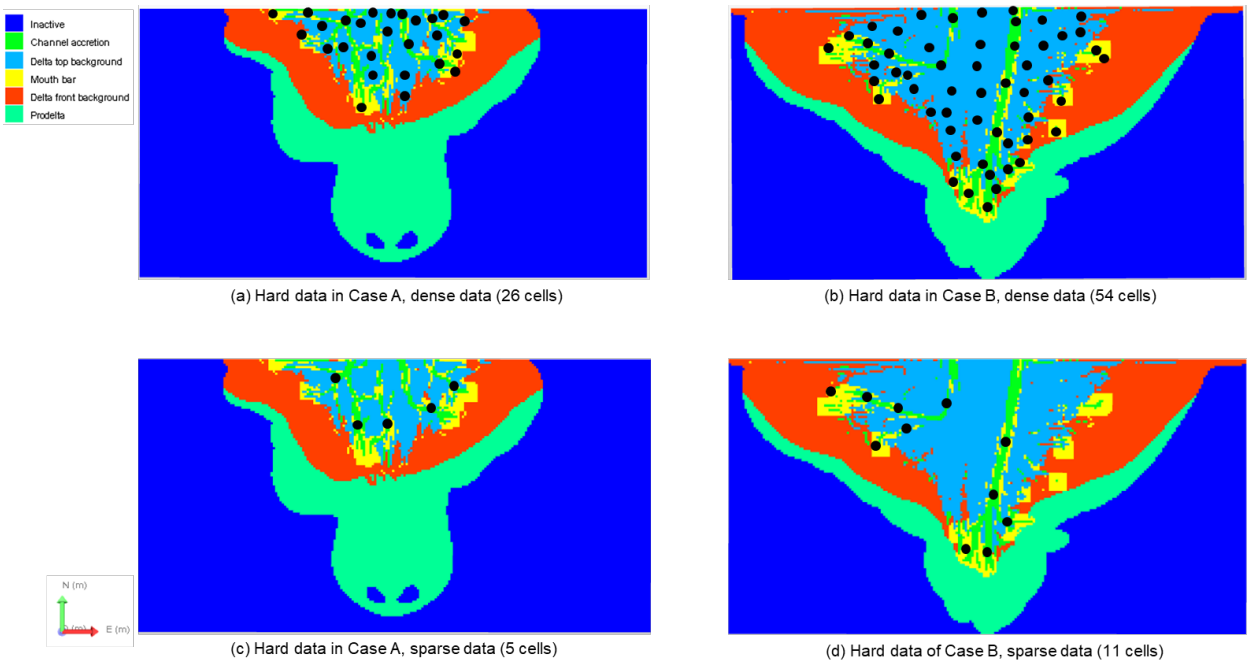

(a) Hard data in Case A, dense data (26 cells)

(b) Hard data in Case B, dense data (54 cells)

(c) Hard data in Case A, sparse data (5 cells)

(d) Hard data of Case B, sparse data (11 cells)

Figure 3.12. Hard data placement for Case A and Case B. In sparse hard data distribution, the placement of the hard data took place in the distal area and the sandy deposit's facies that offers advantage in evaluating the unilateral simulation path.

4

Results

This chapter describes the results from unconditional and conditional MPS simulations using zonation and control map approaches. The study used visual inspection to determine the method in unconditional MPS simulations that produces the patterns of the sandy deposit (channel accretion and mouth bar facies) properly, then further evaluated using connectivity function. There were several approaches with different simulation paths that have been taken in Case A and Case B, termed with Method I-IV:

- Method I, zonation approach with random simulation path
- Method II, zonation approach with unilateral -J+I simulation path
- Method III, control map approach with random simulation path
- Method IV, control map approach with unilateral -J+I simulation path

The conditional MPS simulations were carried out with using the methods from unconditional simulation that have passed the visual inspection, using dense and sparse hard data. This decision helps to ensure that the approved methods can mimic the patterns in Delft3D model correctly and can be evaluated for both unconditional and conditional MPS simulations (Arpat and Caers, 2007). E-type model, conditional variance model, and analysis of distance (ANODI) were adopted to obtain further in-depth information on the conditional capabilities. The final stage of this chapter comprised an evaluation on the best performance in mimicking the patterns within the performed method for both unconditional and conditional MPS simulation in fluvial-dominated delta model using process-bases simulation model.

4.1 Unconditional MPS simulation results

In zonation approach, azimuth map was used to apply the data events transformation in order to mimic the Delft3D data. For control map approach, there are no additional data events transformation variable other than control map to handle the nonstationarity in the MPS simulation.

To evaluate the whole fluvial-dominated delta development in MPS simulation, this study used two cases based on two different time-slices: 240th k-layer as Case A that has high repetition in its sandy deposit's patterns, depicted in Figure 4.1, and 100th k-layer as Case B that has low repetition in its sandy deposit's patterns, shown in Figure 4.2. The sandy deposit are channel accretion and mouth bar facies, in the delta top and delta front subenvironment.

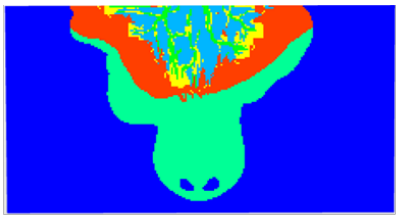

(a) Case A: 240th k-layer

Legend for facies

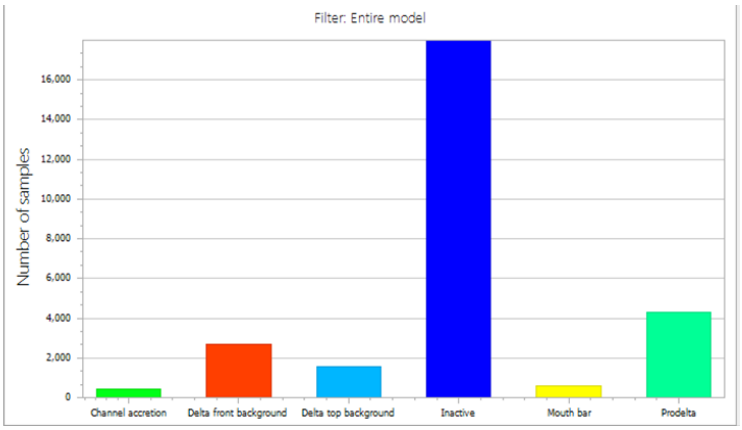

Histogram for facies of Case A

Figure 4.1. Case A and its histogram for its facies. Case A has high repetition in its sandy deposit's facies, which are channel accretion and mouth bar facies.

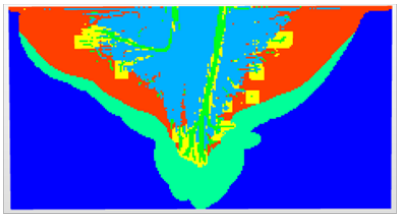

(a) Case B: 100th k-layer

Legend for facies

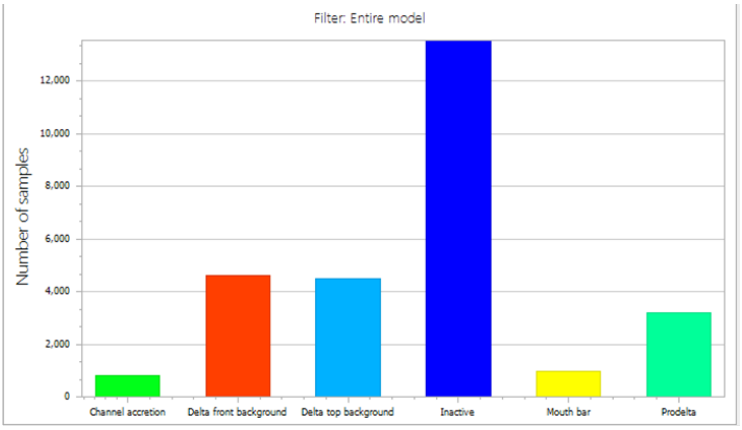

Histogram for facies of Case B

Figure 4.2. Case B and its histogram for its facies. Case B has low repetition in its sandy deposit's facies, which are channel accretion and mouth bar facies.

4.1.1 Case A

4.1.1.1 Method I

All the result in Method I was carried out using zonation approach with random simulation path (Figure 4.3). This method utilised four different TI for each of the zonations and azimuth map as additional input.

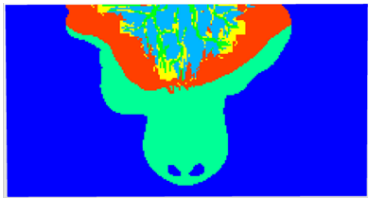

(a) Case A: 240th k-layer

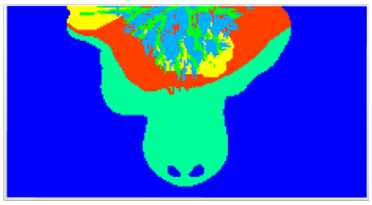

(b) Method I: realisation 1

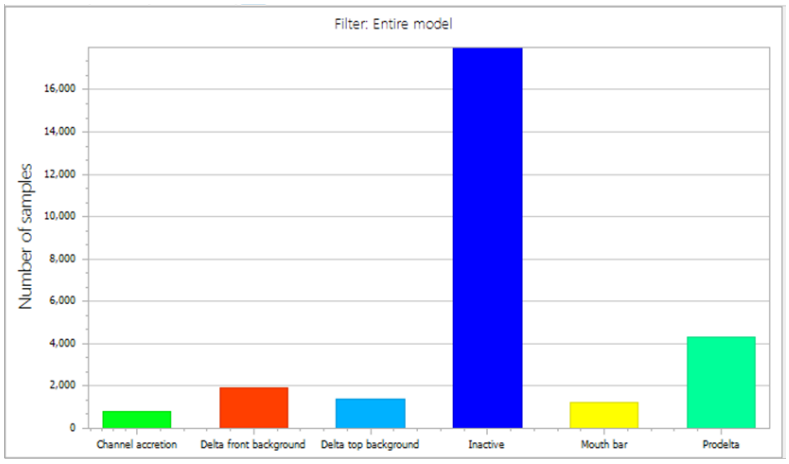

Histogram for facies of realisation 1

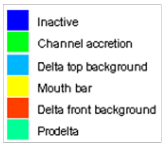

Legend for facies

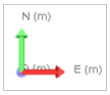

Figure 4.3. Unconditional simulation results from Case A and its facies' histogram using Method I.

As shown in Figure 4.3, results from Method I showed good continuity with the channel accretion facies, continued by the mouth bar facies advancing through the end of the channels. There were several dispersed delta front facies in the delta top zonation caused by the original mouth bar facies shown in the Delft3D model. On average, Method I delivered visually similar results to the original Delft3D model.

4.1.1.2 Method II

Method II was carried out using zonation approach and unilateral simulation path with -J+I direction (Figure 4.4). This method utilised four different TI for each of the zonations and azimuth map as additional input.

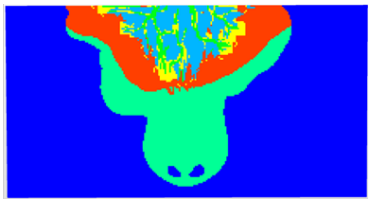

(a) Case A: 240th k-layer

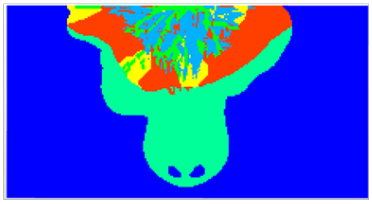

(b) Method II: realisation 1

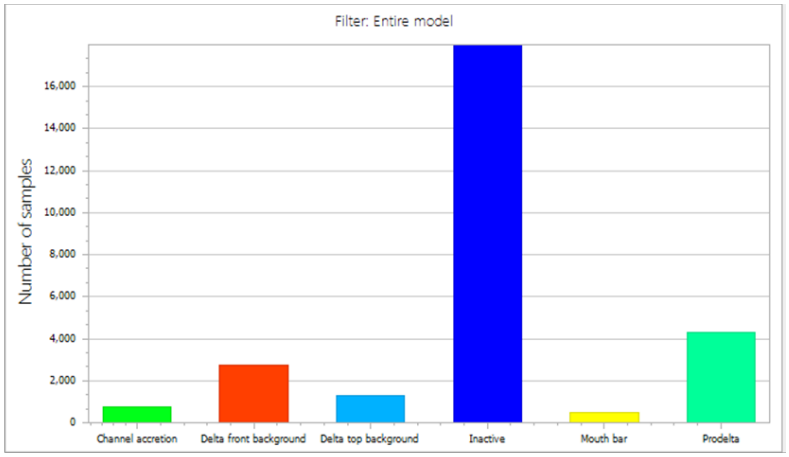

Histogram for facies of realisation 1

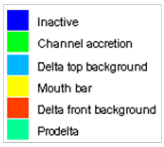

Legend for facies

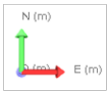

Figure 4.4. Unconditional simulation results from Case A and its facies' histogram using Method II.

Looking at Figure 4.4, it is apparent that the realisation from Method II were comparable to Method II and the original Deltf3D model. The channel continuity was good, and the mouth bar facies were constructed correctly in the end of the channel accretion facies. The dispersed delta front background facies was also found in Method II's realisations. In summary, a positive visual correlation was found between the Method II realisations and the original Delft3D model.

4.1.1.3 Method III

Method III simulated the TI using control map approach and random simulation path (Figure 4.5). This method only utilises single Delft3D k-layer as its TI with no additional input.

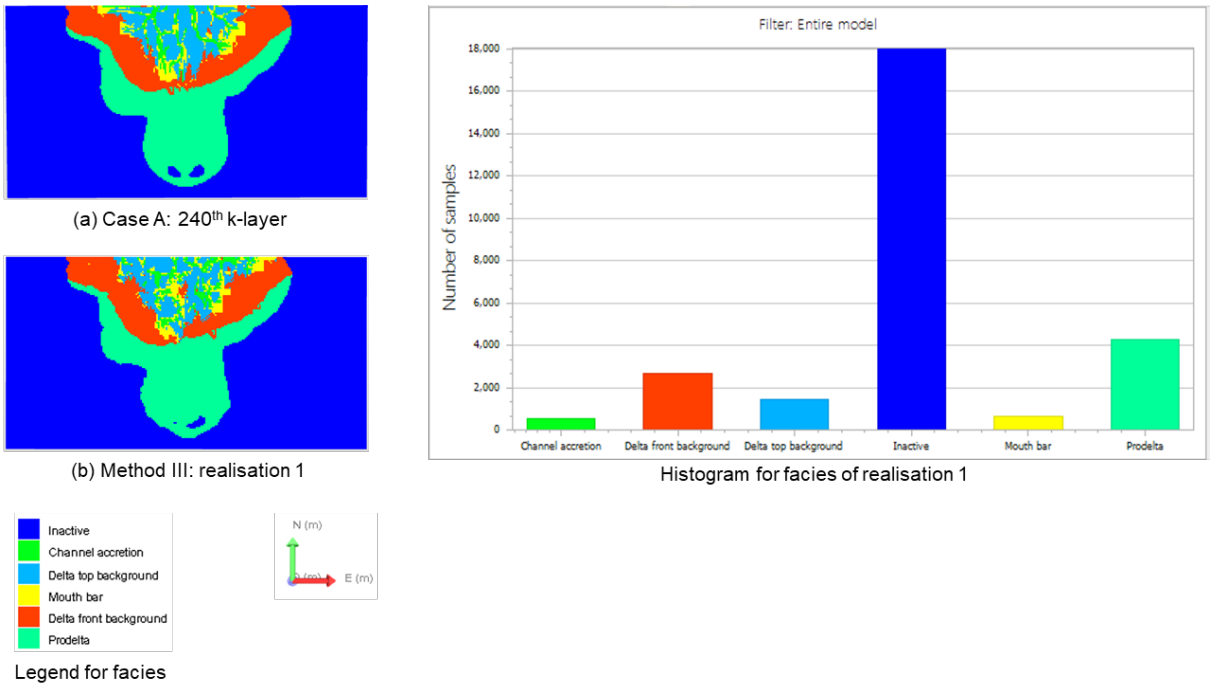

Figure 4.5. Unconditional simulation results from Case A and its facies' histogram using Method III.

As can be seen from the Figure 4.5 above, the realisation from Method III did not show any satisfactory channel continuity and the simulation of the mouth bar facies. Interestingly, there were also differences between the realisations of Method III with control map approach compared to Method I and Method II with zonation approach. Control map approach gave less smooth results compared to the zonation approach, and there were more artefacts found in the realisations. The findings clearly indicate that Method III had failed in mimicking the original Delft3D model.

4.1.1.4 Method IV

Method IV was performed using control map approach with unilateral simulation path in -J+I direction (Figure 4.6). This method only utilises single Delft3D k-layer as its TI with no additional input.

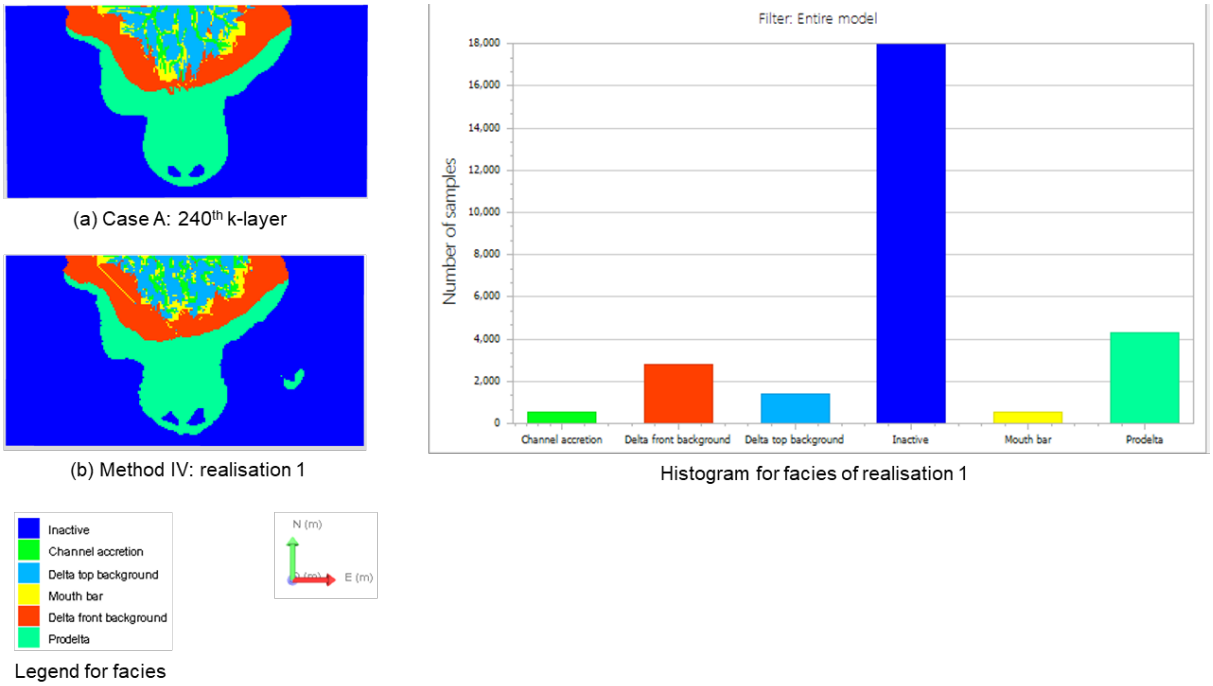

Figure 4.6. Unconditional simulation results from Case A and its facies' histogram using Method IV.

The difference between Method III and Method IV was significant. Compared to Method III, Method IV gave a more appealing results in using the control map approach. Method IV has successfully simulated the channel continuity owing to the unilateral simulation path, supported with the mouth bars that was recreated in the end of the channel accretion facies. These results suggest that Method IV with the combination of unilateral simulation path in control map approach had managed the nonstationarity well.

4.1.2 Case B

4.1.2.1 Method I

Using the zonation approach with random simulation path, Method I was conducted to the Case B with low repetition in the patterns. This method made use of four different TI in each zonations and azimuth map as additional input.

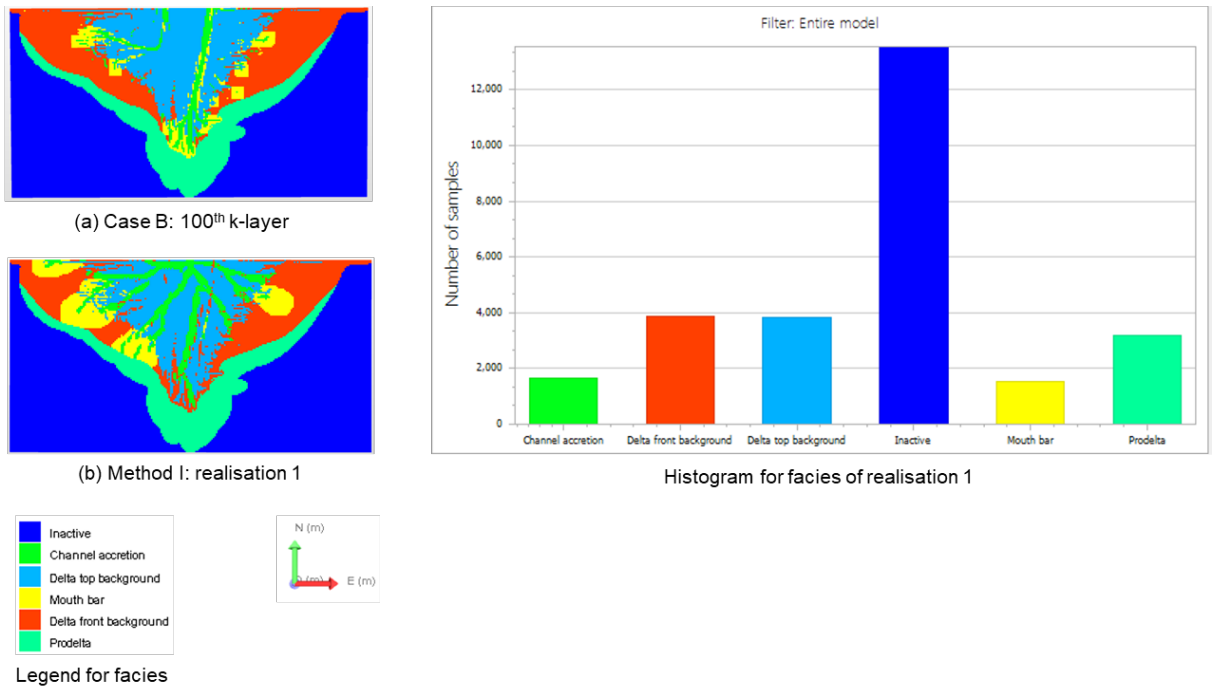

Figure 4.7. Unconditional simulation results from Case B and its facies' histogram using Method I.

The figure above illustrates the realisations from Method I. What stands out in the realisation is the channel accretion facies, where more proportions and much higher repetitions were created. While the channels were developing correctly where mouth bars facies were identifiable at the end of the channels, this method suffered from channel discontinuity.

4.1.2.2 Method II

Nonstationarity was being handled using Method II with zonation approach and unilateral -J+I path. This method employed four different TIs for each zonations and additional input of azimuth map.

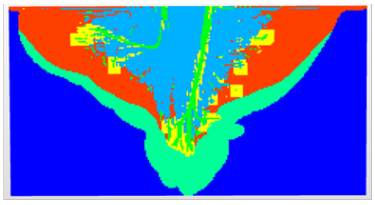

(a) Case B: 100th k-layer

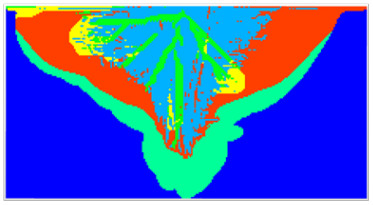

(b) Method II: realisation 1

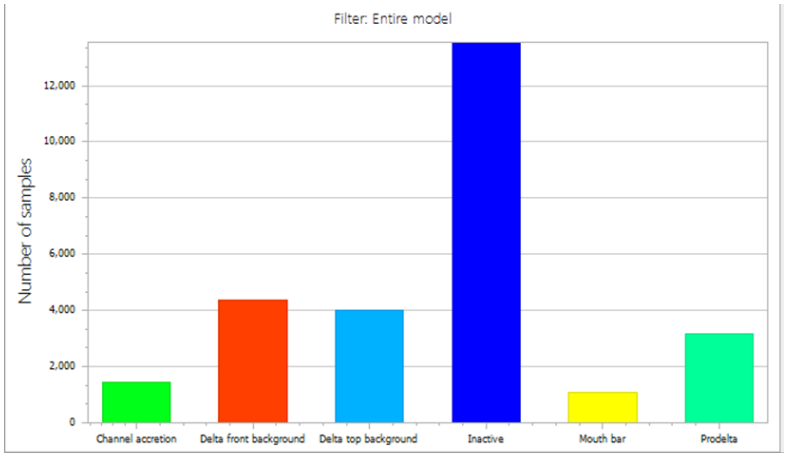

Histogram for facies of realisation 1

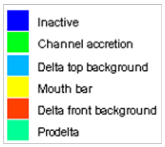

Legend for facies

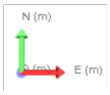

Figure 4.8. Unconditional simulation results from Case B and its facies' histogram using Method II.

Method II brought equivalent results to Method I, notably in the channels' patterns reproduction. Channels discontinuity was also found in the realisations. No significant similarity was found from this method to the original Delft3D model, that leads us to the incapability of the zonation map in delivering good results from the Case B with low repetition in the patterns.

4.1.2.3 Method III

Method III was carried out using control map approach and unilateral -J+I path. Single TI based on the original Delft3D data was used with no additional input in azimuth map.

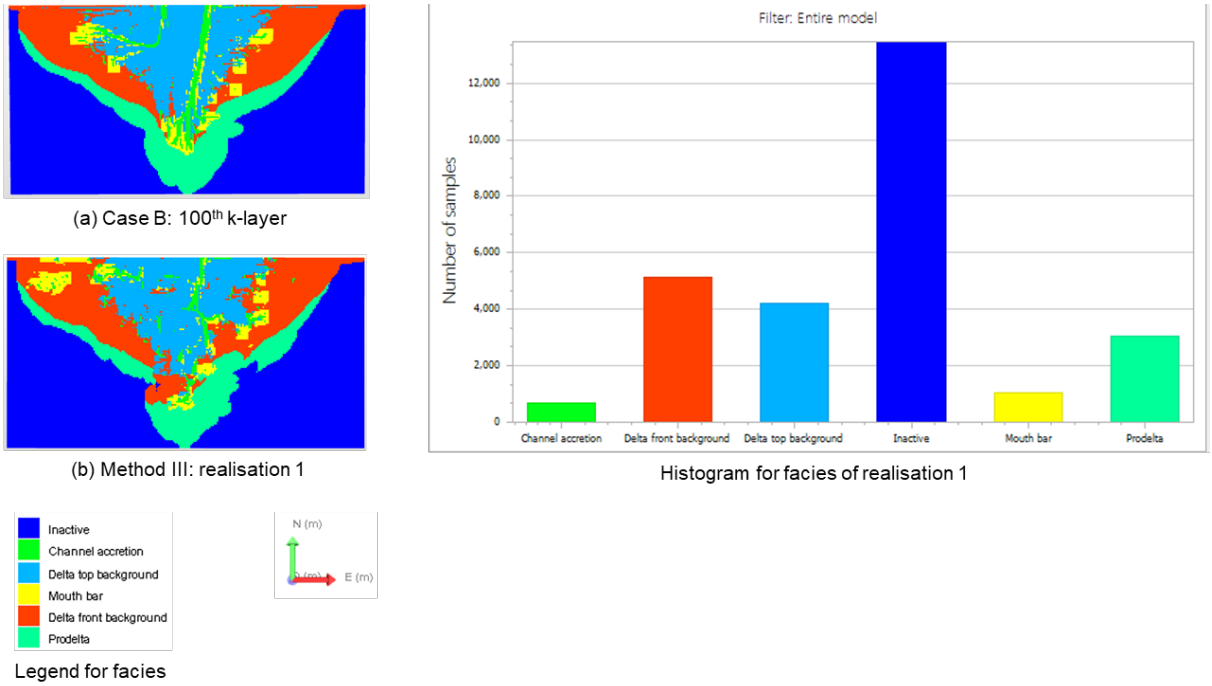

Figure 4.9. Unconditional simulation results from Case B and its facies' histogram using Method III.

From the realisation, it can be seen that Method III gave disorganised patterns in both of channels accretion facies and mouth bars. The boundaries between facies were roughly simulated and several artefacts were identified. But we can see from the realisation that the centre channel accretion facies was simulated, although it is disconnected. Overall, the combination of control map approach with random simulation path did not give favourable results to the simulation, so we see how the results were in using unilateral simulation path with Method IV, explained in the next section.

4.1.2.4 Method IV

Method IV simulated the single TI using control map approach and unilateral -J+I map. No additional input was introduced in azimuth map.

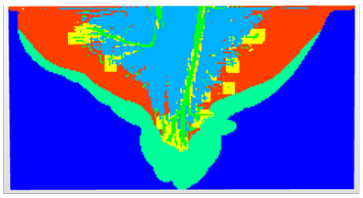

(a) Case B: 100th k-layer

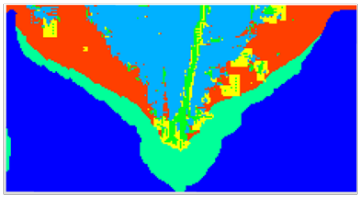

(b) Method IV: realisation 1

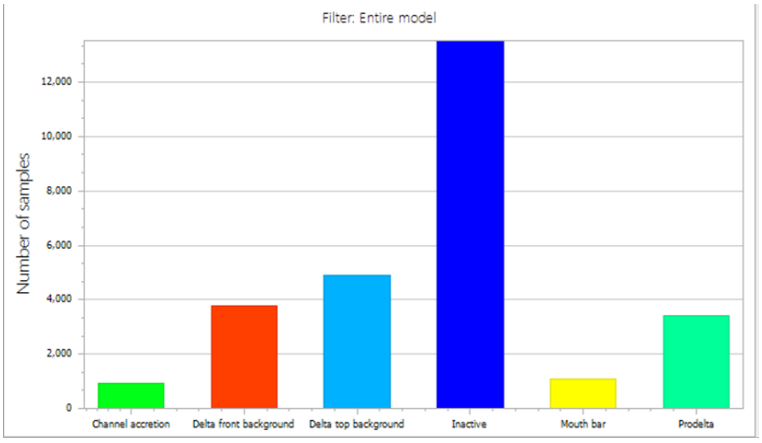

Histogram for facies of realisation 1

Legend for facies

Figure 4.10. Unconditional simulation results from Case B and its facies' histogram using Method IV.

The correlation of the realisations between Method IV and Method III is interesting because while using the same control map approach in the same Case B, the difference in the use of unilateral simulation path delivered proper results to the simulation. The main channel was simulated correctly with good continuity, at the same time keeping the boundaries between the facies reasonably smooth. Comparing those four methods in simulating Case B, only this method had successfully simulated the complete sandy deposit facies in low repetitive patterns.

4.1.3 Evaluation of the results

4.1.3.1 Visual inspection of Case A and Case B

In this evaluation, all the realisations from four methods for each Case A and Case B were assessed based on the features of the original Delft3D model, which are the continuity of the channels pattern, the recreation of the mouth bar facies in the end of the channel accretion facies, and the proportion of the patterns' repetition. The judgment of the visual inspection from the realisation is a decision of the geomodeler, so subjectivity of the geomodeler become the uncertainty in the evaluation. The appropriate methods in unconditional MPS simulation are important to determine which method that simulate the patterns correctly, and later to be used in the conditional MPS simulation.

In Case A, zonation approach represented in Method I and Method II delivered good results in recreating Delft3D patterns. The channels and mouth bar patterns were simulated similarly to the Delft3D model, along with proportion of the channel accretion facies. In the control map approach

of Method III and Method IV, only Method IV showed acceptable results in channels continuity. Together these results provide important insights to the acceptable methods in simulating TI with high repetitions, and they are Method I, Method II, and Method IV.

Case B showed pleasing results only in Method IV where the channels continuity was simulated correctly. The other methods revealed either poor continuity, a much higher facies proportion, or rough edges along the facies. Taken together, the methods that passed the visual inspection for Case B in low repetition patterns is only Method IV; nevertheless, Method III was tested next in the conditional results to see its conditional capability and be compared to Method IV within the same control map approach.

4.1.3.2 Connectivity function

By using MATLAB, connectivity function calculation was performed to analyse the similarity between the realisations of the methods and the TI from the original data of Delft3D simulation model. The comparations of the connectivity function in each method tested were to support the visual inspection.

The facies used in the analysis was the sandy deposit consisting of the combination between channel accretion facies and mouth bar facies. This was because the variation of the patterns lies in those two facies, so performing connectivity function in those facies would be the most appropriate way. The carried-out connectivity function calculation was on the north-south direction where the delta was developing.

In the connectivity function plot, the x-axis depicts the separation between the two locations in y-direction as lag distance (measured in pixels), and the y-axis shows the connectivity function defined as the probability of the connection between two locations. The similarity of the appearance of the connectivity function between the realisations and the TI represents the similarity of the sandy deposit's patterns between the results. For better visual representation, only 10 realisations were displayed in the plot.

4.1.3.2.1 Case A

It can be seen in the connectivity functions results through Figure 4.11 that in general, there was a variability in the plots between the TI and the realisations for all the methods. Some of the realisations managed to get a close similarity, visible in Method II and Method IV, while most of the realisations did not manage to get a reasonable similarity to the TI in Method I and Method III.

A distinct anisotropy, shown in the dissimilarity of the connectivity function of the TI and its realisations, was present amongst most of the realisations. Most of the anisotropy were at a lag distance above 10 pixels where the connectivity functions started to diverge. In higher lag distances, the plateau of connectivity function was reached with the value of 1 in some of the realisations in all approaches and paths, most prominent in Method IV that is zonation approach with the unilateral simulation path. Higher connectivity function in the higher lag distance where the TI's connectivity function had reached 0 means that the simulated realisations were able to simulate longer geobodies and better connectivity contrast to the TI's geobodies.

While there were no results that shown close similarity, Case A with high repetition in its patterns shown better similarity in connectivity function in Method II and Method IV, both made use of unilateral path as the simulation path.

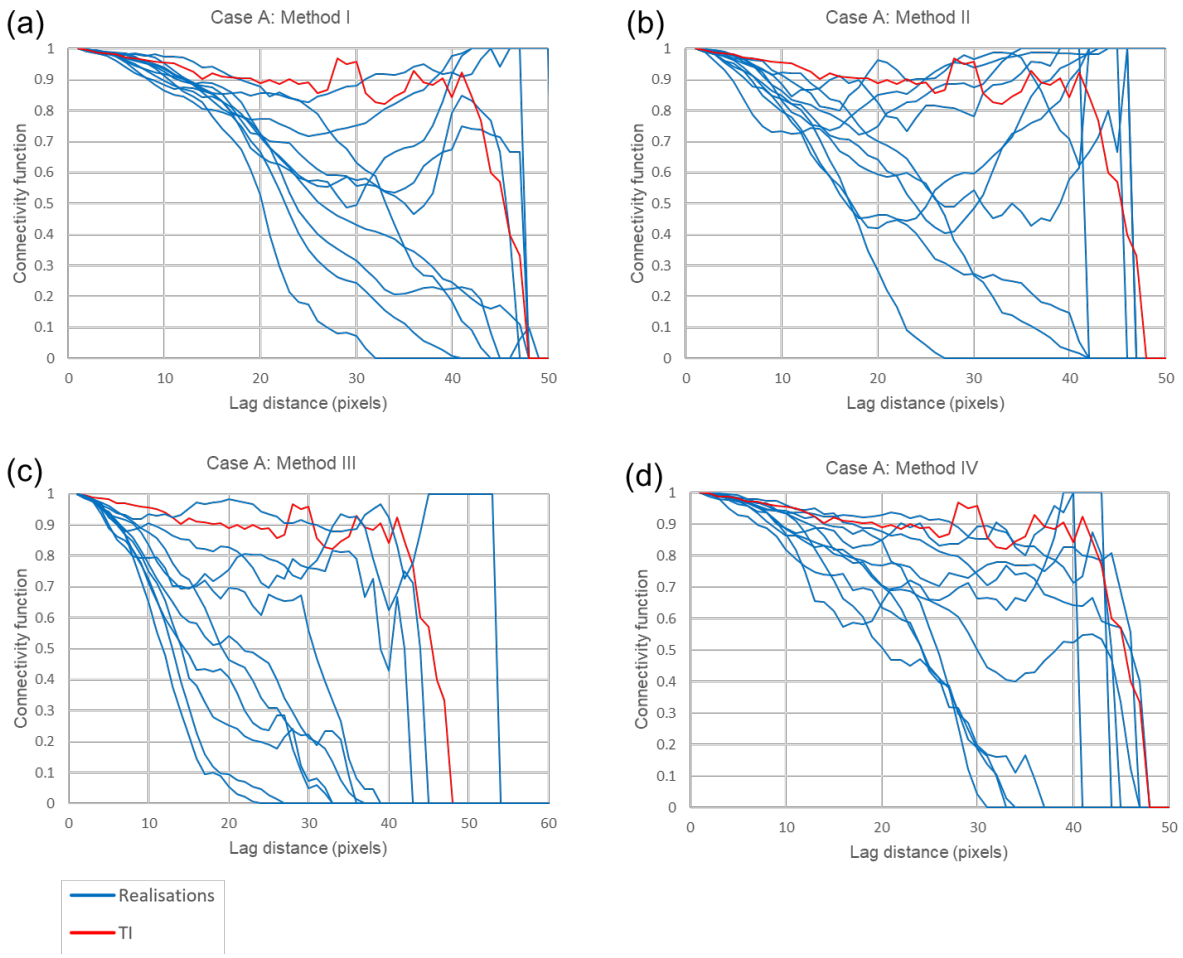

Figure 4.11. Connectivity function of Method I, Method II, Method III, and Method IV in Case A. The similarity of the connectivity function reflects good patterns' reproduction between realisations and TI. Only 10 realisations are displayed in the plot to show better visual representation.

4.1.3.2.2 Case B

In the evaluation of Case B with low repetition in sandy deposit's patterns through connectivity function, unilateral path as the simulation path revealed better results through Method II and Method IV as shown in Figure 4.12.

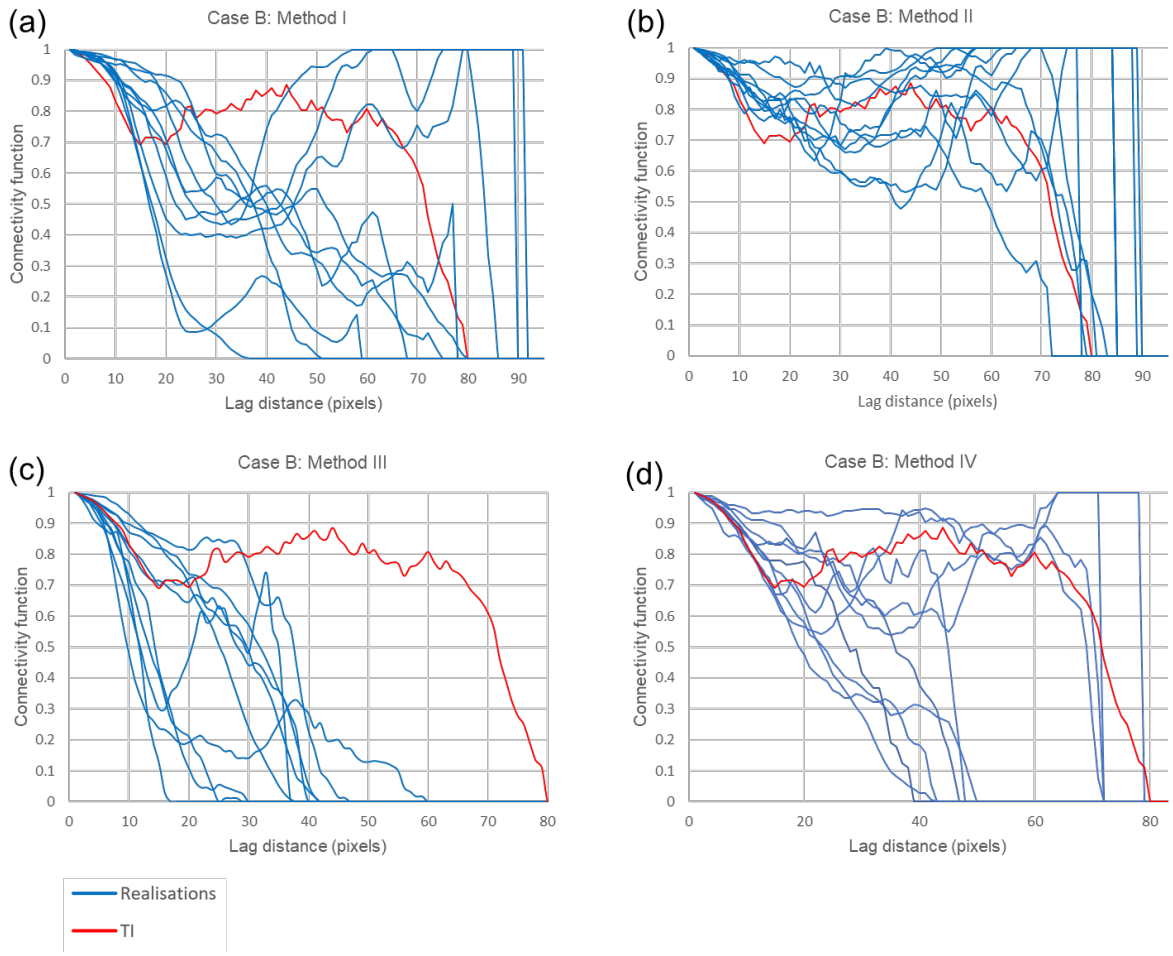

Figure 4.12. Connectivity function of Method I, Method II, Method III, and Method IV in Case B. The similarity of the connectivity function reflects good patterns' reproduction between realisations and TI. Only 10 realisations are displayed in the plot to show better visual representation.

In Method I and Method III, which were both using random simulation path, had failed to manage good connectivity. Method I depicts a high anisotropy with high divergence in connectivity function. In Method III, none of the realisations had succeeded in achieving similar connectivity function nor reached the same connectivity function as the TI.

The realisations in the Method III and Method IV appeared much better in connectivity function, while some of them also did not have the similar connectivity as the TI by reaching the value 0 before the lag distance achieved by the TI. The most interesting aspect of those two methods is in Method II, where the realisations achieved similar connectivity function with the TI. From its realisation (Figure 4.8), Method III is visually not similar to the original Delft3D data but managed to get good results in connectivity function. The connectivity function evaluates connectivity within the sandy deposit where in some cases like Method III supports good connectivity with the method but failed to mimic the patterns from the TI.

The results from connectivity function in Case B with low repetition in the patterns had shown that the unilateral simulation path in Method II and Method IV succeeded in reproducing low repetition

in patterns and delivered better connectivity compared to random simulation path in Method I and Method III.

4.1.4 Summary of the unconditional MPS simulation results

After performing all the unconditional results using Method I-IV and evaluating the results using visual inspection and connectivity function, this study has identified the applicable method to handle nonstationarity in unconditional MPS simulations using Delft3D simulation model data. The chosen methods were based from the visual inspection where the facies were simulated correctly and similar to the original Delft3D data, and also supported by the connectivity function:

- In Case A with high repetition in the patterns, the good results from visual inspection were obtained from Method I (zonation approach with random simulation path), Method II (zonation approach with unilateral simulation path), and Method IV (control map approach with unilateral simulation path). Those methods have succeeded in simulating distributary channels in channel accretion facies and its sandy mouth bar in the mouth bar facies, added with the acceptable similarity of the patterns.
- In Case B with low repetition in the patterns, Method IV (control map approach with unilateral simulation path) had passed the visual inspection. Although only Method IV had managed to get a good continuity within the channels, Method III (control map approach with random simulation path) was included in the next simulation and evaluation to be a comparison with the Method IV.
- All of the connectivity function calculation results had a range of variability between the TI and the realisations, shown with diverging connectivity functions in the plots. The use of unilateral simulation path in MPS simulation showed better connectivity for the sandy deposit compared to the random simulation path and succeeded to simulate Case B combined with control map approach.

4.2 Conditional MPS simulation results

Having conducted the unconditional MPS simulation and evaluated the method through visual inspection and connectivity function analysis, we have acquired acceptable methods in mimicking the patterns in Delft3D model. Those method will be tested in conditional MPS simulation using dense and sparse hard data for both Case A and Case B to evaluate the conditional capabilities using hard data:

- Case A
    - Method I, zonation approach with random simulation path
    - Method II, zonation approach with unilateral -J+I simulation path
    - Method IV, control map approach with unilateral -J+I simulation path
- Case B
    - Method III, control map approach with random simulation path
    - Method IV, control map approach with unilateral -J+I simulation path

4.2.1 Case A

4.2.1.1 Method I

Method I used zonation approach with random simulation path. The inputs were the same as the unconditional simulations, where four different TIs were used with azimuth map as the additional input.

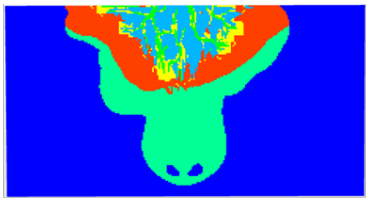

(a) Case A: 240th k-layer

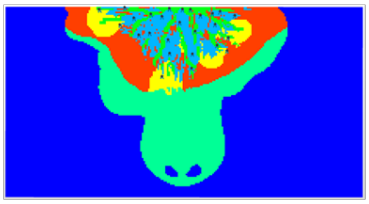

(b) Method I: realisation 1 with dense hard data

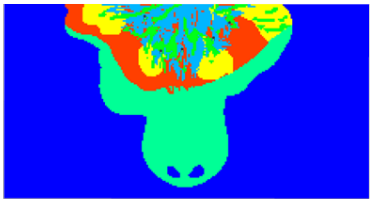

(c) Method I: realisation 1 with sparse hard data

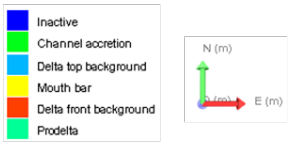

Legend for facies

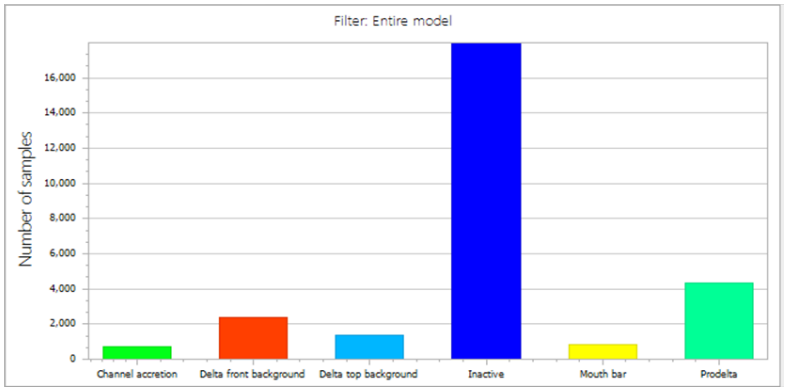

Histogram for facies of realisation 1 with dense hard data

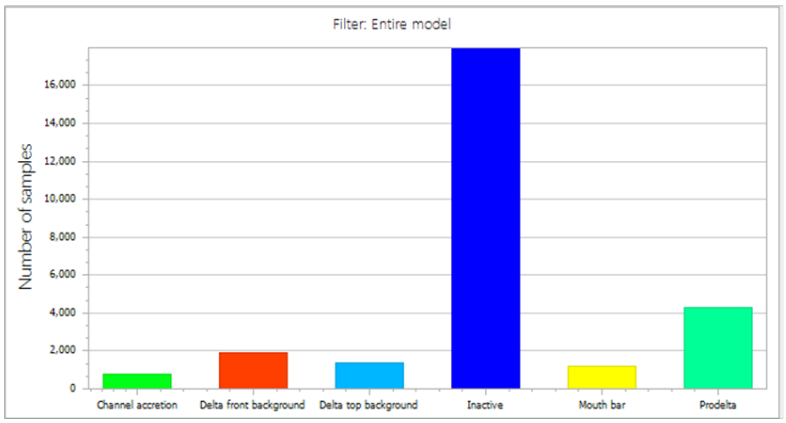

Histogram for facies of realisation 1 with sparse hard data

Figure 4.13. Conditional simulation results from Case A using Method I.

As shown in Figure 4.13, the results in using dense and sparse data were visually similar. Closer inspection of the channel accretion facies revealed that there was more discontinuity in the sparse hard data. Other than that, both of the hard data distribution contributes to the conditional MPS simulation performance.

4.2.1.2 Method II

Method II incorporated zonation approach with unilateral -J+I path in four different TIs in each zonations. Azimuth map as rotation was used as additional input data.

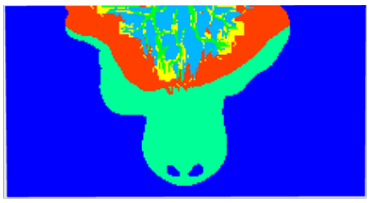

(a) Case A: 240th k-layer

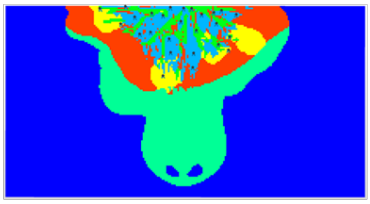

(b) Method II: realisation 1 with dense hard data

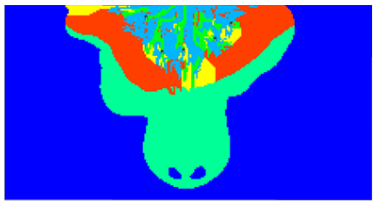

(c) Method II: realisation 1 with sparse hard data

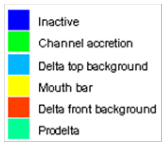

Legend for facies

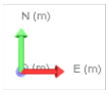

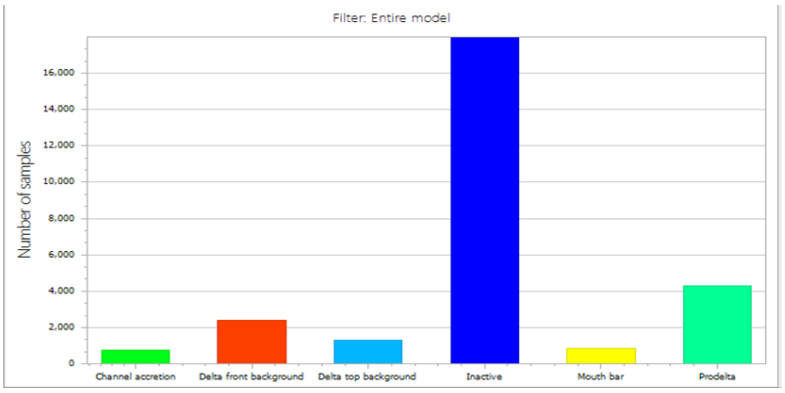

Histogram for facies of realisation 1 with dense hard data

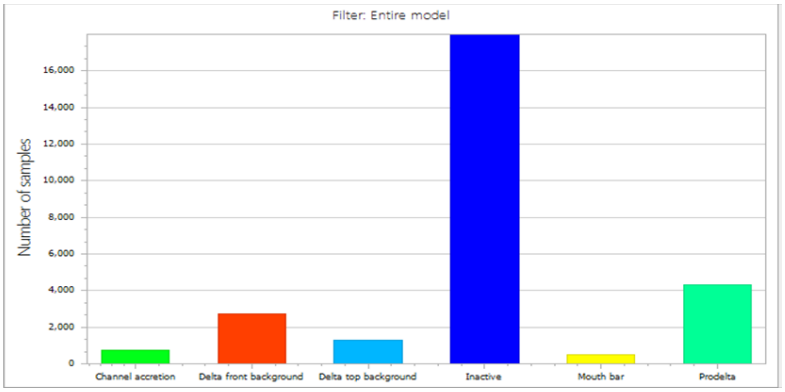

Histogram for facies of realisation 1 with sparse hard data

Figure 4.14. Conditional simulation results from Case A using Method II.

The capability of unilateral simulation path had shown its shortcomings, strikingly in the sparse hard data realisations. It is apparent from Figure 4.14 that more discontinuity had appeared in the channel accretion facies in sparse hard data. In the other hand, there was no problem in mimicking the Delft3D patterns using dense hard data.

4.2.1.3 Method IV

Using the control map with unilateral -J+I path, Method IV was performed to Case A with both dense and sparse data. Single TI from the original Delft3D simulation model data was used, and the results were expressed in realisations for each hard data distribution.

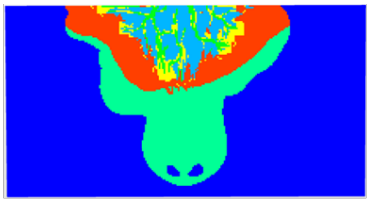

(a) Case A: 240th k-layer

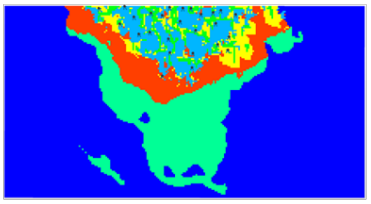

(b) Method IV: realisation 1 with dense hard data

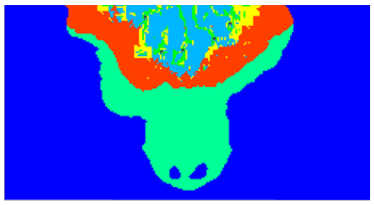

(c) Method IV: realisation 1 with sparse hard data

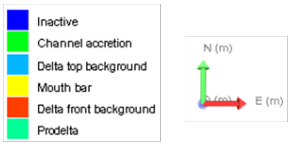

Legend for facies

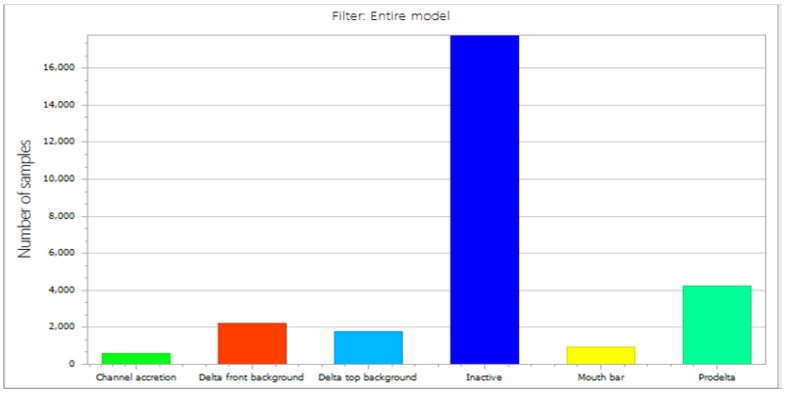

Histogram for facies of realisation 1 with dense hard data

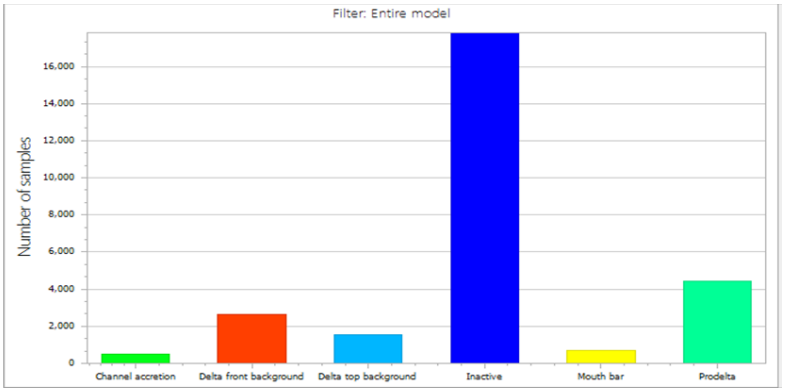

Histogram for facies of realisation 1 with sparse hard data

Figure 4.15. Conditional simulation results from Case A using Method IV.

As Figure 4.15 shows, there is an indicative difference between conditional and unconditional MPS simulations of Method IV. In conditional simulations, the appearance of the facies' patterns was disordered, particularly in the case with dense hard data. The prodelta facies in dense hard data gave the chaotic patterns with artefacts that was not found in sparse hard data or unconditional MPS simulations. In terms of the channel continuity, both dense and sparse hard data struggled to achieve good continuity.

4.2.2 Case B

4.2.2.1 Method III

Method III simulated the single TI based on the Delft3D model data with using control map and random simulation path. There was no additional azimuth required in the simulation.

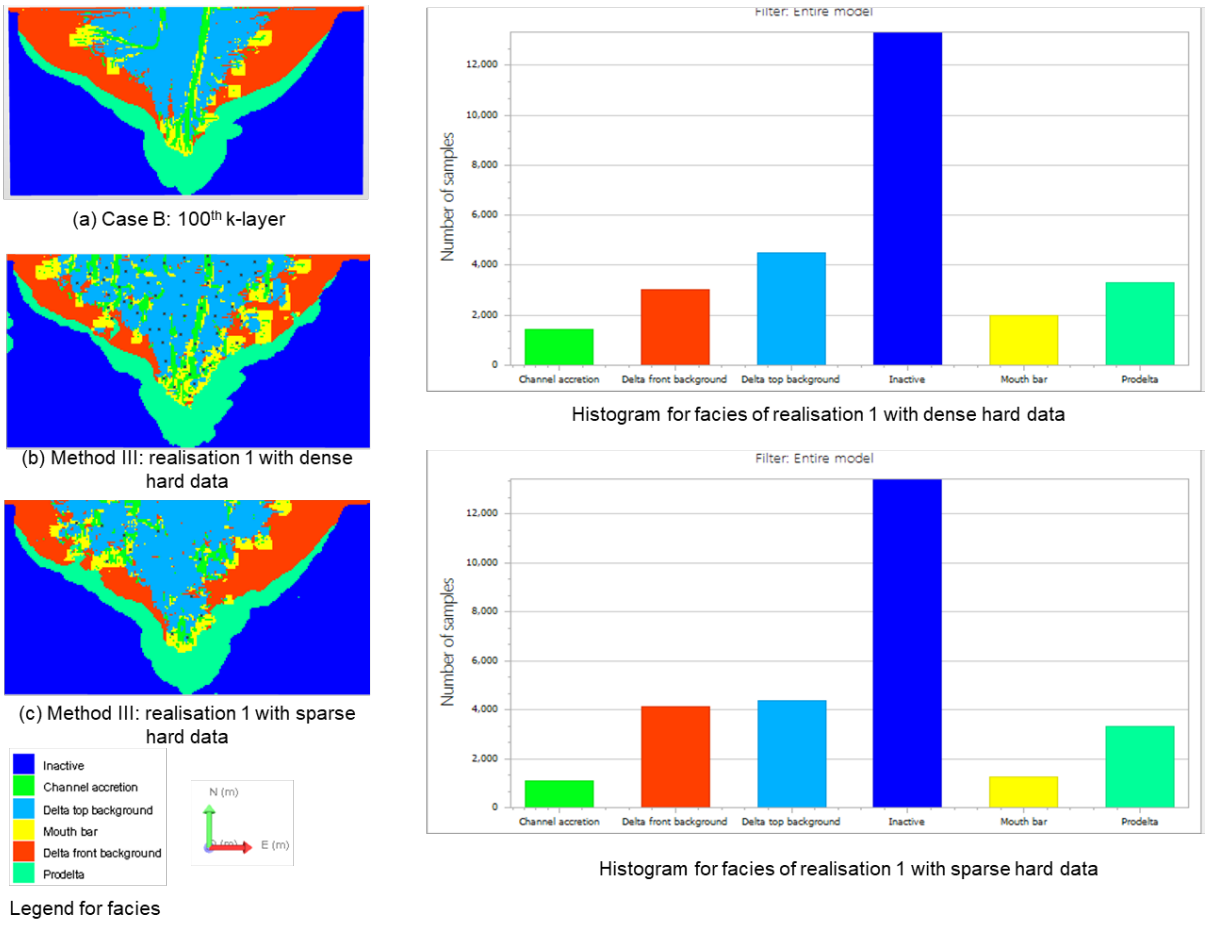

Figure 4.16. Conditional simulation results from Case B using Method III.

From this Figure, we can see that Method III resulted in poor channels continuity from the channel accretion facies. Dense hard data did not make the continuity better, and it was more discontinued in the sparse hard data. There was also a tendency in making the main channel in the centre in the dense hard data. The results expressed that random simulation path strived in giving continuity of the channels' pattern.

4.2.2.2 Method IV

Method IV conditionally simulated the single TI from Delft3D simulation model with control map in unilateral -J+I path. Realisations were represented for dense hard data and sparse hard data.

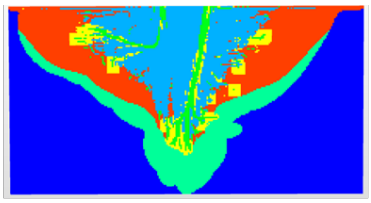

(a) Case B: 100th k-layer

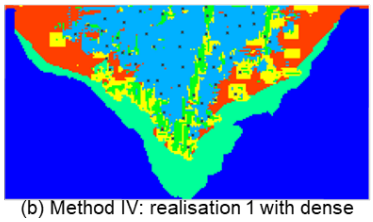

(b) Method IV: realisation 1 with dense hard data

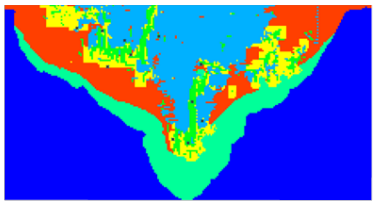

(c) Method IV: realisation 1 with sparse hard data

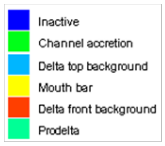

Legend for facies

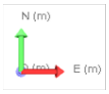

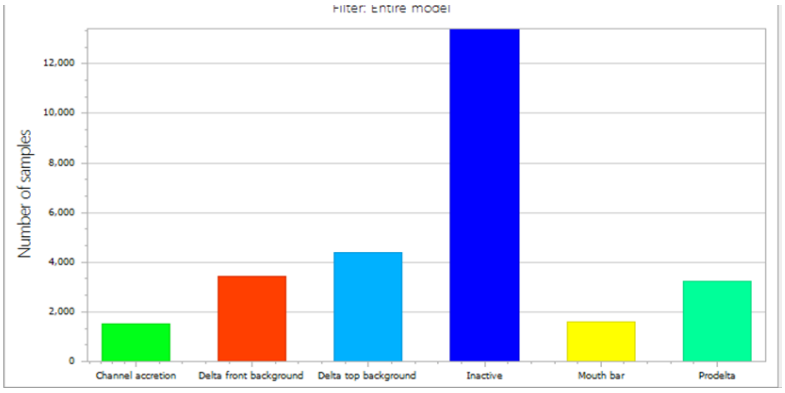

Histogram for facies of realisation 1 with dense hard data

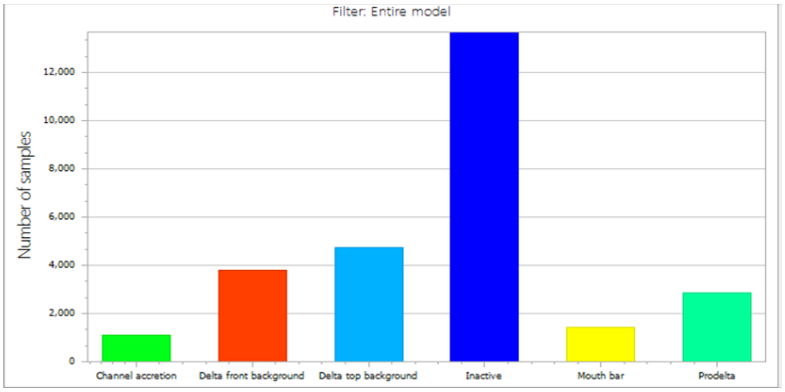

Histogram for facies of realisation 1 with sparse hard data

Figure 4.17. Conditional simulation results from Case B using Method IV.

The results from conditional simulation using Method IV is revealing in several ways. First, unlike the other methods, this method had successfully stochastically simulated channel continuity with low repetitions. The realisations, shown in Figure 4.17, had channels simulated from north to south. Trouble in simulating the channel was apparent in Figure 4.17c where the channels was finally simulated after had encountered the hard data, leaving delta top background in cells in the north side of the grid.

4.2.3 Evaluation of the results

4.2.3.1 Connectivity function

4.2.3.1.1 Case A

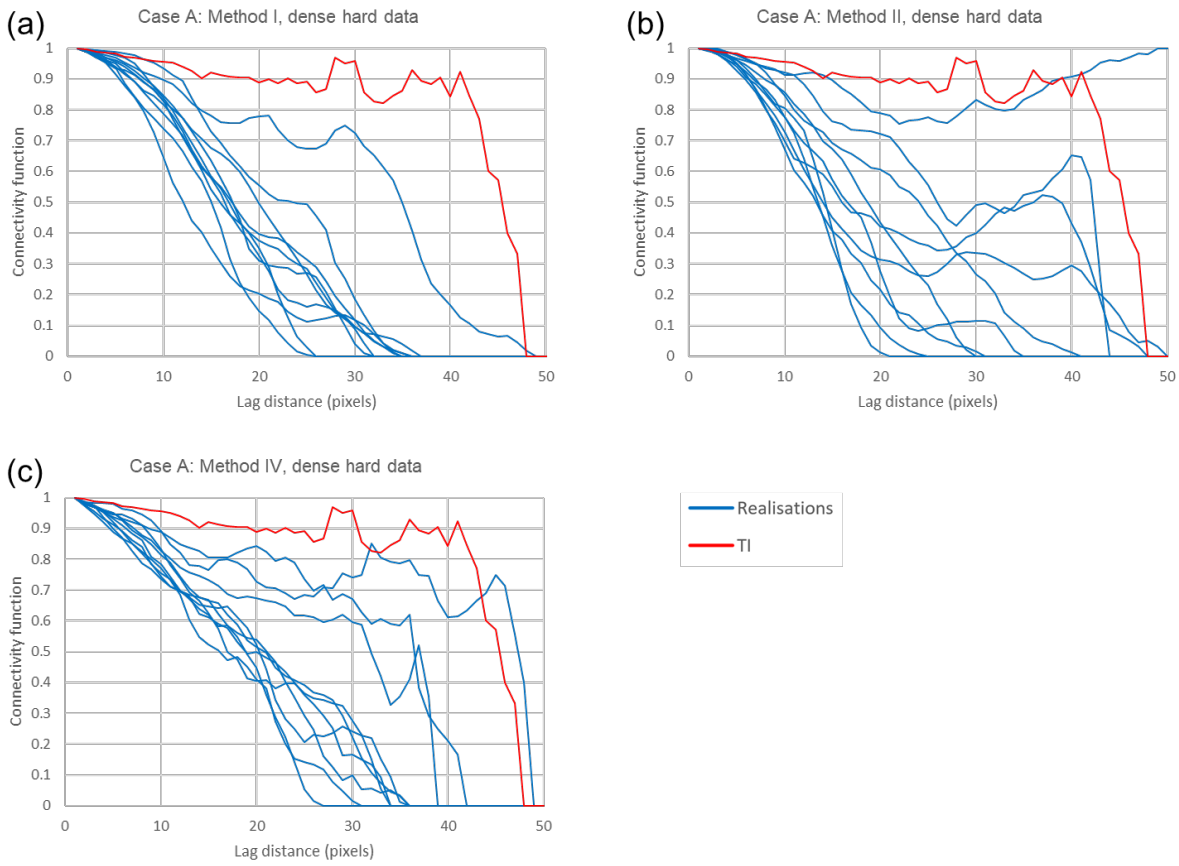

Figure 4.18. Connectivity function of Method I, Method II, and Method IV in Case A with dense hard data. The similarity of the connectivity function reflects good patterns' reproduction between realisations and TI. Only 10 realisations are displayed in the plot to show better visual representation.

Interestingly, in overall judging from the connectivity results in Figure 4.18 where the dense hard data were applied in Case A, the realisations has lower connectivity compared to its TI. Unilateral simulation path results in Method II and Method IV has higher connectivity in contrast to the random simulation path in Method I.

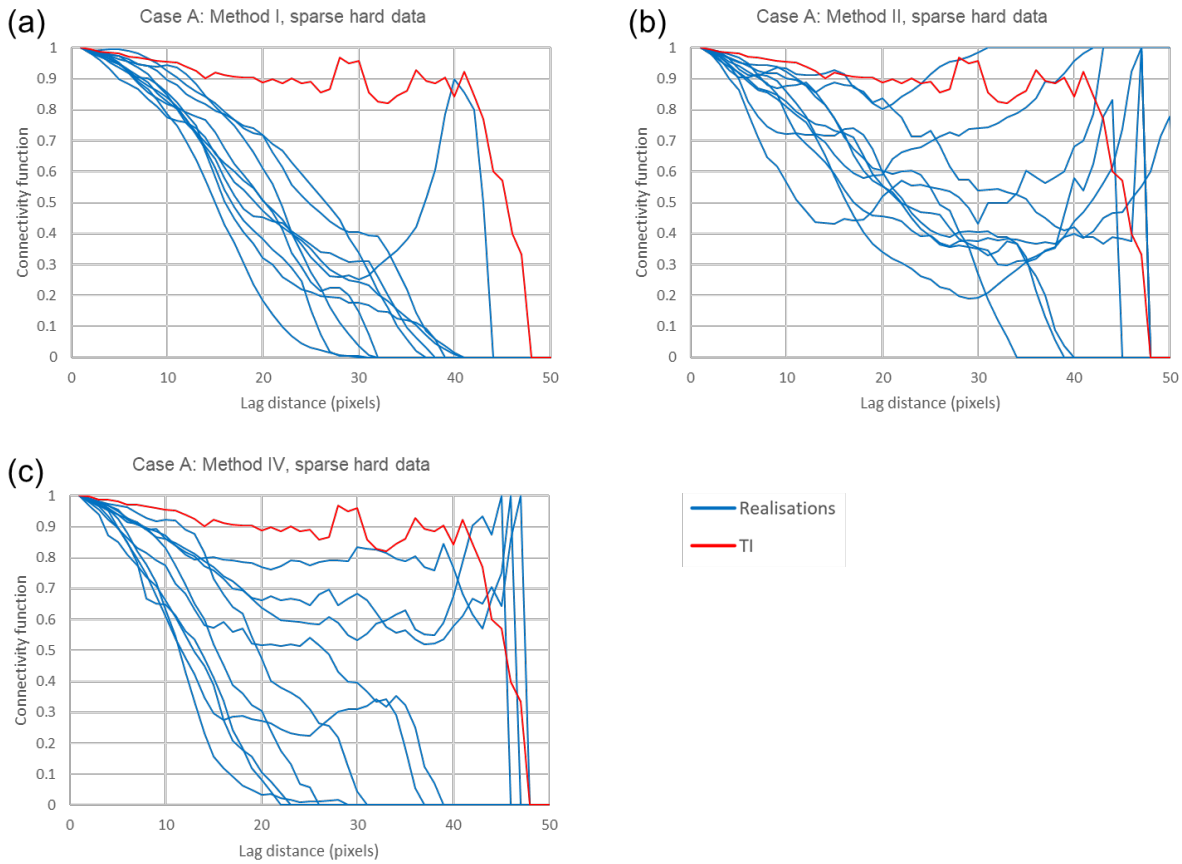

Figure 4.19. Connectivity function of Method I, Method II, and Method IV in Case A with sparse hard data. The similarity of the connectivity function reflects good patterns' reproduction between realisations and TI. Only 10 realisations are displayed in the plot to show better visual representation.

The results from Case A using sparse hard data again shown better connectivity in unilateral simulation path in Method II and Method IV (Figure 4.19). Random simulation path shown in Method I reflects low connectivity where MPS simulation with random simulation path struggled to simulate channels' patterns in sparse data. From Method II and Method IV with unilateral simulation path, connectivity function of the realisations has the tendency to increase in higher lag distance, especially in Method II with zonation approach.

Taken together, these results suggest that there is an association between better connectivity with unilateral simulation path in conditional MPS simulation, for both dense and sparse hard data distribution. Correlated with the unconditional MPS simulation, the presence of hard data decreases the overall connectivity in the realisations.

4.2.3.1.2 Case B

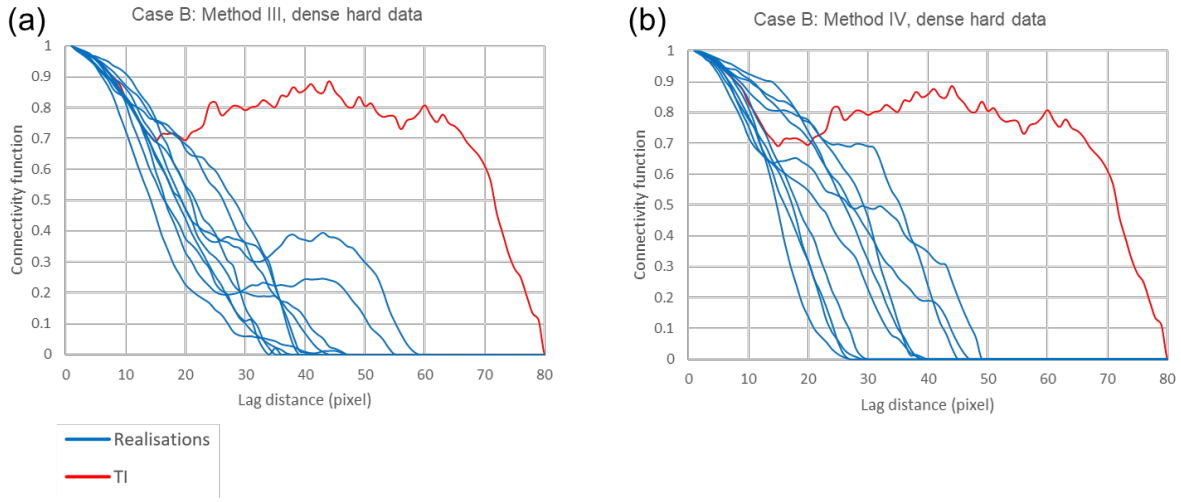

Figure 4.20. Connectivity function of Method III and Method IV in Case B with dense hard data. The similarity of the connectivity function reflects good patterns' reproduction between realisations and TI. Only 10 realisations are displayed in the plot to show better visual representation.

Similar to Case A, testing the connectivity of conditional MPS simulation of Case B has shown much lower connectivity in the realisations. Figure 4.21 shows clearly that none of the realisations has similar connectivity function compared to the TI, with all of them showing low connectivity.

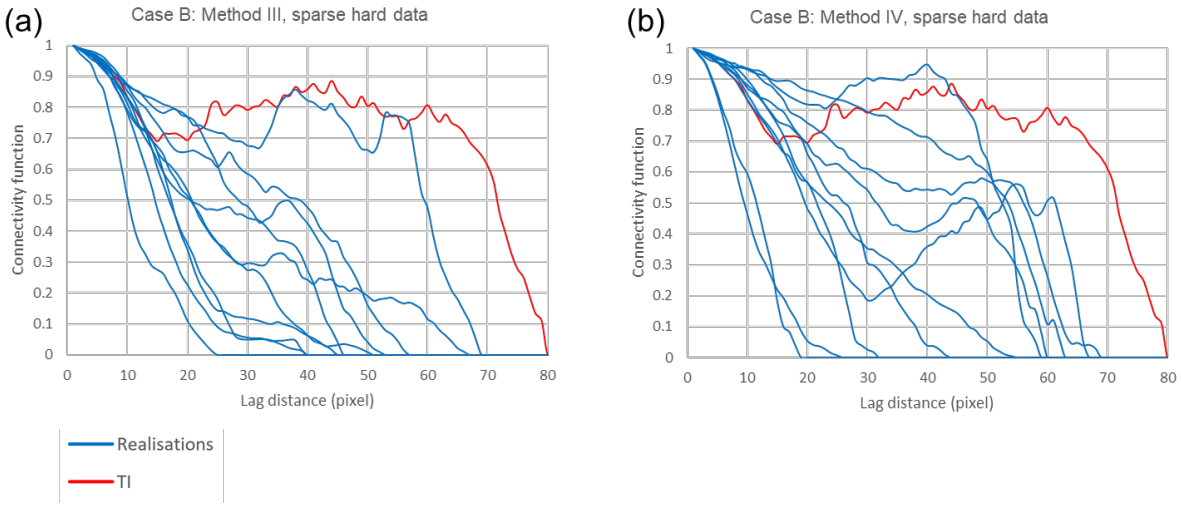

Figure 4.21. Connectivity function of Method III and Method IV in Case B with sparse hard data. The similarity of the connectivity function reflects good patterns' reproduction between realisations and TI. Only 10 realisations are displayed in the plot to show better visual representation.

In Figure 4.21 with sparse hard data, lower connectivity is again depicted in the realisations' connectivity function. The absence of the connectivity function that has high similarity with the TI has shown that the MPS struggled in conditionally simulating patterns with low repetition. The results

indicate that in conditionally simulating Case B with low repetitive patterns will give lower connectivity in the realisations, for both dense and sparse distribution of hard data.

4.2.3.2 E-type and conditional variance models of Case A

E-type model represented the local average (expected value) of the realisations tested, while conditional variance model measured the variance of the realisations as well. Both models were constructed from 50 realisations in each method.

4.2.3.2.1 Method I

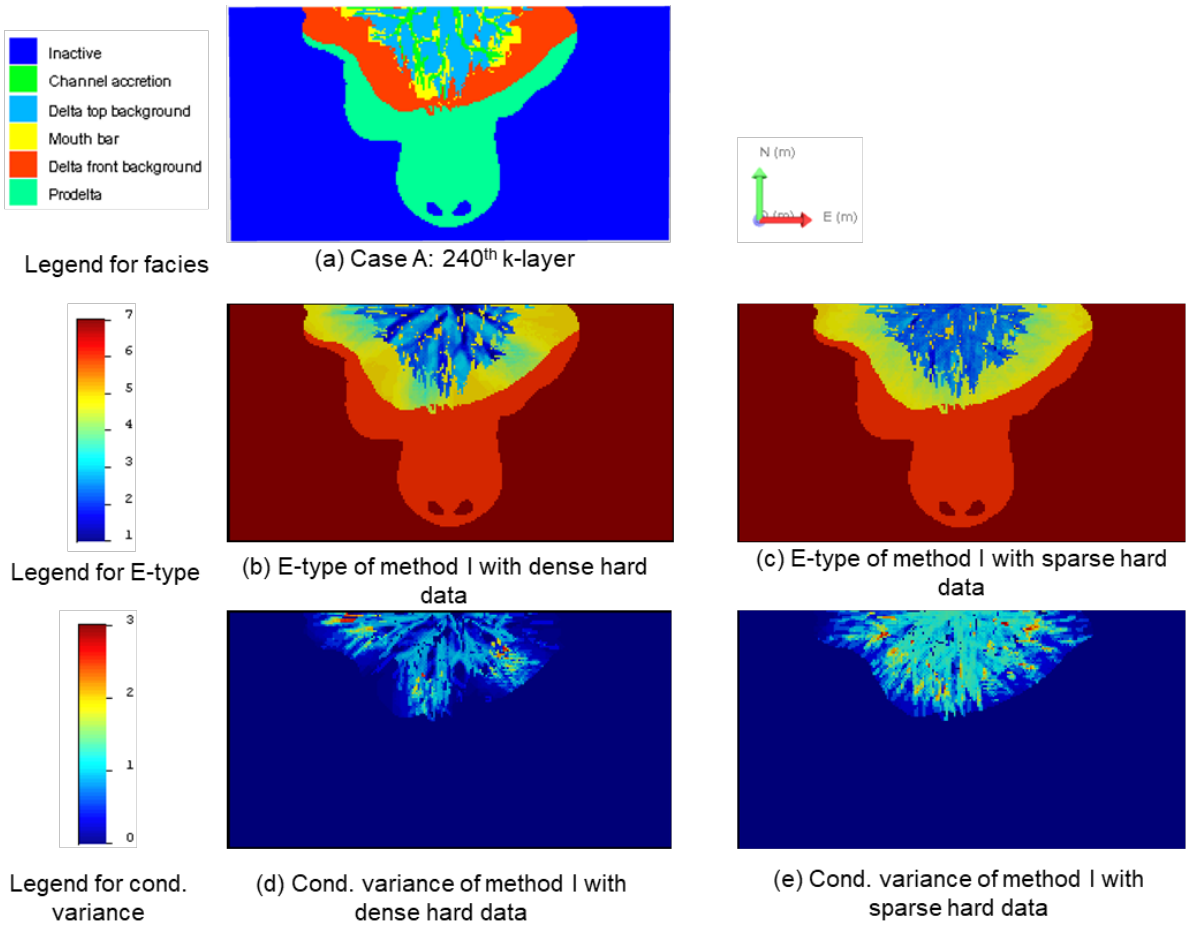

Figure 4.22. E-type and conditional variance models of Method I for conditional MPS simulations in Case A. The channels accretion facies in the E-type model was shown by the value of 1.

Dense hard data distribution in conditional MPS simulation using Method I (zonation approach with random simulation path) tend to simulate the patterns in specific location. In contrast, sparse hard data E-type and conditional variance models revealed smooth expressions, showing insignificant trend in patterns reproduction. The value 0 in the location of the hard data revealed the quality of the conditional capability with Method I.

4.2.3.2.2 Method II

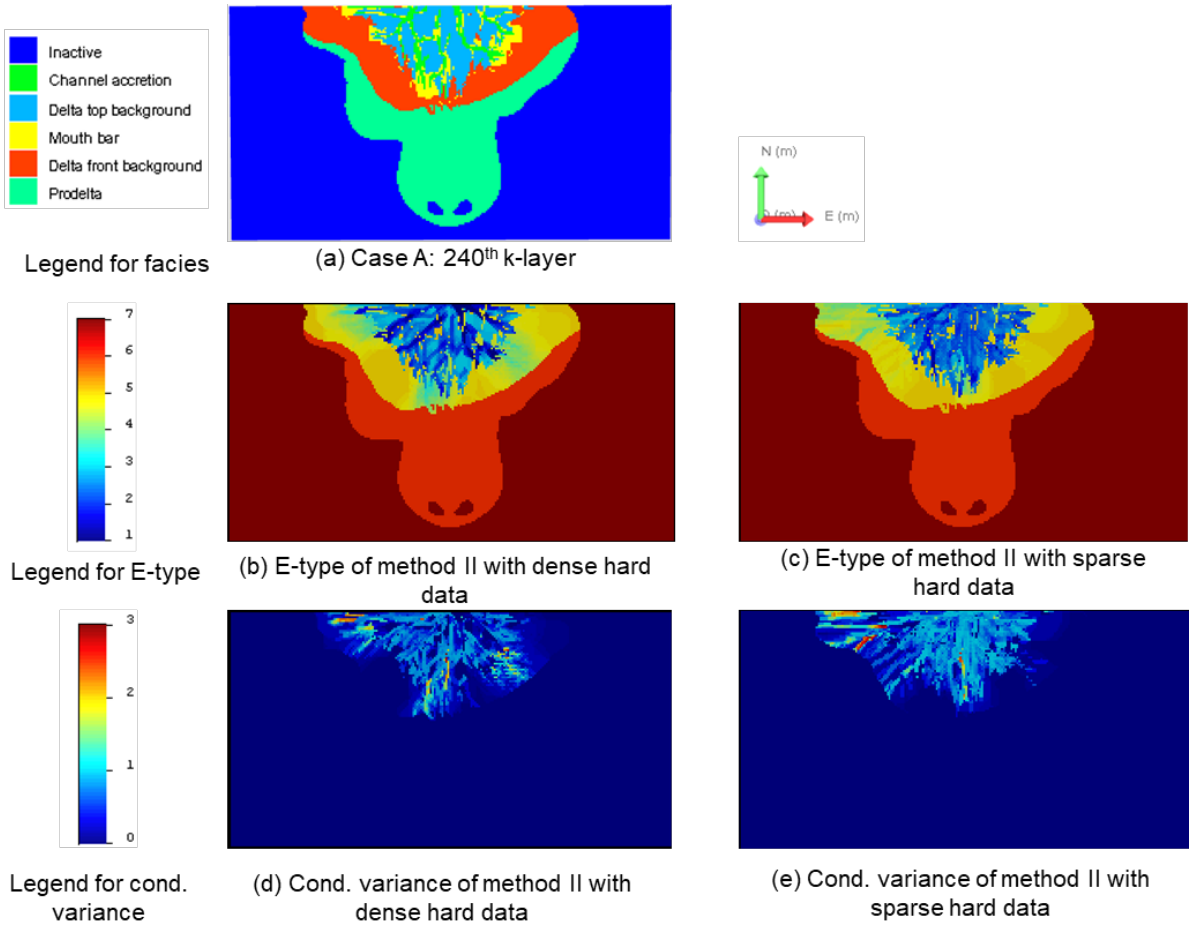

Figure 4.23. E-type and conditional variance models of Method II for conditional MPS simulations in Case A. The channels accretion facies in the E-type model was shown by the value of 1.

Both Method II (zonation approach with unilateral simulation path) and Method I (zonation approach with random simulation path) share a similarity in the E-type and conditional variance models. Dense hard data gave inclination in creating particular patterns, where sparse hard data did not give any tendency by showing smooth appearance in the models.

4.2.3.2.3 Method IV

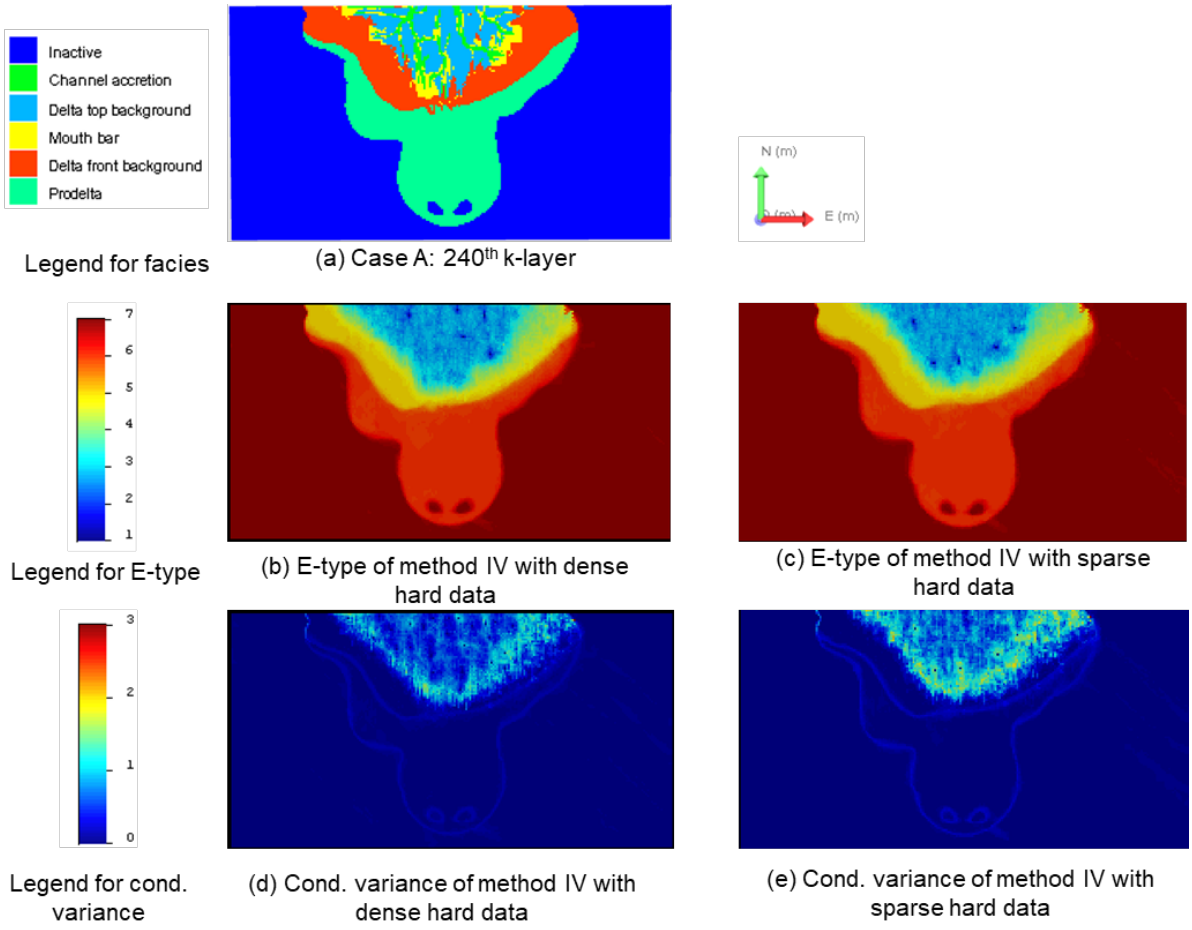

Figure 4.24. E-type and conditional variance models of Method IV for conditional MPS simulations in Case A. The channels accretion facies in the E-type model was shown by the value of 1.

In contrast to the Method I and Method II where using zonation approach, Method IV in using control map approach with unilateral simulation path did not show any significant trend in the results of E-type and conditional variance models. Both of the E-type were smooth, supported by the variance where there was a number of variance across the simulation grid, even in the dense hard data simulation.

4.2.3.3 E-type and conditional variance models of Case B

4.2.3.3.1 Method III

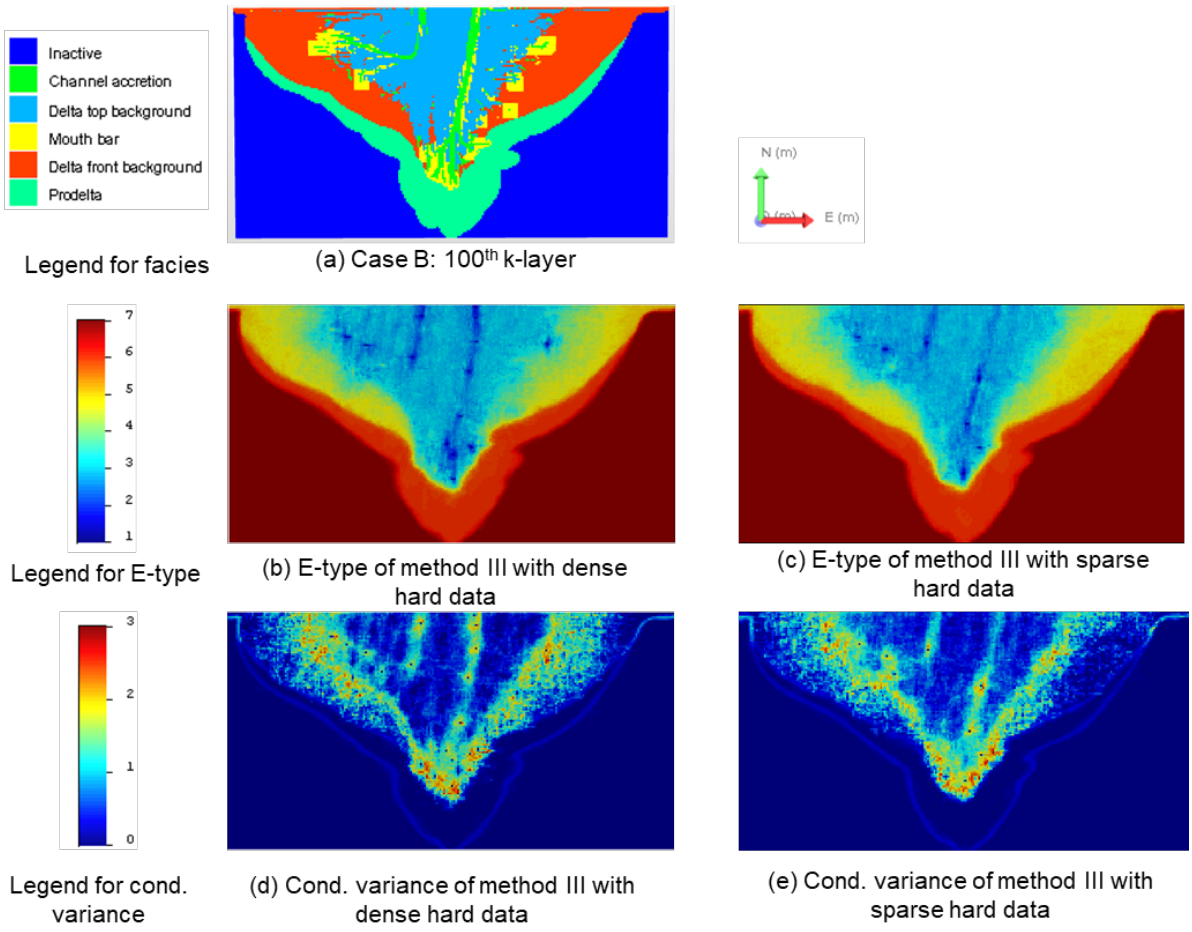

Figure 4.25. E-type and conditional variance models of Method III for conditional MPS simulations in Case B. The channels accretion facies in the E-type model was shown by the value of 1.

In Method III (control map approach with random simulation path), we can see the trend in E-type and conditional variance for the two channels in Case B with low patterns' repetition. Discontinuity of the results were apparent for both the hard data distribution, supporting the poor continuity in the conditional MPS simulation results.

4.2.3.3.2 Method IV

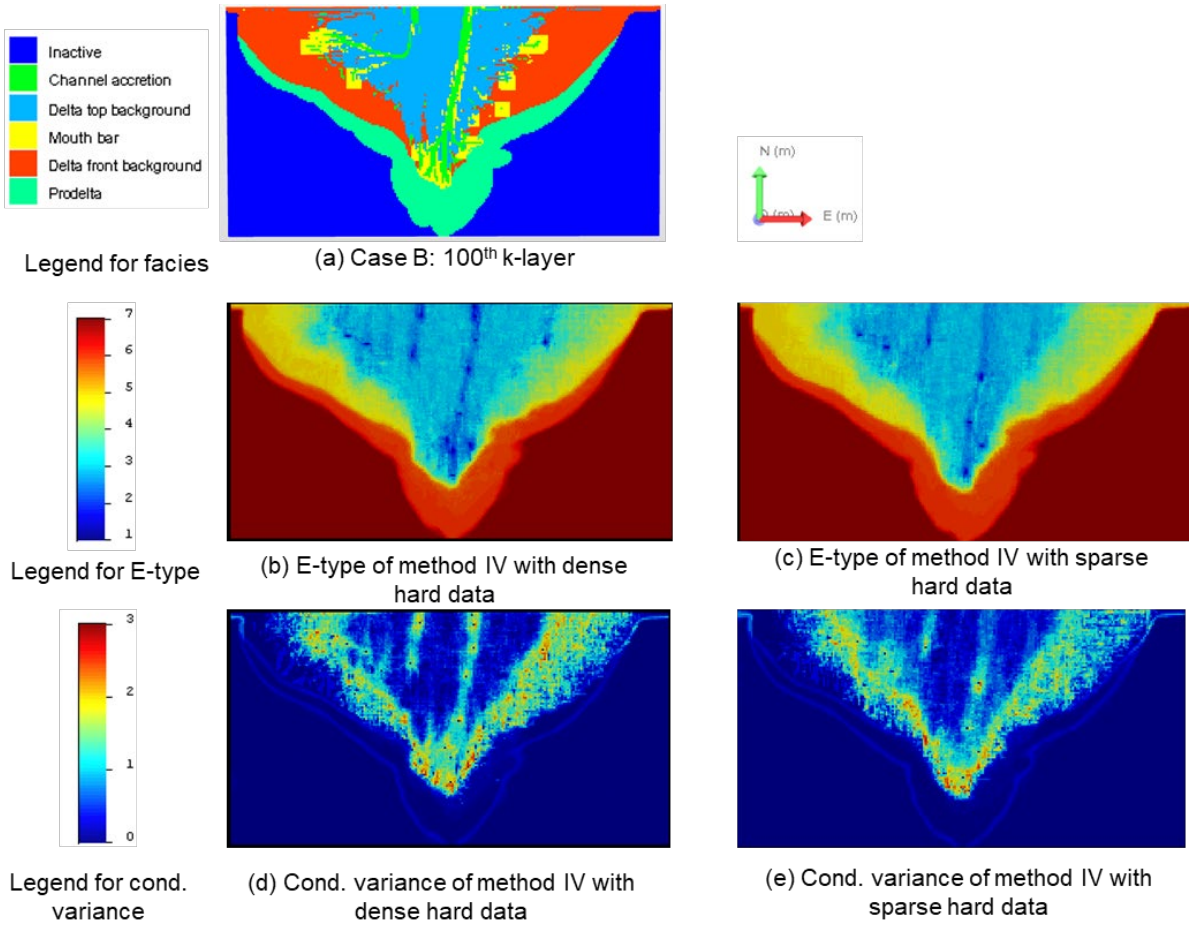

Figure 4.26. E-type and conditional variance models of Method IV for conditional MPS simulations in Case B. The channels accretion facies in the E-type model was shown by the value of 1.

Compared to the E-type and conditional variance models of Method III (control map approach with random simulation path), Method IV (control map approach with unilateral simulation path) gave a much better trend in the channels reproduction, especially in the dense hard data results. In sparse hard data, the conditional simulations tend to simulate the main channel in the centre after encountering the hard data. In overall, the presence of hard data aided the unilateral simulation path in constructing the channels' continuity.

4.2.3.4 Analysis of distance (ANODI)

Prior to analysis of distance (ANODI), the template size of each grid was defined using "elbow" from the scree-plots based on the correlation between the eigenvalues of the covariance matrix and its dimensions. With using MATLAB, principal component analysis (PCA) were performed to determine the scree-plots and supported by maximum likelihood estimate (MLE) for the decrease of the covariance matrix whose dimensions is the same with the "elbow" value.

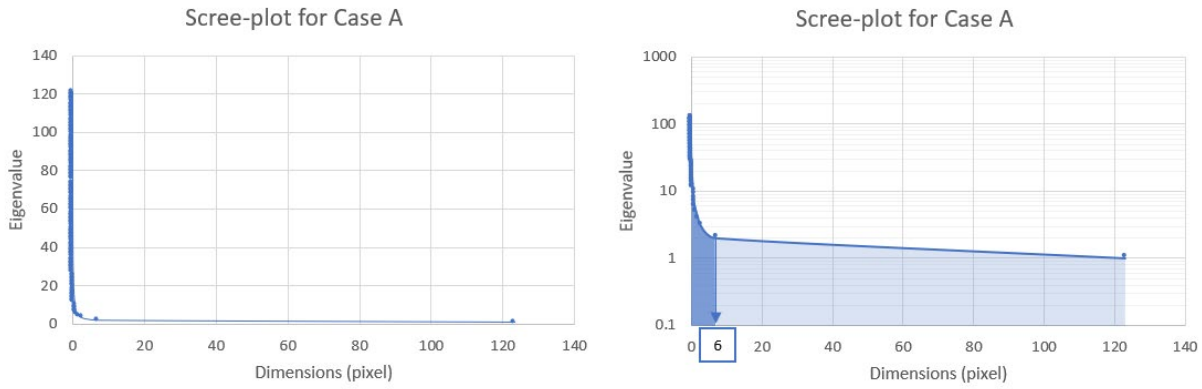

Figure 4.27. Left picture shows scree-plot for case A with eigenvalue in normal scale, and the right picture shows scree-plot for Case A with logarithmic scale for the eigenvalues.

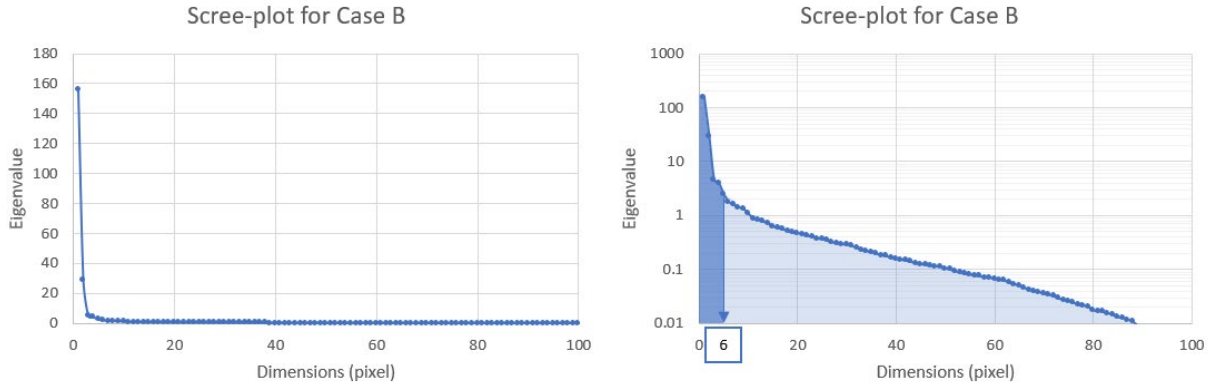

Figure 4.28. Left picture shows scree-plot for case B with eigenvalue in normal scale, and the right picture shows scree-plot for Case B with logarithmic scale for the eigenvalues.

Resulting eigenvalues of the covariance matrix were plotted against the dimensions to determine the “elbow” which can be conjured up with a sharp decrease in eigenvalues up to the elbow location, then a nearly flattening behaviour for the remaining points. To make it easier to find the “elbow” in scree-plots, the eigenvalues are shown in the logarithmic scale (Figure 4.27 and Figure 4.28). The best choice for the dimensions is 6 for both Case A and Case B as the slope changed significantly and started to stabilise. This result was supported by the MLE, which was 6.26 and 5.62 for Case A and Case B respectively. Lastly, we could use the template size of 6 x 6 for scanning the patterns in each subresolution.

Statistical variations as described by Tan et al. (2014) occur at multiple scales, so we divided the training image and realisations into three different levels of subresolution g to compare the statistical variations on the different resolution. The process started in TI's original resolution (228 x 121 cells) and divided the resolution into two between each level with bicubic interpolation with the resolution 114 x 61 and 57 x 30 cells, respectively.

The patterns within close similarity were classified and clustered as cluster-based histograms of patterns (CHP), which then later be used in calculating JS-divergence distances for the MDS plots.

4.2.3.4.1 MDS plot of Case A

JS-divergence distances were calculated with the CHPs between TI-realisation and realisation-realisation in three subresolutions, resulting in a table of 51 x 51 x 3 distances in each method. Multidimensional scaling (MDS) plot was used to visually show the distances between methods with eigenvalue decomposition, consequently between TI and the realisations of each method. The closer the visual distance, the more similar in statistics reproduction between the TI and the realisations. The x-axis on the MDS plot indicates the largest eigenvalue, y-axis to the second largest eigenvalue, and z-axis to the third largest eigenvalue. The results obtained from the MDS plot are provided in Figure 4.29 and Figure 4.30 for both dense and sparse hard data conditional MPS simulation.

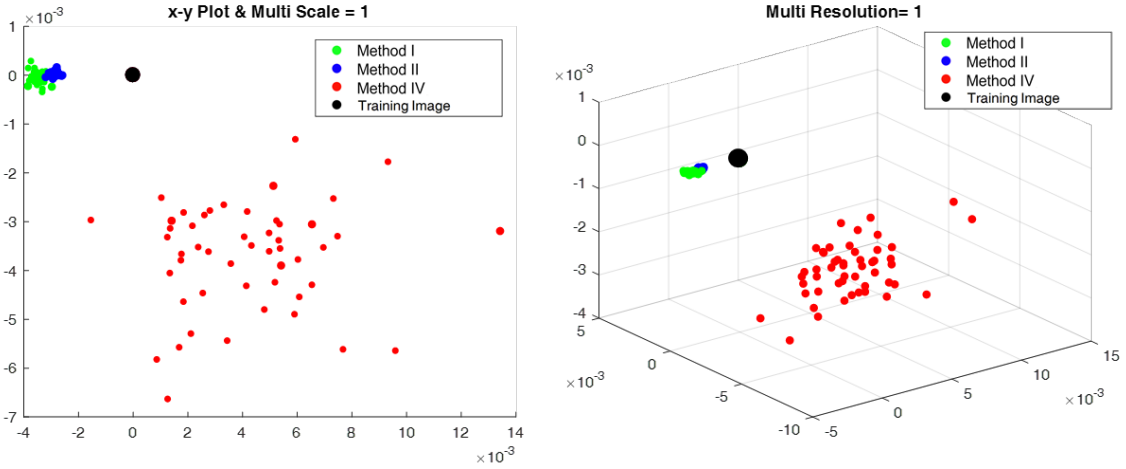

Figure 4.29. MDS plot of Case A with dense hard data. The left plot depicts the x-y plot, and the right plot depicts the x-y-z plot.

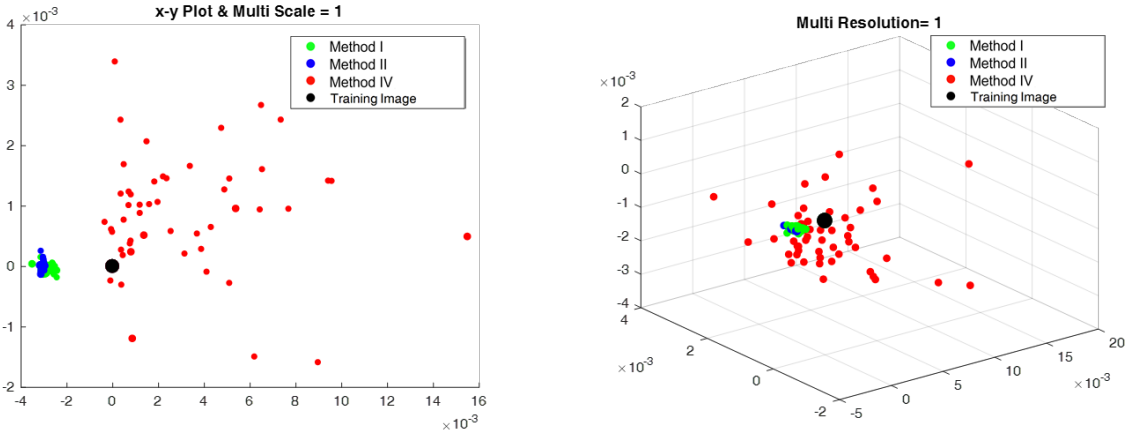

Figure 4.30. MDS plot of Case A with sparse hard data. The left plot depicts the x-y plot, and the right plot depicts the x-y-z plot.

From both of the hard data distribution in both figures, it is apparent that the size of the point clouds was similar in each method. The largest point cloud of data was the Method IV indicating high variability in the generated realisations, while Method I and Method II share the close-packed

distribution depicting low variability in the realisations. One can see that none of the methods was plotted close to the TI, saying that all of those methods were not performing well in reproducing the statistics of the TI, while the relatively nearest methods to the TI were Method II in dense hard data and Method IV in sparse hard data.

4.2.3.4.2 MDS plot of Case B

In Case B, same procedures were run in order to determine JS-divergence distances with the CHP between TI-realisation and realisation-realisation in three subresolutions. The distances then displayed in Multidimensional scaling (MDS) plot where distances in its eigenvalue decomposition can be visually displayed. The x-axis indicated the largest eigenvalue, the y-axis to the second largest eigenvalue, and the z-axis to the third largest eigenvalue.

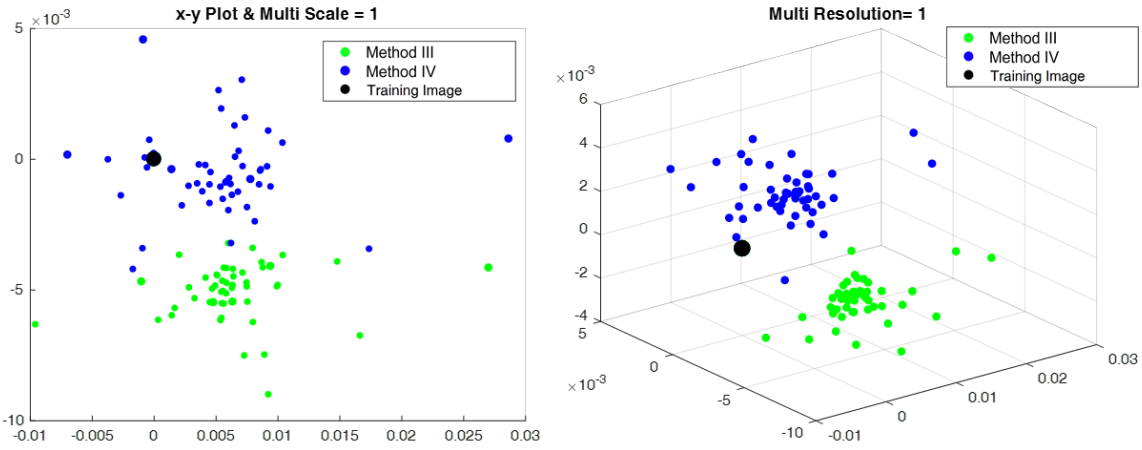

Figure 4.31. MDS plot of Case B with dense hard data. The left plot depicts the x-y plot, and the right plot depicts the x-y-z plot.

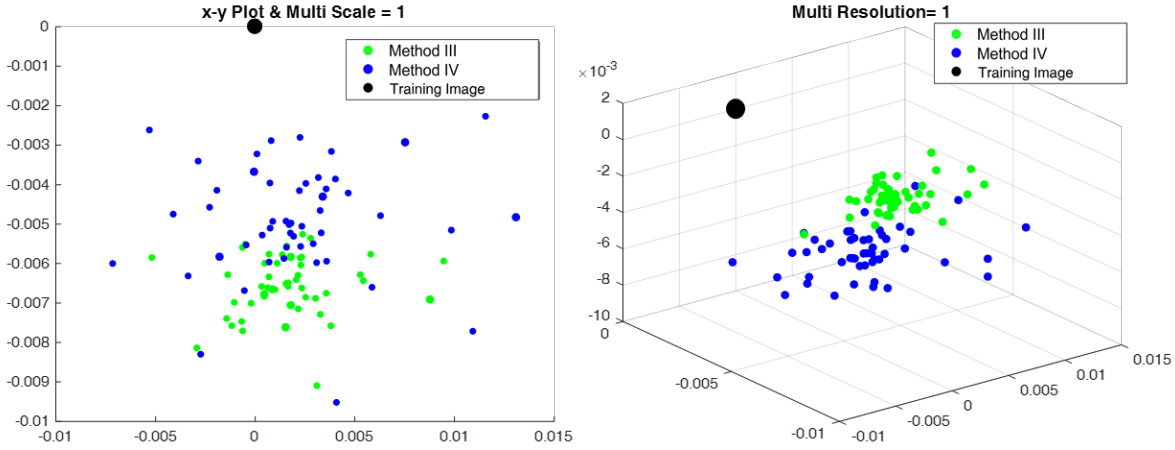

Figure 4.32. MDS plot of Case B with sparse hard data. The left plot depicts the x-y plot, and the right plot depicts the x-y-z plot.

The visual appreciation of Case B in MDS plot indicated that both Method III and Method IV had high variability in the realisations generated, showed by the massive size of the point cloud. Method IV gives a relatively closer statistic to the TI compared to Method III in dense hard data distribution, while in sparse hard data, the point cloud Method IV were plotted further against the TI.

4.2.3.4.3 Ranking algorithms of Case A

With the JS-divergence distances, we can now summarise the variability between the realisations ("between-realisation" distance) and the resemblance between realisation and the TI ("within-realisation" distance) of each method in each subresolution. The study calculated the sum of the variabilities from these subresolutions to get the overall relative ordering. The ANODI scores are a comparison between methods, so all the methods that have been tested are compared relative to Method IV (control map approach with unilateral simulation path), resulting in the value 1 for the score of Method IV.

The ratios that quantify "between-realisation" and "within-realisation" distance between algorithms in all subresolution grid are presented in Table 4.1 and Table 4.2. The better performing methods compared to Method IV will give a higher “between” distance, lower “within” distance, and higher “total” distance.

Table 4.1. ANODI scores for Case A with dense hard data.

Distance	Method I	Method II	Method III	Method IV
Space of uncertainty ("between")	0.04	0.02	0.37	1
Pattern reproduction ("within")	0.60	0.49	1.15	1
Total ("between/within")	0.06	0.05	0.32	1

Table 4.2. ANODI scores for Case A with sparse hard data.

Distance	Method I	Method II	Method III	Method IV
Space of uncertainty ("between")	0.04	0.02	0.31	1
Pattern reproduction ("within")	0.63	0.72	1.19	1
Total ("between/within")	0.06	0.02	0.26	1

In the case of conditional MPS simulation capability in Case A with dense hard data, we can confirm that using Method IV (control map approach with unilateral simulation path) had the highest space of uncertainty, shown by the largest point cloud in the MDS plot, Method III as the second largest space of uncertainty, while Method I had a marginally larger "between-realisation" distance to Method II. The results were similar to sparse hard data distribution.

In the aspect of pattern reproduction (“within” distances) with dense and sparse hard data, Method I and Method II outperformed Method III and Method IV. It was proven in the MDS plot by the lower relative distances to the TI compared to the Method IV. The total ratio concluded that Method IV is the best algorithm in performing conditional MPS simulation in Case A for both dense and sparse hard data distribution.

4.2.3.4.4 Ranking algorithms of Case B

For Case B, the variability between the realisations ("between-realisation" distance) and the resemblance between realisation and the TI ("within-realisation" distance) of each method were calculated in each subresolution. The sum of the variabilities from the subresolutions were then used to get the overall relative ordering in distances ranking, depicted in Table 4.3 and Table 4.4.

Again, ANODI scores are a comparison between methods, so all the methods that have been tested are compared relative to Method IV (control map approach with unilateral simulation path), resulting in the value 1 for the score of Method IV. The better performing methods compared to Method IV will give a higher "between" distance, lower "within" distance, and higher "total" distance.

Table 4.3. ANODI scores for Case B with dense hard data.

Distance	Method I	Method II	Method III	Method IV
Space of uncertainty ("between")	0.15	0.28	0.82	1
Pattern reproduction ("within")	0.63	1.08	1.19	1
Total ("between/within")	0.23	0.26	0.69	1

Table 4.4. ANODI scores for Case B with sparse hard data

Distance	Method I	Method II	Method III	Method IV
Space of uncertainty ("between")	0.24	0.22	0.60	1
Pattern reproduction ("within")	0.98	0.65	0.88	1
Total ("between/within")	0.25	0.34	0.69	1

The issue of conditioning using low repetitive patterns were supported in the ANODI scores. Dense hard data in conditional MPS simulation of Case B proved to be different with sparse hard data. For example, Method III outperformed the pattern reproduction of Method I in sparse hard data while the opposite in the dense hard data. Method IV in both hard data distribution held the first place in performance.

In overall, using control map is the better performing method in conditional MPS simulation with low patterns' repetition (Method III and Method IV). Combined with unilateral simulation path, control map approach had successfully surpassed the other methods.

4.2.4 Summary of the conditional MPS simulation results

After performing all the conditional results using different methods and evaluating the results using connectivity function, E-type models, conditional variance models, and ANODI, this study has identified the applicable method to handle nonstationarity in conditional MPS simulations using Delft3D simulation model data:

- In Case A, the visually good results in reproducing the sediment bodies with conditional simulation with both dense and sparse hard data were Method I (zonation approach with random simulation path) and Method II (zonation approach with unilateral simulation path). Method IV (control map approach with unilateral simulation path) delivered rough edges

and disorganised in the reproduced facies. In Case B, Method IV successfully simulate the channel continuity through the realisations.

- In connectivity function from conditional MPS simulation, unilateral simulation path shown better connectivity compared to the random simulation path methods. But, in contrast to the unconditional MPS simulation, the presence of hard data lowers the connectivity from the realisations.
- In E-type and conditional variance models, only Method IV in Case A that had low variability and low tendency in the patterns' reproduction. In Case B, Method IV tend to simulate the main channel in the centre with the significant effect of the hard data. This feature was most visible in sparse hard data where low possibility of the channel reproduction in the north side in the absent of hard data.
- In MDS plot, Method I and Method II had condensed point cloud, compared to the Method IV that had large point cloud. The point cloud indicated the variability between the realisations, where the variability is proportional to the size of the point cloud. In Case A, the relatively nearest point of cloud to the TI was the Method II in dense hard data, and Method IV in sparse hard data. In Case B, Method IV had the distance relatively closer to the TI.
- In ranking algorithms of both cases, Method IV had the best performance indicated by the highest total ratio compared to the other methods. Methods with unilateral simulation path gives better results to those method with random simulation path.

5

Discussion

5.1 Unconditional MPS IMPALA simulation

5.1.1 Determining assumed stationarity zonations in unconditional MPS simulation

There are two different approaches in simulating unconditional MPS simulation using 2D nonstationary TI from the process-based model in the fluvial-dominated delta that this study focuses on, which are zonation approach (Method I and Method II) and control map approach (Method III and Method IV). Both methods had successfully simulated the TI in MPS, but the selection of nonstationary TI delivered different results in different simulation paths. The repetition of patterns ruled these aspects in MPS simulation, shown in Case A where less difficulty in reproducing the patterns compared to Case B with low repetition. This finding is consistent with that of Zhang et al., (2006) who expressed the necessity of enough repetition in successful nonstationary MPS simulation.

It is critical to identify the stationary area in the TI in modelling nonstationarity in MPS. MPS depends on its assumption of stationarity in order to be successfully simulated. Subenvironment has similar hydrodynamic processes and sediment supply composition within each zonations, so this study used subenvironment variable from the process-based simulation model to become the base of assumed stationary zonations. The choice delivered successful unconditional MPS simulation for both zonation approach (Method I and Method II) and control map approach (Method III and Method IV).

5.1.2 Comparing the realisations from zonation approach and control map approach in unconditional MPS simulation

Zonation approach in Method I (zonation approach with random simulation path) and Method II (zonation approach with unilateral simulation path) only produced satisfactory visual inspection results in using a TI with high repetition like Case A. It was challenging to reproduce low repetitive patterns using new assumed stationary TIs in zonation approach without creating a much higher repetition in the realisations. The resulting zonation approach simulations in the low repetition TI like Case B always produce realisations with a higher proportion of sandy deposit facies (channel accretion and mouth bar facies), as shown in Figure 4.7 and Figure 4.8.

Choice of correct rotational angle in creating the azimuth map also contributed in reproducing original TI's patterns. For instance, the bending channels in the west part of the grid in Case A (Figure 3.3). This study decided not to constrain the delta development by creating freedom for

the MPS simulation in simulating the facies, but to recreate the similar patterns, we need a narrower restrict in the azimuth that would violate our stochastic simulation basis. We can only create a TI with an assumption of stationarity; and if we honour the stationarity, it was just simply impossible to reproduce such highly nonstationary patterns without restricting the variables into a higher order of controls. Again, MPS was designed to generate stochastic models, not to force a particular behaviour.

Control map approach (Method III and Method IV) has different characteristics in creating realisations compared to the zonation approach (Method I and Method II). To illustrate, the realisations from the direct control approach make less-smooth channel accretion and mouth bars facies. An explanation for this result is the use of the whole statistics from control map approach in Method III (control map approach with random simulation path) and Method IV (control map approach with unilateral simulation path). Compared to the zonation approach, control map approach uses the whole TI and utilises control map to determine the patterns' location in the simulation grid Figure 5.1. In this manner, there is a higher possibility of artefact within the simulation in connection with search template and MPS algorithm. In the other hand, zonation approach only addressed variations in the delta top and delta front subenvironments, so the simulated statistics is limited to those two subenvironments.

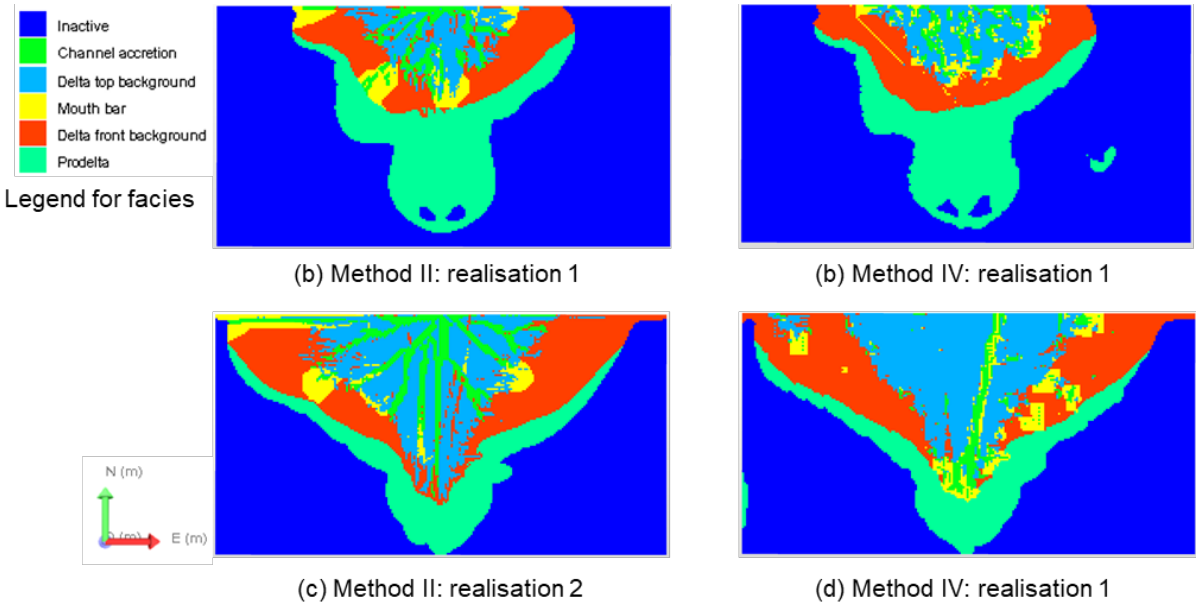

Figure 5.1. An example of comparation between Method II (zonation approach with unilateral simulation path) and Method IV (control map approach with unilateral simulation path). Method IV has rougher edges between the boundaries of the facies.

In contrast to the zonation approach that failed in reproducing patterns with low repetition, using the unilateral simulation path in direct control map approach simulated the patterns well. The bending channels in the west part were still becoming the weak point in this method since the unilateral simulation path make the patterns tend to be parallel to the first direction (north-south direction), so the channels with east-west direction would not be simulated well (Figure 4.9 and Figure 4.10).

5.1.3 The effect of various parameters in the connectivity function

The connectivity function of the method also supported the characteristics of random and unilateral simulation path. In the connectivity function plot of Case A using control map approach with the unilateral simulation path (Method IV), some of the connectivity function of the realisations were highly similar to the TI. Based on visual inspection, the use of the direct control map approach has successfully recreated low repetition patterns by not recreating higher repetitions and honour the global statistics from the original TI.

The tendency of reaching high connectivity function value in higher lag distance were caused by the stochastic nature of MPS in recreating mouth bar in the end of the delta, which occurred in higher lag distances. Most of the cases, the mouth bars were reproduced near one another, so it created new connection to the neighbouring channels, resulting in higher connectivity function value (e.g. see Figure 4.3 and Figure 4.7).

Also, higher and similar connectivity function between the realisations and TI does not necessarily a good reproduction of the original TI. For instance, the connectivity function of Method II (zonation approach with unilateral simulation path) in Case B (Figure 4.12b). It shows good connectivity with similar appearance of the connectivity function, but based on the visual inspection, Method II in Case B did not show proper facies reproduction. Its realisation appeared to reproduce more channel accretion facies compared to the original Delft3D model, but with good connectivity along the channels. It is essential to compare both connectivity function and visual inspection to the original TI's features to ensure proper MPS simulation.

5.1.4 Preference of unilateral simulation path in simulating channel features

The decision of a specific simulation path affected the channel construction in the MPS simulation. Based on the unconditional MPS simulation results and evaluation, the choice of the unilateral simulation path is better for the continuity of the fluvial-dominated delta to the random simulation path. These results corroborate the ideas of Mariethoz and Caers (2014) who suggested the use of unilateral simulation path in ensuring the continuity of the channels, especially in simulating features that has orientation parallel to the first direction of the unilateral simulation path. In this study's Case B with only two channels with the major orientation north-south in the original TI, the choice of -J+I direction in unilateral simulation path has sufficiently reproduce the channels in unconditional MPS simulation.

Before moving on to the conditional MPS simulation, it is important to use the approved method throughout visual evaluation and the connectivity function from the unconditional simulations first. The unconditional simulation phase makes certain that the MPS algorithm correctly simulated the patterns from the original TI to mimic the original deterministic model like process-based simulation model.

5.2 Conditional MPS IMPALA simulation

5.2.1 Capability in honouring the hard data

IMPALA as an improvement of SNESIM algorithm did not address any problem in honouring the hard data in conditional MPS simulation. This was proven by the zero variance in conditional variance maps in hard data locations for all the realisations. Pixel-based algorithm like IMPALA estimated the hard data in its location with zero variance, but at the same time, it will affect the

cells around the hard data (Mariethoz and Caers, 2014). The effects become clear in the cases of low repetition in Case B where the highest variance were the parts around the hard data, as shown in Figure 4.25 and Figure 4.26.

One or more thing that may cause high variance around in the hard data is because in the location where the delta top background facies surround the main channel. Especially in the Case B with low repetition in the patterns, the possibility of stochastically simulating the location around hard data not as channel accretion facies is high, resulting in disconnection within the channels. The features may not be apparent in cases with high repetitive patterns because the probability of simulating facies accretion is higher than those with low repetition, referring to the SNESIM algorithm in referring the probability of cells reproduction (Strebelle, 2002).

Disconnection within the channels is also consistent with the connectivity function results in Section 4.2.3.1. The presence of hard data lowers the overall connectivity function, most visible in Case B with low repetition in the patterns (Figure 4.20 and Figure 4.21).

5.2.2 Limitation of unilateral simulation path

Unilateral simulation path showed good results in simulating straight channel, but it depended on the location of the hard data and the cases on which direction the channels went. This feature is most prominent in Case B, especially with Method IV (control map approach with unilateral simulation path). Consistent with Daly in 2005, the study found that the data ahead of the path is not compatible with the structures that built preceding the simulation data. Figure 5.2 indicates the incapability with the circle through the realisations, E-type model, and conditional variance model.

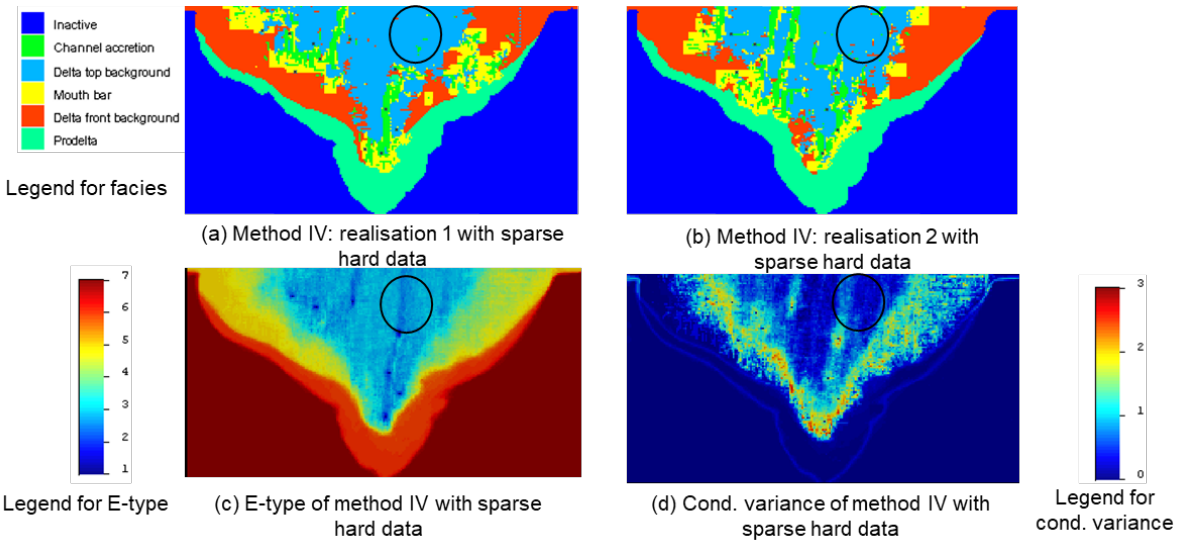

Figure 5.2. An example of incapability of unilateral simulation path in conditional MPS simulation with Method IV (control map approach with unilateral simulation path) in Case B. The circle represents the discontinuity of the facies before it encountered the hard data.

5.2.3 Interpolation capability in conditional MPS simulation

Conditional MPS simulation with unilateral simulation path expressed an interpolation in the case of low repetition in Case B (Figure 5.3). A tendency of new channel development on the east part

of the grid where there are none hard data was revealed in both E-type and conditional variance map. When we look closer to the channel, actually it shows approximately the same gap distance from the original TI. The algorithm of the pixel-based method compared the patterns from the original TI and matched it with the simulation grid, and the interpolation of the new channel in the east side of the simulation grid is comparable with the two channels in original TI.

The interpolation capability shown in control map approach with unilateral simulation path motivated a positive side in stochastic simulations. The results validated the choice of control map approach in reproduce channels' pattern in the assumed stationary zonations. MPS simulation is capable of creating patterns that are learned from the original TI, even with low repetition, and applied it to the new zones with the absence of hard data.

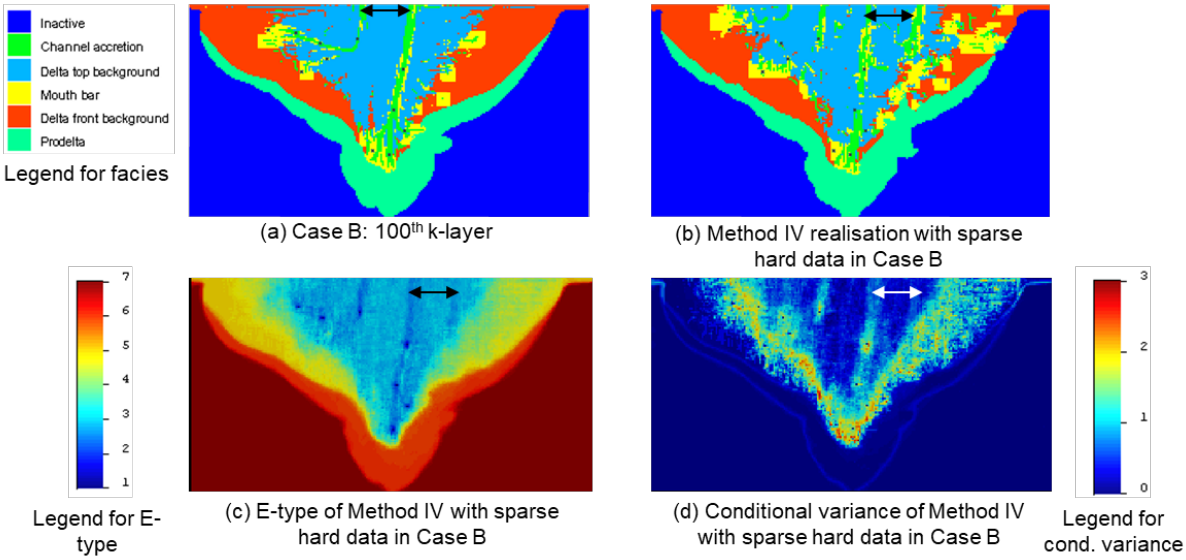

Figure 5.3. Interpolation capability in reproducing new channel in a specific location with Method IV in Case B. Notice the arrow indicating the same length to the new channel in the realisation, E-type model and conditional variance model.

5.2.4 Variability of realisations between zonation and control map approaches

Comparing zonation approach and control map in handling Case A and Case B, control map inclines to create a higher variability in the realisations. Most imminent in the E-type and conditional variance map that showing smoother results compared to the zonation approach. The explanation to this is referring to the SNESIM algorithm in simulating the whole statistics for the control map approach (Daly, 2005).

By taking account of the whole statistics in the simulation grid, there are more possibility of reproducing different patterns in accordance to its search template (Figure 2.2). The resulting realisations' patterns would be more varied compared to the realisations from zonation approach in Method I and Method II, where only making use of delta top and delta front subenvironments.

5.2.5 ANODI scoring results compared to the other evaluation

Analysis of distance (ANODI)'s objective in ranking the best algorithm compared to the others was depended on two distance aspects: the space of uncertainty between the realisations ("between" distance) and the pattern reproduction based on the TI ("within" distance). The results have shown the dominance of any control map approach's results (Method III and Method IV) to the zonation approaches (Method I and Method II).

One thing to be noted that the zonations approach only simulated the delta top and delta front subenvironment, where the control map approach technically simulated the whole simulation grid. ANODI rankings are based on the total statistics of the simulation grid compared to the TI grid. The control map took account of the non-simulated cells wherein the zonations approach stay untouched. Therefore, the space uncertainty of the control map approaches performed poorly, where the cells other than the simulated cells remain the same through the realisations. An optimum comparison should be within the same methods but different paths or parameter (between Method I-II or Method III-IV), so the rankings would be more objective.

If we compare the results between distance ranking and the visual evaluation of Method IV in Case B, the results were contradicting with another. Visual evaluation gave poor results on the channel continuity (Figure 4.17), while the distance ranking of Method IV outperformed Method III (Table 4.4), making Method IV the best method compared to the others. One thing to remember is the total ratio of the ranking takes account of the space uncertainty and the pattern reproduction within the realisations. From the visual evaluation, we can say that the pattern reproduction is unsatisfactory (for the sparse hard data), but the space of uncertainty of Method IV supported the poor pattern reproduction score. The space of uncertainty in Method IV significantly surpass the Method III. This is the objective of creating ANODI by Tan et al. in 2014: to create unbiased evaluation between different methods in conditional MPS simulation.

The final score, contributing to both "between" and "within" distances, still makes Method IV the preferred method in modelling the Case B.

5

Conclusions and future recommendation

This study had tested and validated the unconditional and conditional MPS simulation in using 2D nonstationary TI of fluvial-dominated delta reservoir model. From the results, we have concluded some of the critical remarks that become the recommendation of the optimised workflow in MPS simulation with a process-based model and might be applicated in similar other cases.

6.1 Ideal TI for MPS simulation using nonstationary fluvial-dominated delta simulation model

The study has done two different approaches to model the nonstationarity in the case of two representative TI (Case A and Case B) that have high and low repetition of patterns in fluvial-deltaic environment. The approaches were zonation approach (Method I and Method II) and control map approach (Method III and Method IV).

An ideal TI used for MPS simulation must have enough repetition in the patterns because of the MPS' inferring of multiple point facies joint correlation moments from the provided TI. In the case of simulating model with low repetition of patterns like Case B, the geomodeler can use the original TI with low repetition in the control map approach to get the desired results.

Zonation approach requires the construction of new TIs that represent each of the stationary zonations. The obvious limitation in this method appeared when we tried to model low repetition in the TI, where MPS tends to make higher repetition in new patterns. This approach could only deliver pleasing simulation models with the high repetition in the original TI, so it is preferable to only use zonation approach in the case with high repetition in the patterns. The high subjectivity of the modeller was also a concern in this approach that necessitates the modeller to mimic the model as similar as possible with different parameters which capture the patterns in the governing TI.

In practice, the process of constructing new TI in zonation approach is an often-exceedingly demanding task. The modeller not only have built the appropriate TI that captures the pattern and the stationarity of the original TI but also has to establish the correct parameters and data event transformation properties for mimicking the complexity in the original TI's patterns. Frequently this process is a trial-and-error attempt that is indirect and unsystematic.

In the other hand, control map approach does not require the construction of new TI owing to the use the original TI, and the control map will decide which patterns in the TI would occur in the

simulation grid. The subjectivity comes when determining the assumed stationary zonations for the values of the control map, and in this study's case, the choice of subenvironment as the stationary zonations.

6.2 The optimised method to unconditionally model the nonstationarity in fluvial-dominated delta reservoir model based on the study's methods

The results have shown the nonstationary could be modelled in a non-ideal TI even with low repetition in acceptable results, with few caveats.

First, the importance of choosing the considered stationary zonations in the original TI. The defined stationary zonations must have a similar characteristic in the patterns. In the zonation approach, a distinct geobodies pattern in each zonation is simulated with MPS, while the zonation with no distinct reservoir patterns is not going to be simulated. Control map approach simulates the entire TI, with a distinction of the values in the control map as the substitute of the zonations. In the study results, we chose the zonations with the basis of subenvironment in the process-based simulation of the original TI because of the same hydrodynamic processes and resulting patterns underlying in each subenvironment. The similarity of the patterns exhibits similar statistics that are used in the MPS' inferring statistics existing at different spatial locations.

One can see this task of determining stationary zonations as a subjective one for the modeller, because in most of the cases it is difficult to be accurately defined the boundaries between the zonations. The boundary commonly comprised of gradual transition from zonations to the other. Zonation approach can overcome this problem by the presence of the same facies in between TI that allows MPS to connect the facies across the boundary between the zonations. Control map approach uses gradual values in between the boundary to map the smooth transition. One improvement was made by Honarkhah and Caers in 2012 with the propose of Gabor filters to automatically segment a TI into stationary zonations, which was not covered in this study.

Second, the uses of simulation path within the MPS simulation. The method of unilateral simulation path proved to carry out satisfactory connectivity in the case of the fluvial-deltaic environment by correctly simulate the end of the channel accretion facies which feeds the mouth bar facies with sediments. This path also made the modelling of low repetition such as Case B possible by simulating the connectivity from the proximal-to-distal parallel to the first unilateral simulation path direction with control map approach.

In brief, the optimised approach to perform an unconditional MPS simulation in the case of high repetitions were both the zonation and control map approach with the unilateral simulation path. In modelling the case of low repetitions, the use of control map approach with unilateral simulation path proved able to overcome the patterns reproduction capability of zonation approach with random simulation path. This study recommends the use of the control map with the unilateral simulation path for performing successful continuing patterns of fluvial-dominated delta reservoir model and the ease in preparing the data without any additional TI construction.

6.3 The optimised method to conditionally model the nonstationarity in fluvial-dominated delta reservoir model based on the study's methods

Conditional simulation using MPS demonstrated the capability of conditioning with the IMPALA algorithm. The algorithm honoured the data well with zero variance in the hard data location. Between the simulation paths, unilateral simulation path proved to be superior in conditional MPS simulations compared to random simulation path. While this may be true, there are several outlooks to be in consideration in the optimised way of utilising unilateral simulation path in different conditions.

First, when the TI has little repetition in the patterns, and there are only several hard data available, we have to consider the position of the hard data compared to the simulated geobody. If the hard data are in the middle of the geobody, one has to validate the realisations whether it has simulated the geobody properly or not. The unilateral simulation path tends to simulate parallel to the first direction, and conditioning will be applied to the cells after it has encountered the hard data. It means that the patterns can only be correctly simulated if the patterns are parallel to the first direction of unilateral simulation path and encounter the hard data. If a high number of hard data is available, the conditioning the nonstationary TI should not be much of a problem other than the direction of the patterns whether is parallel or not to the first direction of unilateral simulation path.

Second, the effect of interpolation capability in IMPALA algorithm. Despite the favourable results in the case of stochastic simulations, the new stochastic channels have to be considered in building the model where no data is available. One has to make sure of the validation of the new stochastic variables in accord to the original TI.

In summary, similar as the previous unconditional MPS recommendation, this study recommends the use of control map approach with unilateral simulation path for performing successful conditional MPS simulation using nonstationary fluvial-dominated delta reservoir model and the ease in preparing the data without any additional TI construction.

6.4 Future recommendations

The tedious work of selecting assumed stationary zonations can be overcome with techniques introduced by Honarkhah and Caers in 2012 termed spatial-similarity method (SSM) and automatic segmentation method (ASM). Those methods eliminate the subjectivity of the modeller in choosing the boundaries within the assumed stationarity zonations and provide auxiliary variables that serve as the control map that aids the MPS simulation.

The nonstationary model used in this study is a 2D model, so the use of a 3D model should be beneficial in determining optimised MPS workflow in the 3D model. MPS simulation in 3D case requires different approach compared to the 2D case, and the complexity lies in the introduction of the vertical axis. The flow simulation also can be used in both the underlying reservoir model as TI and the resulting realisations model from MPS simulation, so we can see that the MPS could reproduce the connecting geobodies in 3D.

The E-type invalidating the realisations in this study used a simple averaging calculation that expressed the expected value at each location, but it proved difficult in distinguishing facies in low repetitions such as Case B that the background facies surround the channels accretion. A different weighting approaches can be applied to the E-type generation, so better identification can be achieved with distinct patterns.

References

Arpat, G. B., and Caers, J. (2007). Conditional simulation with patterns. *Mathematical Geology*, 39(2), 177–203. DOI:10.1007/s11004-006-9075-3

Boisvert, J. B., Pyrcz, M. J., and Deutsch, C. V. (2007). Multiple-point statistics for training image selection. *Natural Resources Research*, 16(4), 313–321. DOI:10.1007/s11053-008-9058-9

Campedel, M., Moulines, E., Matre, H., and Datcu, M. (2005). Feature selection for satellite image indexing. *ESA-EUSC: Image Information Mining*.

Chugunova, T. L., and Hu, L. Y. (2008). Multiple-Point simulations constrained by continuous auxiliary data. *Mathematical Geosciences*, 40(2), 133–146. DOI:10.1007/s11004-007-9142-4

Colombera, L., Felletti, F., Mountney, N. P., and McCaffrey, W. D. (2012). A database approach for constraining stochastic simulations of the sedimentary heterogeneity of fluvial reservoirs. *AAPG Bulletin*, 96(11), 2143–2166. DOI:10.1306/04211211179

Cover, T. M., and Thomas, J. A. (2005). Elements of Information Theory. Hoboken, NJ, USA: John Wiley & Sons, Inc. DOI:10.1002/047174882X

Daly, C. (2005). Higher Order Models Using Entropy, Markov Random Fields and Sequential Simulation. *Springer Netherlands*, 215–224. DOI:10.1007/978-1-4020-3610-1_22

Daly, C., and Caers, J. (2010). Multi-point geostatistics – an introductory overview. *First Break*, 28(September), 39–47. DOI:10.3997/1365-2397.2010020

Dastgheib, A., Roelvink, J. A., and Wang, Z. B. (2008). Long-term process-based morphological modeling of the Marsdiep Tidal Basin. *Marine Geology*, 256(1–4), 90–100. DOI:10.1016/j.margeo.2008.10.003

Delft, H. V. D. V. T. U., Mullins, J., van der Vegt, H., and Howell, J. (2018). Combining Multiple Point Geostatistics and Process-based Models for Improved Reservoir Modelling. *80th EAGE Conference & Exhibition 2018*, (June 2018). DOI:10.3997/2214-4609.201800772

Deutsch, C. V., and Tran, T. T. (2002). FLUVSIM: A program for object-based stochastic modeling of fluvial depositional systems. *Computers and Geosciences*, 28(4), 525–535. DOI:10.1016/S0098-3004(01)00075-9

Ephesia Consult. (2017). Ephesia - DeeSse Multipoint Simulation. Retrieved October 8, 2018, from https://www.petromehras.com/petroleum-software-directory/geology-software/ephesia-deesse-multipoint-simulation

Fadlelmula F., M. M., Killough, J., and Fraim, M. (2016). TiConverter: A training image converting

tool for multiple-point geostatistics. *Computers and Geosciences*, 96, 47–55. DOI:10.1016/j.cageo.2016.07.002

Feng, W., and Wu, S. (2016). A multiple-point geostatistical method based on geological vector information. *Arabian Journal of Geosciences*, 9(10). DOI:10.1007/s12517-016-2595-3

Goovaerts, P. (1997). Geostatistics for natural resources characterization. New York: Oxford University Press. DOI:10.1007/978-94-009-3699-7

Granjeon, D., and Joseph, P. (1999). Concepts and applications of a 3D multiple lithology, diffusive model in stratigraphic modeling. *SEPM Special Publication*, 62(May), 197–210. DOI:10.2110/pec.99.62.0197

Guardiano, F. B., and Srivastava, R. M. (1993). Multivariate Geostatistics: Beyond Bivariate Moments. In *Geostatistics Troia '92* (pp. 133–144). Springer. DOI:10.1007/978-94-011-1739-5_12

Hoffimann, J., Scheidt, C., Barfod, A., and Caers, J. (2017). Stochastic simulation by image quilting of process-based geological models. *Computers and Geosciences*, 106(May), 18–32. DOI:10.1016/j.cageo.2017.05.012

Honarkhah, M., and Caers, J. (2010). Stochastic Simulation of Patterns Using Distance-Based Pattern Modeling. *Mathematical Geosciences*, 42(5), 487–517. DOI:10.1007/s11004-010-9276-7

Honarkhah, M., and Caers, J. (2012). Direct Pattern-Based Simulation of Non-stationary Geostatistical Models. *Mathematical Geosciences*, 44(6), 651–672. DOI:10.1007/s11004-012-9413-6

Hu, L. Y., and Chugunova, T. (2008). Multiple-point geostatistics for modeling subsurface heterogeneity: A comprehensive review. *Water Resources Research*, 44(11), 1–14. DOI:10.1029/2008WR006993

Journel, A. G. (2003). Multiple-point Geostatistics: A State of the Art. *Stanford Center for Reservoir Forecasting*, 1–52.

Jung, A., and Aigner, T. (2012). Carbonate geobodies: Hierarchical classification and database - a new workflow for 3D reservoir modelling. *Journal of Petroleum Geology*, 35(1), 49–65. DOI:10.1111/j.1747-5457.2012.00518.x

Lesser, G. R., Roelvink, J. A., van Kester, J. A. T. M., and Stelling, G. S. (2004). Development and validation of a three-dimensional morphological model. *Coastal Engineering*, 51(8–9), 883–915. DOI:10.1016/j.coastaleng.2004.07.014

Li, L., Storms, J. E. A., and Walstra, D. J. R. (2018). On the upscaling of process-based models in deltaic applications. *Geomorphology*, 304, 201–213.

DOI:10.1016/j.geomorph.2017.10.015

Liu, Y. (2006). Using the Snesim program for multiple-point statistical simulation. *Computers and Geosciences*, 32(10), 1544–1563. DOI:10.1016/j.cageo.2006.02.008

Lochbühler, T., Pirot, G., Straubhaar, J., and Linde, N. (2014). Conditioning of Multiple-Point Statistics Facies Simulations to Tomographic Images. *Mathematical Geosciences*, 46(5), 625–645. DOI:10.1007/s11004-013-9484-z

Maharaja, A. (2008). TiGenerator: Object-based training image generator. *Computers and Geosciences*, 34(12), 1753–1761. DOI:10.1016/j.cageo.2007.08.012

Mariethoz, G., and Caers, J. (2014). Multiple-Point Geostatistics: Stochastic Modeling with Training Images. Chichester, UK: John Wiley & Sons, Ltd. DOI:10.1002/9781118662953

Mariethoz, G., and Kelly, B. F. J. (2011). Modeling complex geological structures with elementary training images and transform-invariant distances. *Water Resources Research*, 47(7), 1–14. DOI:10.1029/2011WR010412

Mariethoz, G., and Lefebvre, S. (2014). Bridges between multiple-point geostatistics and texture synthesis: Review and guidelines for future research. *Computers and Geosciences*, 66, 66–80. DOI:10.1016/j.cageo.2014.01.001

Mariethoz, G., Renard, P., and Straubhaar, J. (2010). The direct sampling method to perform multiple-point geostatistical simulations. *Water Resources Research*, 46(11), 1–14. DOI:10.1029/2008WR007621

Michael, H. A., Li, H., Boucher, A., Sun, T., Caers, J., and Gorelick, S. M. (2010). Combining geologic-process models and geostatistics for conditional simulation of 3-D subsurface heterogeneity. *Water Resources Research*, 46(5), 1–20. DOI:10.1029/2009WR008414

Miller, J. K., Sun, T., Li, H., Stewart, J., Genty, C., Li, D., and Lyttle, C. (2008). Direct Modeling of Reservoirs through Forward Process-based Models: Can We Get There? In *International Petroleum Technology Conference* (pp. 1–12). International Petroleum Technology Conference. DOI:10.2523/12729-MS

Orton, G. J., and Reading, H. G. (1993). Variability of deltaic processes in terms of sediment supply, with particular emphasis on grain size. *Sedimentology*, 40(3), 475–512. DOI:10.1111/j.1365-3091.1993.tb01347.x

Pardo-Igúzquiza, E., and Dowd, P. A. (2003). CONNEC3D: A computer program for connectivity analysis of 3D random set models. *Computers and Geosciences*, 29(6), 775–785. DOI:10.1016/S0098-3004(03)00028-1

Parra, Á., and Ortiz, J. M. (2011). Adapting a texture synthesis algorithm for conditional multiple point geostatistical simulation. *Stochastic Environmental Research and Risk Assessment*,

25(8), 1101–1111. DOI:10.1007/s00477-011-0489-1

Pourfard, M., Abdollahifard, M. J., Faez, K., Motamedi, S. A., and Hosseinian, T. (2017). PCTO-SIM: Multiple-point geostatistical modeling using parallel conditional texture optimization. *Computers & Geosciences*, 102, 116–138. DOI:10.1016/j.cageo.2016.12.012

Pyrcz, M. J., Boisvert, J. B., and Deutsch, C. V. (2008). A library of training images for fluvial and deepwater reservoirs and associated code. *Computers and Geosciences*, 34(5), 542–560. DOI:10.1016/j.cageo.2007.05.015

Pyrcz, M. J., and Deutsch, C. V. (2014). Geostatistical reservoir modeling. *Computers & Geosciences* (Vol. 29). DOI:10.1016/S0098-3004(02)00101-2

Ringrose, P., and Bentley, M. (2015). Reservoir Model Design. Dordrecht: Springer Netherlands. DOI:10.1007/978-94-007-5497-3

Riou, J., and Höcker, C. (2015). Practical Recommendations for Successful Application of the MPS Facies Modelling Method. In *Abu Dhabi International Petroleum Exhibition and Conference*. Society of Petroleum Engineers. DOI:10.2118/177675-MS

Saripally, I., and Caers, J. (2008). Evaluating data conditioning accuracy of MPS algorithms and the impact on flow modeling. *21th SCRF Meeting, Stanford University*.

Straubhaar, J., Renard, P., Mariethoz, G., Froidevaux, R., and Besson, O. (2011). An improved parallel multiple-point algorithm using a list approach. *Mathematical Geosciences*, 43(3), 305–328. DOI:10.1007/s11004-011-9328-7

Strebelle, S. (2002). Conditional Simulation of Complex Geological Structures Using Multiple-Point Statistics. *Mathematical Geology*, 34(1), 1–21. DOI:10.1023/A:1014009426274

Strebelle, S., and Chevron, E. T. C. (2012). Multiple-Point Geostatistics: from Theory to Practice. *Expanded Abstract Collection from Ninth International Geostatistics Congress. Norwegian Computing Center*, 1–65.

Suzuki, S., and Caers, J. K. (2006). History Matching With an Uncertain Geological Scenario. *Annual Technical Conference and Exhibition*. DOI:10.2118/102154-ms

Tahmasebi, P., Sahimi, M., and Caers, J. (2014). MS-CCSIM: Accelerating pattern-based geostatistical simulation of categorical variables using a multi-scale search in fourier space. *Computers and Geosciences*, 67, 75–88. DOI:10.1016/j.cageo.2014.03.009

Tan, X., Tahmasebi, P., and Caers, J. (2014). Comparing training-image based algorithms using an analysis of distance. *Mathematical Geosciences*, 46(2), 149–169. DOI:10.1007/s11004-013-9482-1

van der Vegt, H. (2018). From Fluvial Supply to Delta Deposits: Simulating Sediment Delivery,

Transport, and Deposition. Delft University of Technology. https://doi.org/10.4233/uuid:c049ea67-23a1-4e7e-af52-1275802839f1

Wu, J., Zhang, T., and Boucher, A. (2007). Non-stationary Multiple-point Geostatistical Simulations with Region Concept. In *Proceedings of the 20th SCRF meeting, Stanford, CA, USA* (pp. 1–53).

Zhang, T. (2008). Incorporating Geological Conceptual Models and Interpretations into Reservoir Modeling Using Multiple-Point Geostatistics. *Earth Science Frontiers*, 15(1), 26–35. DOI:10.1016/S1872-5791(08)60016-0

Zhang, T., Bombarde, S., Strebelle, S., and Oatney, E. (2006). 3D Porosity Modeling of a Carbonate Reservoir Using Continuous Multiple-Point Statistics Simulation. *SPE Journal*, 11(03), 375–379. DOI:10.2118/96308-PA

Zhu, M., and Ghodsi, A. (2006). Automatic dimensionality selection from the scree plot via the use of profile likelihood. *Computational Statistics and Data Analysis*, 51(2), 918–930. DOI:10.1016/j.csda.2005.09.010

Ziegel, E. R., Deutsch, C., and Journel, A. (1995). GSLIB: Geostatistical Software Library and User's Guide. *Technometrics*, 37(1), 126. DOI:10.2307/1269177

A

Appendix

Appendix A contains unconditional MPS simulation realisations for Method I, Method II, Method III, and Method IV in Case A and Case B. Three representative realisations were shown in each method.

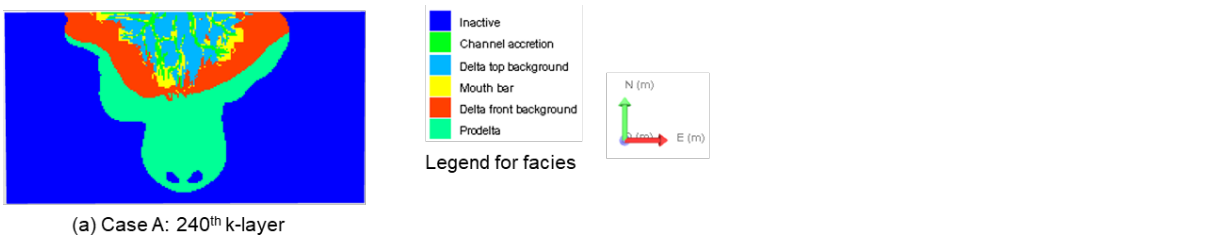

Legend for facies

(a) Case A: 240th k-layer

(b) Method I: realisation 1

(c) Method I: realisation 2

(d) Method I: realisation 3

Figure 7.1 Unconditional simulation results from Case A using Method I.

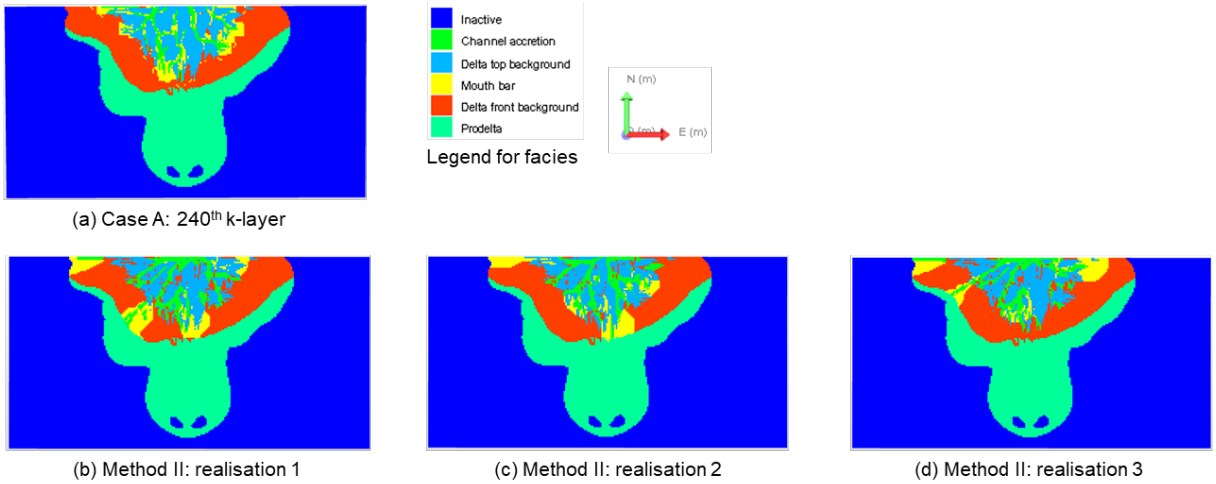

(a) Case A: 240th k-layer

(b) Method II: realisation 1

(c) Method II: realisation 2

(d) Method II: realisation 3

Figure 7.2. Unconditional simulation results from Case A using Method II.

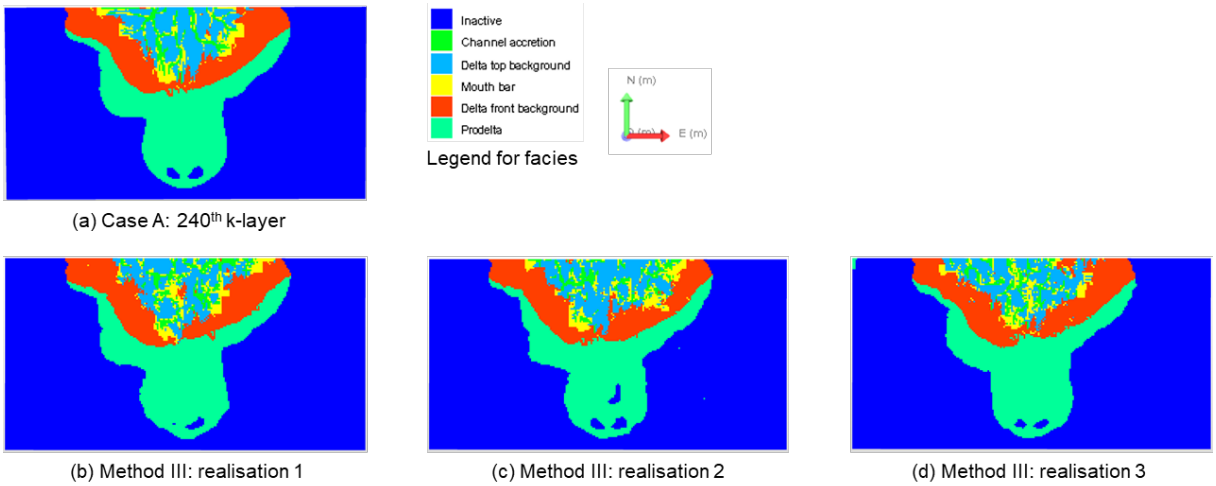

(a) Case A: 240th k-layer

(b) Method III: realisation 1

(c) Method III: realisation 2

(d) Method III: realisation 3

Figure 7.3. Unconditional simulation results from Case A using Method III.

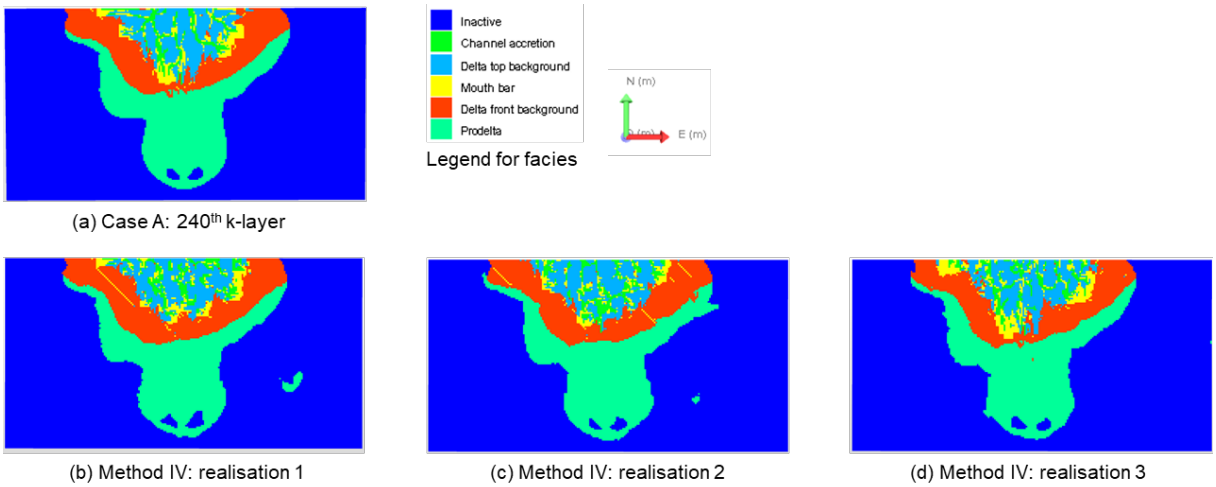

(a) Case A: 240th k-layer

(b) Method IV: realisation 1

(c) Method IV: realisation 2

(d) Method IV: realisation 3

Figure 7.4. Unconditional simulation results from Case A using Method IV.

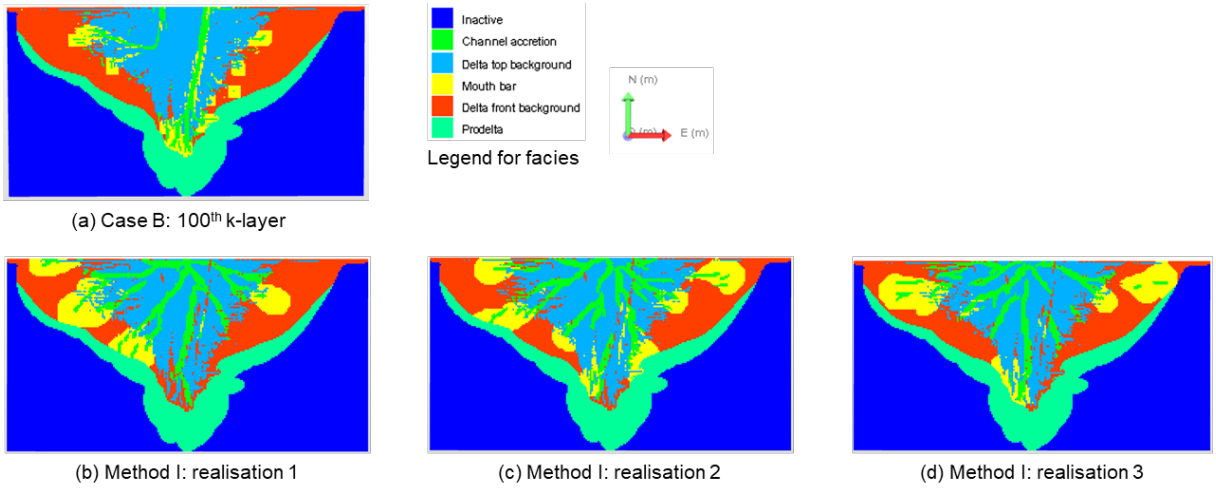

(a) Case B: 100th k-layer

(b) Method I: realisation 1

(c) Method I: realisation 2

(d) Method I: realisation 3

Figure 7.5. Unconditional simulation results from Case B using Method I.

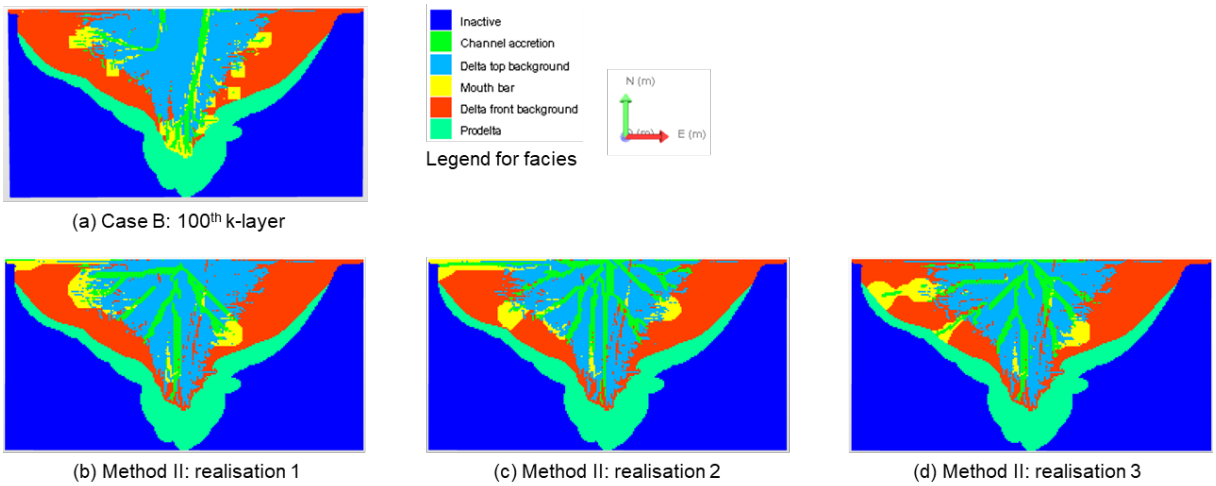

(a) Case B: 100th k-layer

(b) Method II: realisation 1

(c) Method II: realisation 2

(d) Method II: realisation 3

Figure 7.6. Unconditional simulation results from Case B using Method II.

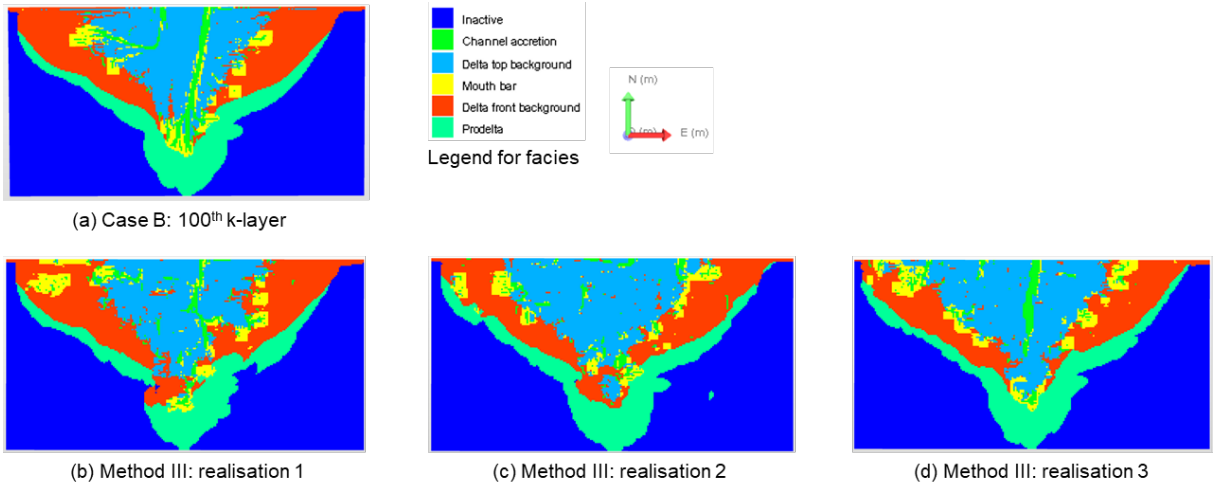

(a) Case B: 100th k-layer

(b) Method III: realisation 1

(c) Method III: realisation 2

(d) Method III: realisation 3

Figure 7.7. Unconditional simulation results from Case B using Method III.

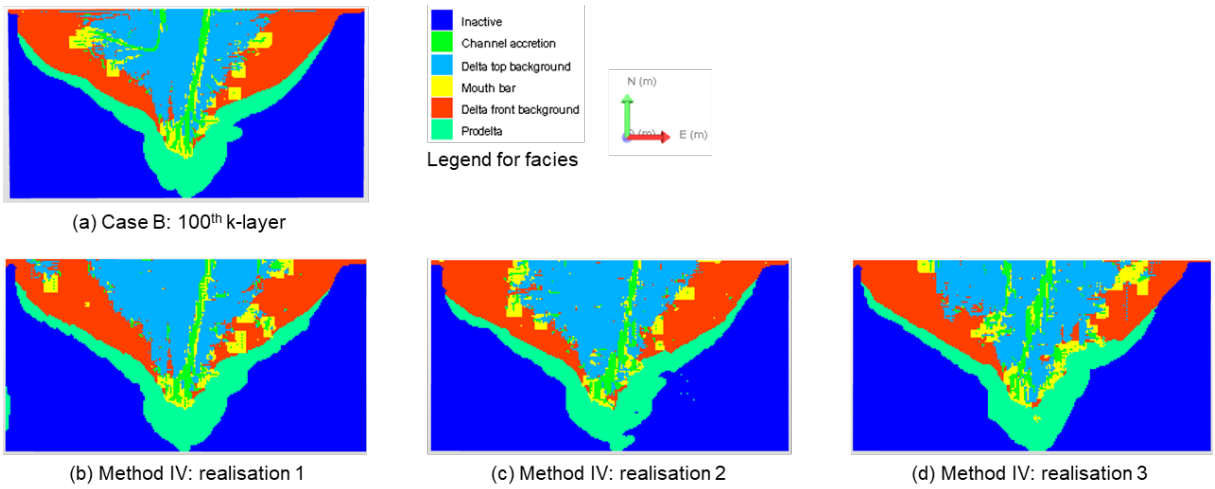

(a) Case B: 100th k-layer

Legend for facies

(b) Method IV: realisation 1

(c) Method IV: realisation 2

(d) Method IV: realisation 3

Figure 7.8. Unconditional simulation results from Case B using Method IV.

B

Appendix

Appendix B contains conditional MPS simulation realisations for methods used in Case A and Case B. Three representative realisations were shown in each method.

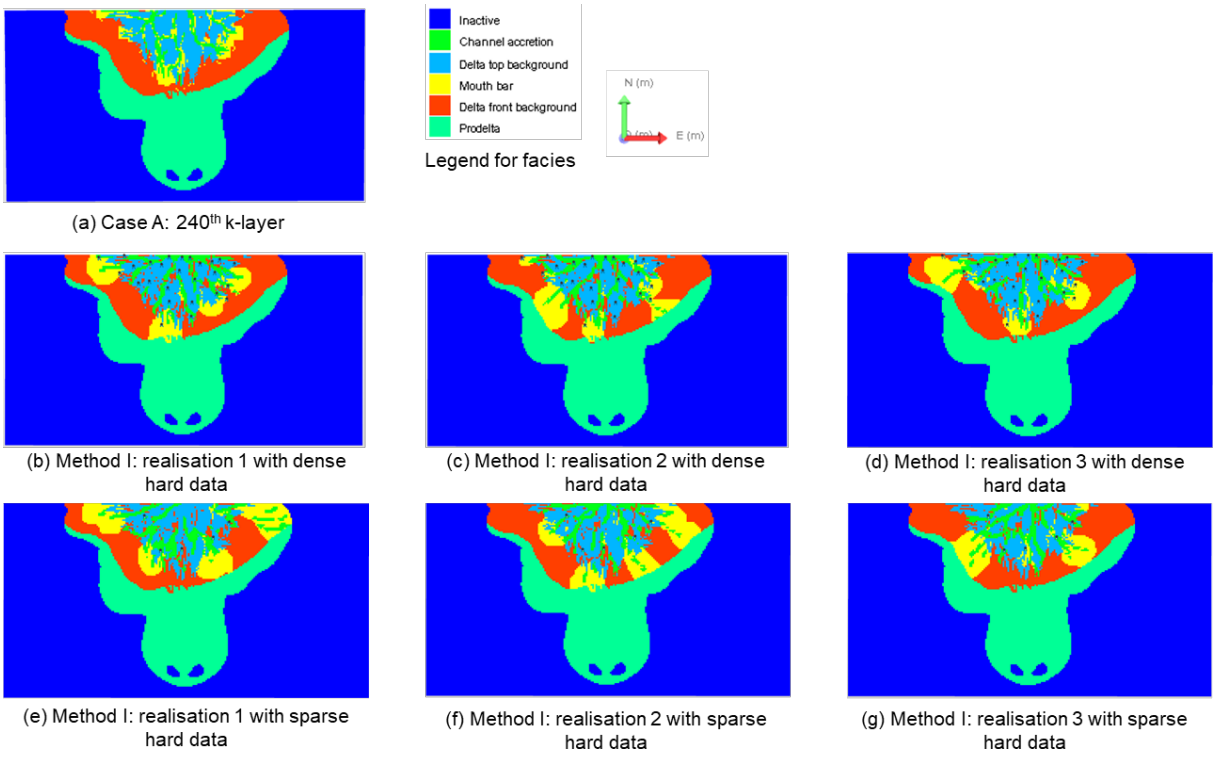

(a) Case A: 240th k-layer

Legend for facies

(b) Method I: realisation 1 with dense hard data

(c) Method I: realisation 2 with dense hard data

(d) Method I: realisation 3 with dense hard data

(e) Method I: realisation 1 with sparse hard data

(f) Method I: realisation 2 with sparse hard data

(g) Method I: realisation 3 with sparse hard data

Figure 7.9. Conditional simulation results from Case A using Method I for dense and sparse hard data.

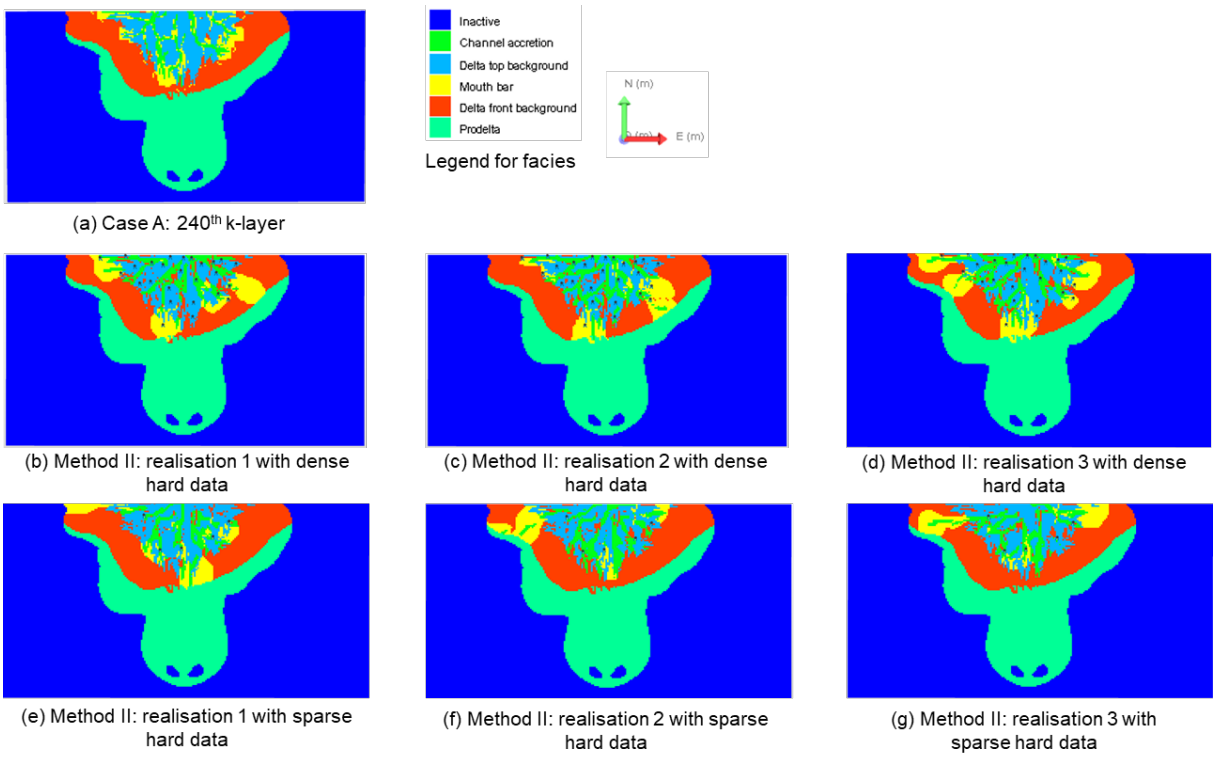

(a) Case A: 240th k-layer

Legend for facies

(b) Method II: realisation 1 with dense hard data

(c) Method II: realisation 2 with dense hard data

(d) Method II: realisation 3 with dense hard data

(e) Method II: realisation 1 with sparse hard data

(f) Method II: realisation 2 with sparse hard data

(g) Method II: realisation 3 with sparse hard data

Figure 7.10. Conditional simulation results from Case A using Method II for dense and sparse hard data.

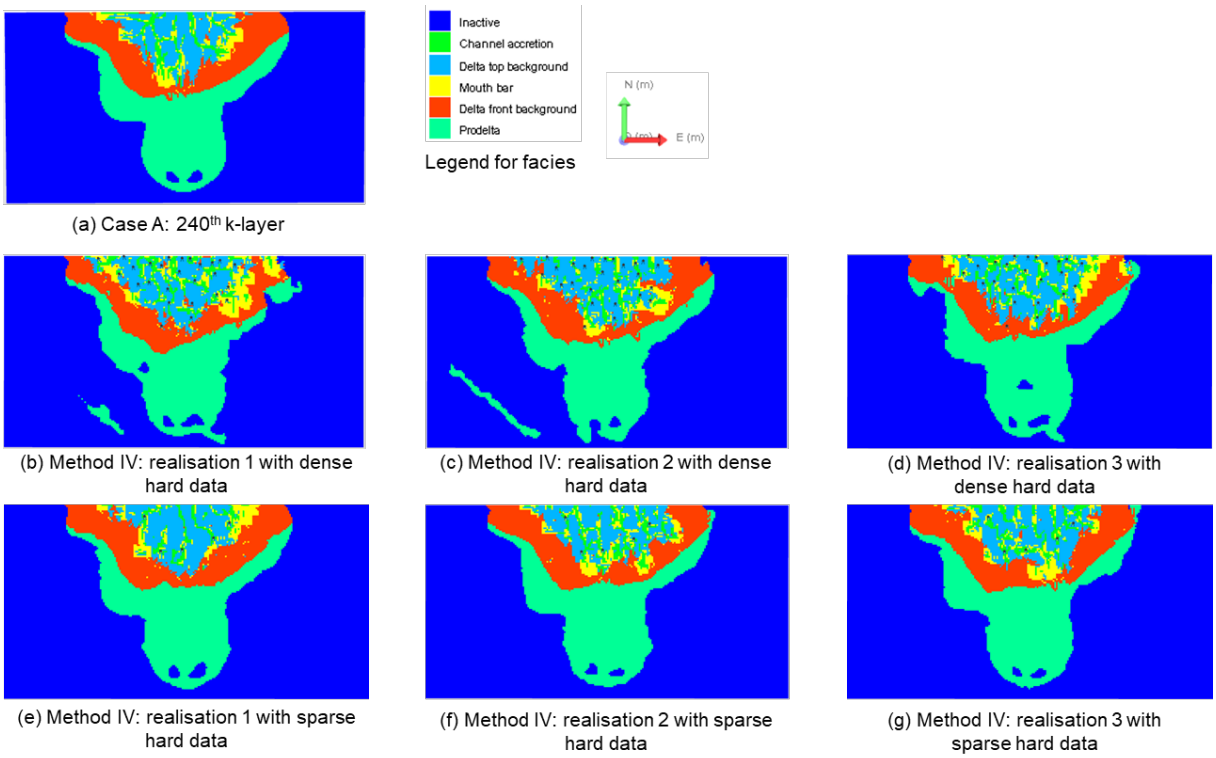

(a) Case A: 240th k-layer

Legend for facies

(b) Method IV: realisation 1 with dense hard data

(c) Method IV: realisation 2 with dense hard data

(d) Method IV: realisation 3 with dense hard data

(e) Method IV: realisation 1 with sparse hard data

(f) Method IV: realisation 2 with sparse hard data

(g) Method IV: realisation 3 with sparse hard data

Figure 7.11. Conditional simulation results from Case A using Method IV for dense and sparse hard data.

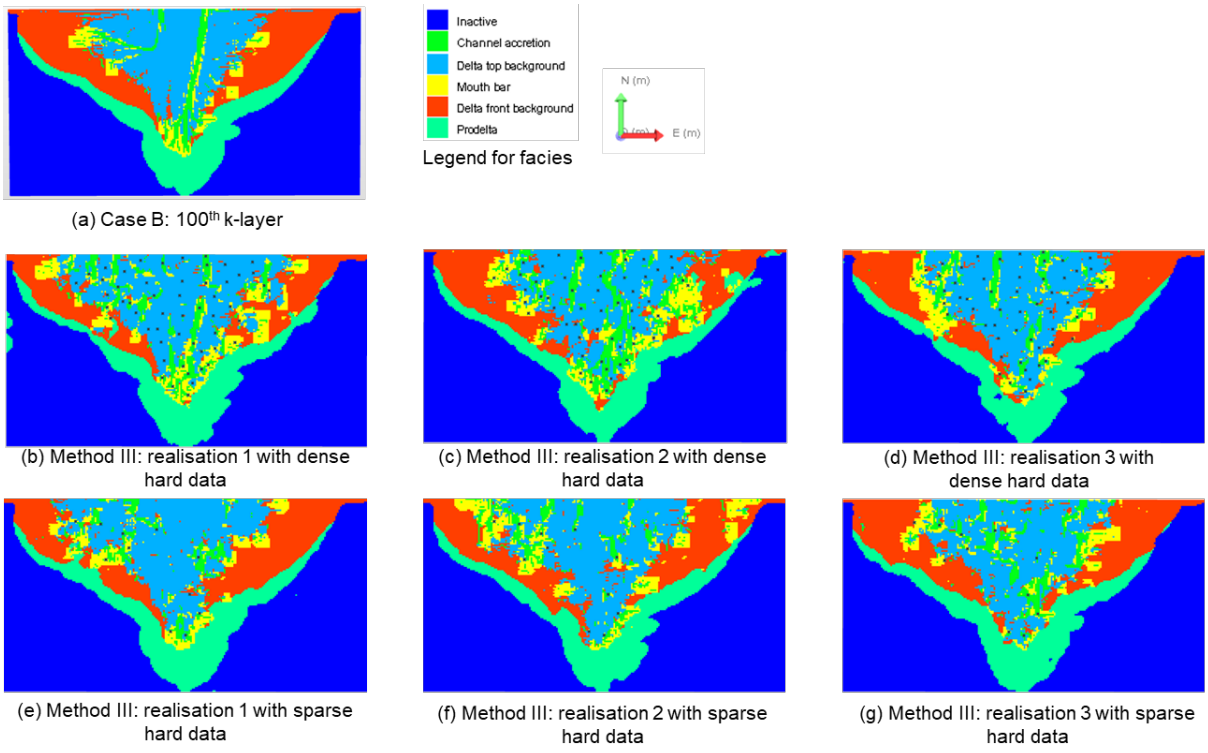

(a) Case B: 100th k-layer

(b) Method III: realisation 1 with dense hard data

(c) Method III: realisation 2 with dense hard data

(d) Method III: realisation 3 with dense hard data

(e) Method III: realisation 1 with sparse hard data

(f) Method III: realisation 2 with sparse hard data

(g) Method III: realisation 3 with sparse hard data

Figure 7.12. Conditional simulation results from Case B using Method III for dense and sparse hard data.

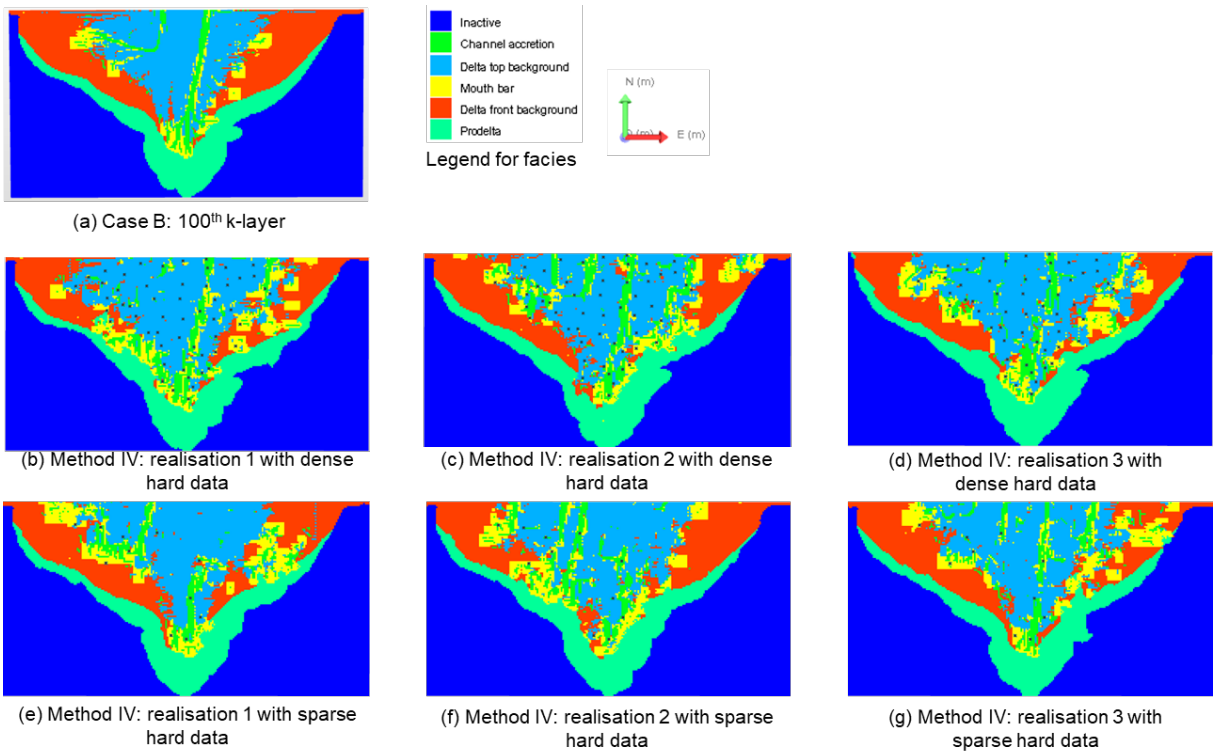

(a) Case B: 100th k-layer

Legend for facies

(b) Method IV: realisation 1 with dense hard data

(c) Method IV: realisation 2 with dense hard data

(d) Method IV: realisation 3 with dense hard data

(e) Method IV: realisation 1 with sparse hard data

(f) Method IV: realisation 2 with sparse hard data

(g) Method IV: realisation 3 with sparse hard data

Figure 7.13. Conditional simulation results from Case A using Method IV for dense and sparse hard data.